이학석사학위논문

# Mechanistic Elucidation Guided by Covalent Inhibitors for the Development of Anti-diabetic PPARγ Ligands

# 항당뇨성 퍼옥시좀 증식자 활성화 수용체 감마 리간드의 개발을 위한 공유결합성 저해제를 사용한 메카니즘적 설명

2016년 2월

서울대학교 대학원

화학부 유기화학전공

배 환

# Abstract

## Mechanistic Elucidation Guided by Covalent Inhibitors for the Development of Anti-diabetic PPARγ Ligands

Hwan Bae

Department of Chemistry

Seoul National University

Peroxisome proliferator-activated receptor γ (PPARγ) is a ligand-regulated transcription factor that plays crucial roles in adipogenesis, lipid metabolism, and glucose homeostasis. There are several PPARγ ligands having anti-diabetic activity and they commonly inhibit phosphorylation of PPARγ at Serine 273 (Ser273). Recently reported PPARγ ligand SR1664, which selectively block the phosphorylation with no classical agonism, has potent anti-diabetic activity, indicating that the inhibition of Ser273 phosphorylation is sufficient to provoke anti-diabetic effects.

In this study, we revealed the x-ray structure of PPARγ co-crystallized with SR1664 bound to the alternate binding site of PPARγ, and we confirmed that this binding directly blocks phosphorylation of Ser273. Furthermore, by using synthesized covalent inhibitors as chemical tools, we demonstrated that the

inhibition of phosphorylation is attributed to the occupation of a specific site which is a hydrophobic region between Helix 3 (H3) and β3–β4 at the binding pocket of PPARγ. In high-fat diet-induced obese mice, we confirmed anti-diabetic activity of a covalent inhibitor which is rationally designed to bind at the specific site in PPARγ to block phosphorylation of Ser273. Lastly, the target selectivity of the covalent inhibitor was demonstrated by fluorescence-based visualization of target proteins complexed with its covalent probe containing a bioorthogonal functional group.

**Keywords**: PPARγ, Ser273 phosphorylation, alternate binding site, covalent inhibitor, rational design, chemical tool, anti-diabetic activity, target selectivity

**Student Number**: 2013-22925

# Contents

# 1. Introduction

Insulin resistance is a condition in which cells of body become resistant to the normal actions of insulin hormone, and it is a typical symptom of type Ⅱ diabetes[1]. Because of potent insulin-sensitizing effects of PPARγ-targeting drugs such as rosiglitazone and pioglitazone, PPARγ has been considered one of major therapeutic targets for the treatment of type Ⅱ diabetes although the underlying molecular mechanisms are still unclear[2–4]. However, Choi et al. proposed a plausible mechanism of how anti-diabetic PPARγ ligands affect insulin sensitivity[5]. They demonstrated that the obesity-induced phosphorylation of PPARγ at Ser273 results in dysregulation of a subset of genes involved in insulin resistance and revealed that anti-diabetic PPARγ ligands effectively block this phosphorylation. Based on these findings, they suggested that the efficacy of anti-diabetic PPARγ ligands is attributed to their ability to inhibit the phosphorylation of PPARγ. Moreover, it was recently elucidated that an extracellular signal-regulated kinase (ERK) / cyclin-dependent kinase 5 (Cdk5) axis regulates the diabetogenic actions of PPARγ through the phosphorylation of Ser273[6], and that Ser273-phosphorylated PPARγ is selectively recognized by thyroid hormone receptor-associated protein 3 (Thrap3) and the interaction between them regulates a diabetic gene set[7].

Although glitazones have remarkable effects in the treatment of type Ⅱ diabetes, they have lost their footing on the drug market because of their serious side effects including weight gain, fluid retention and congestive heart failure[8,9]. Glitazones not only inhibit the phosphorylation of Ser273 but also fully activate

expression of PPARγ target genes, which is referred to as classical transcriptional agonism[5]. The full classical agonism has been suspected of causing serious side effects, so there have been consistent efforts to find a selective PPARγ modulator (SPPARγM), which shows reduced classical agonism while retaining potent effects in insulin sensitization[10–12]. Since PPARγ has a huge binding pocket and multiple interaction points with ligands, it is expected that PPARγ activities can be selectively regulated through site-specific binding of ligands[13]. Recently, development of a SPPARγM, SR1664 demonstrated that completely selective modulation of PPARγ activities is possible by the specific ligand binding. Unlike glitazones, SR1664, which does not alter the transcriptional activity of PPARγ but has an ability to inhibit the phosphorylation of Ser273, shows potent anti-diabetic effects while not causing fluid retention and weight gain that are serious adverse effects of conventional PPARγ-targeting drugs represented by glitazones[14]. In consideration of these results, there is no doubt that designing a selective inhibitor of PPARγ phosphorylation can be a powerful strategy for the development of a novel anti-diabetic agent targeting PPARγ. However, one problem is that we do not have a molecular understanding of exact structural mechanism of how anti-diabetic PPARγ ligands block Ser273 phosphorylation.

In this study, we revealed that SR1664 binds to the alternate binding site of PPARγ, blocking phosphorylation of Ser273. Based on this finding, we narrowed down a specific binding site that can be responsible for the inhibition of Ser273 phosphorylation of PPARγ. To verify whether the specific site binding of PPARγ ligands affects the phosphorylation of Ser273, we designed and synthesized several covalent inhibitors that could specifically bind at this

site. By comparing their phosphorylation inhibiting abilities with their crystal structures, we demonstrated that occupation of the specific binding site by PPARγ ligands is necessary to block the phosphorylation of Ser273. Moreover, we confirmed that a rationally designed covalent PPARγ phosphorylation inhibitor showed anti-diabetic effects in high-fat diet-induced mice without promoting adipogenesis. Lastly, target identification using fluorescence labeling revealed that our covalent inhibitor selectively binds to PPARγ.

## 2. Results and Discussion

### 2.1. SR1664 binds to the alternate binding site of PPARγ, blocking its phosphorylation at Ser273

In order to understand the exact molecular mechanism of how anti-diabetic PPARγ ligands can inhibit Ser273 phosphorylation, we solved the crystal structure of PPARγ ligand-binding domain (LBD) complexed with SR1664 to a resolution of 2.20 Å (**Fig. 1a** and **supplymentary Fig. 1a**). X-ray crystallography was performed by Jun Young Jang in Prof. Se Won Suh's group at Seoul National University. Since the molecular interaction between PPARγ and SR1664 is mainly associated with the inhibition of Ser273 phosphorylation, we might gain more insight into how anti-diabetic PPARγ ligands block phosphorylation of Ser273 by analyzing co-crystal structure of PPARγ LBD and SR1664. Interestingly, SR1664 had a completely different binding mode from full PPARγ agonists such as rosiglitazone which binds at the deep binding pocket of PPARγ via strong hydrogen bonding with Helix 12 (H12) (**Fig. 1a**, blue)[15]. In contrast, SR1664 bound to the alternate binding site which is defined as the region near entrance of the deep binding pocket occupied by second

MRL-20 molecule when two molar equivalents of MRL-20 ligand bind to PPARγ (**Fig. 1a**, green) [16]. This is the first co-crystal structure that shows a ligand binding to the alternate site of PPARγ in one-to-one binding mode. In fact, Marciano *et al.* recently reported co-crystal structure of PPARγ LBD complexed with SR1664, but its binding mode is exact opposite to our finding and almost the same as that of rosiglitazone (**Supplementary Fig. 2**)[17].

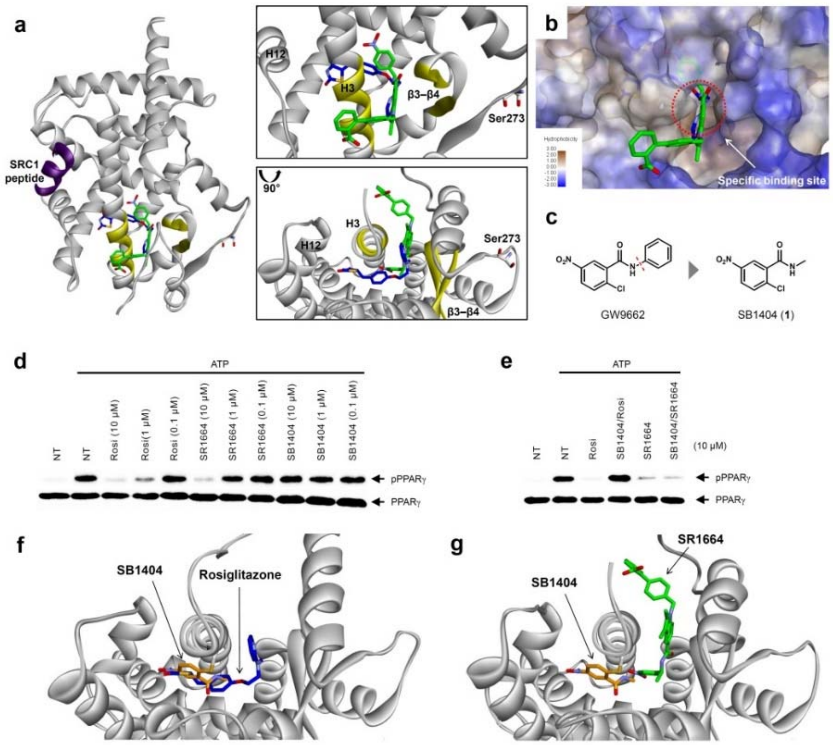


**Figure 1 | Structural elucidation of the binding mode of SR1664 by which it blocks PPARγ phosphorylation at Ser273.** (**a, b**) Alignment of the SR1664–PPARγ LBD (green) and rosiglitazone–PPARγ LBD (blue, PDB: 2PRG) X-ray co-crystal structures. (**c**) Design of a small PPARγ antagonist, SB1404. (**d**) *In vitro* Cdk5 assay of PPARγ in the presence of rosiglitazone, SR1664 or SB1404. (**e**) *In vitro* Cdk5 assay on PPARγ treated by rosiglitazone or SR1664 with or without SB1404. NT, no treatment; pPPARγ, phosphorylated PPARγ. (**f**) Alignment of rosiglitazone–PPARγ LBD (blue, PDB: 2PRG) and SB1404–PPARγ LBD (orange) X-ray co-crystal structures. (**g**) Alignment of SR1664–PPARγ LBD (green) and SB1404–PPARγ LBD (orange) X-ray co-crystal structures.

GW9662 is a synthetic irreversible PPARγ inhibitor that covalently binds to cysteine 313 (Cys313 in PPARγ2; Cys285 in PPARγ1) on H3[18], and completely blocks the ligand engagement at the deep binding pocket while not inhibiting alternate site binding of PPARγ ligands[16]. Therefore, we set to use GW9662 as a chemical tool to determine whether SR1664 does bind to the alternate site. However, there is a problem that SR1664 exhibits a steric clash with phenyl group of GW9662 (**Supplementary Fig. 3**), so we designed and synthesized a smaller covalent inhibitor, SB1404 (**1**) by replacing phenyl group with methyl group (**Fig. 1c**). Compared to rosiglitazone or SR1664, SB1404 did not inhibit Cdk5-mediated phosphorylation of PPARγ at any concentration *in vitro* (**Fig. 1d**). Nevertheless, SB1404 completely blocked the inhibitory effect of rosiglitazone on PPARγ phosphorylation, but does not affect the inhibition of PPARγ phosphorylation by SR1664 (**Fig. 1e**). Furthermore, on the basis of x-ray crystal structure of PPARγ LBD complexed with SB1404 (resolution, 2.80 Å), we confirmed that SB1404 covalently bind to Cys313 on H3 and completely blocks the binding event of rosiglitazone at the deep binding pocket of PPARγ (**Fig. 1f** and **Supplementary Fig. 4**). Unlike GW9662, SB1404 exhibits no steric clash with SR1664, so SB1404-labelled PPARγ can accommodate SR1664 (**Fig. 1g**), which indicated that SR1664 does bind to the alternate binding site of PPARγ. However, it is impossible for SR1664 to bind to SB1404-labelled PPARγ in previously reported binding mode, which is similar to that of rosiglitazone (**Supplementary Fig. 5**)[17]. Although there is a possibility that SR1664 may have different binding modes, as shown in x-ray co-crystal structure and *in vitro* Cdk5 assay, it is uncontroversial that SR1664 binds to the alternate site of PPARγ, blocking the phosphorylation of Ser273 by Cdk5.

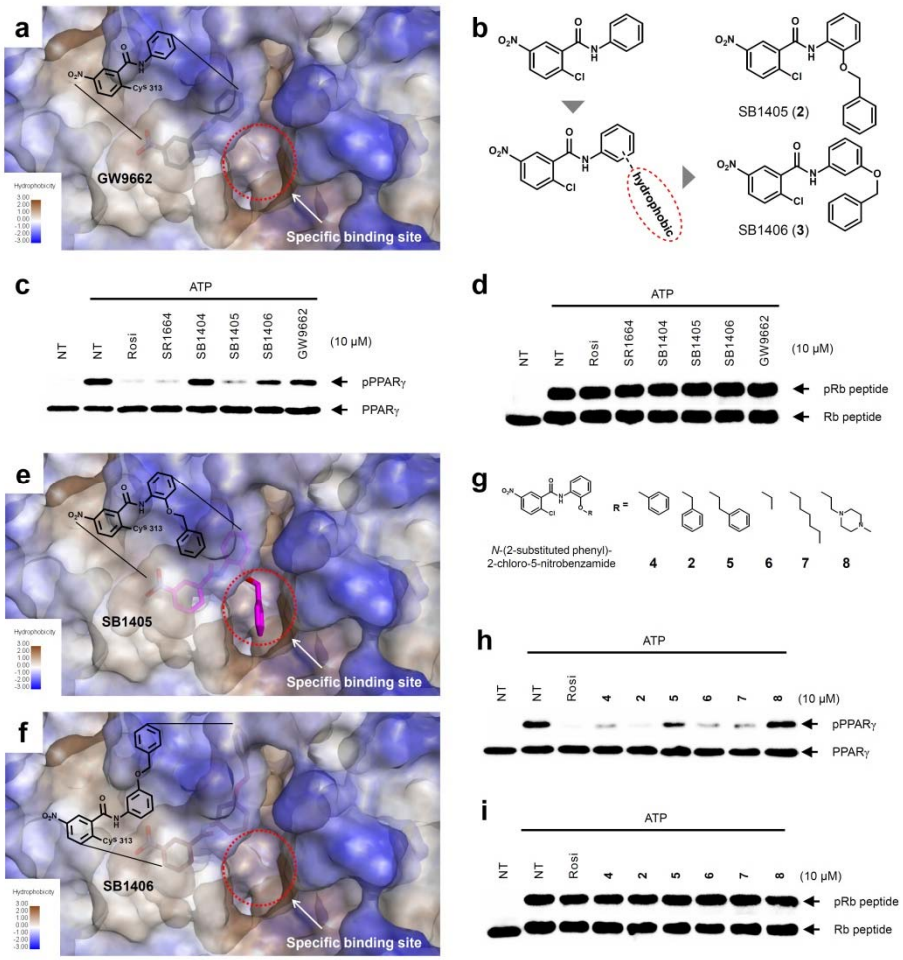


**Figure 2 | Structure-based rational design of covalent inhibitors of PPARγ phosphorylation.** (**a**) The specific binding site on the surface of PPARγ LBD complexed with GW9662 (black, PDB: 3B0R). (**b**) Structure-based design of the covalent inhibitors SB1405 and SB1406 expected to bind at the specific site. (**c, d**) *In vitro* Cdk5 assay of PPARγ or the Rb peptide after treatment with rosiglitazone, SR1664, or the covalent inhibitors. NT, no treatment; pPPARγ, phosphorylated PPARγ; pRb peptide, phosphorylated Rb peptide. (**e, f**) Binding modes of SB1405 (pink) and SB1406 (brown) confirmed by X-ray crystallography. (**g**) Chemical structures of ***N***-(2-substituted phenyl)-2-chloro-5-nitrobenzamides. (**h, i**) *In vitro* Cdk5 assay of PPARγ or the Rb peptide after treatment with rosiglitazone or ***N***-(2-substituted phenyl)-2-chloro-5-nitrobenzamides.

## 2.2. Site-specific binding of PPARγ ligands inhibits the phosphorylation of Ser273

The common biological effect of both SR1664 and rosiglitazone is the specific inhibition of PPARγ phosphorylation at Ser273, which means that they should share a specific characteristic[14]. By analyzing the binding modes of SR1664 and rosiglitazone in x-ray co-crystal structures, we found that a specific hydrophobic region between H3 and β3–β4 occupied by both of them (**Fig. 1b**). Based on this structural insight, we hypothesized that the specific site binding of PPARγ ligands might be responsible to the inhibition of PPARγ phosphorylation at Ser273. To test this hypothesis, we designed a couple of covalent inhibitors that can selectively bind at the specific site. Considering the structures of GW9662 and SB1404, 2-chloro-5-nitrobenzamide moiety can serve as an electrophile and covalently trap Cys313 regardless of functional groups attached to amide. Therefore, based on the GW9662–PPARγ co-crystal structure, we rationally designed SB1405 (**2**) and SB1406 (**3**) containing 2-(benzyloxy)phenyl and 3-(benzyloxy)phenyl group, respectively, instead of phenyl group of GW9662 (**Fig. 2a** and **b**).

With an expectation that additional hydrophobic benzyl moiety would occupy the specific region of PPARγ between H3 and β3–β4, we conducted *in vitro* Cdk5 assay with these covalent inhibitors. Interestingly, only SB1405 inhibited the phosphorylation of PPARγ (**Fig. 2c**) without blocking the phosphorylation of C-terminal fragment of retinoblastoma protein (Rb peptide), one of well-known Cdk5 substrates (**Fig. 2d**)[19]. This indicated that SB1405 does not affect the fundamental kinase function of Cdk5, but blocks the phosphorylation of PPARγ at Ser273 like rosiglitazone and SR1664. However,

we didn't observe this inhibitory activity in the case of SB1406, which is the structural isomer of SB1405. To explain this intriguing result, we resolved the crystal structure of PPARγ LBD complexed either with SB1405 or SB1406 to resolutions of 2.75, 2.95 Å, respectively. Like SB1404, both of them covalently bound to Cys313, but they showed different binding modes (**Supplementary Fig. 6a**). Benzyl group of SB1405 occupied the specific hydrophobic region of PPARγ (**Fig. 2e**), whereas the same moiety of SB1406 did not (**Fig. 2f**). Therefore, these co-crystal structures clearly elucidated why only SB1405 inhibited the phosphorylation of PPARγ at Ser273, demonstrating that the occupation of that hydrophobic region of PPARγ is essential for the inhibition of PPARγ phosphorylation.

When we aligned co-crystal structures of SB1405–PPARγ LBD and SB1406–PPARγ LBD, we didn't observe any considerable differences in their backbone conformation (RMSD Cα = 0.36 Å), and there was no significant difference in their residues' positioning around the specific binding site (**Supplementary Fig. 6b**). This indicates that the inhibition of PPARγ phosphorylation is not an outcome of conformational changes, but is probably caused by ligand-induced changes in the dynamic nature of PPARγ LBD. In fact, recent studies revealed that anti-diabetic PPARγ ligands including rosiglitazone and MRL24 significantly reduced the hydrogen/deuterium exchange (HDX) across H3 and the β-sheet region of PPARγ. This ligand-induced reduction of hydrogen/deuterium exchange rate at that region is an indication of changes in the dynamic nature of H3 and the β-sheet and the subsequent inhibition of Cdk5-mediated PPARγ phosphorylation at Ser273. Actually, the effective inhibition of Ser273 phosphorylation by SB1405 is only

attributed to the occupation at the specific binding site by its benzyl group.

Based on the mechanistic and structural understanding of PPARγ phosphorylation, we selected *N*-(2-substituted phenyl)-2-chloro-5-nitrobenzamide as a suitable molecular framework and synthesized a series of covalent inhibitors of PPARγ phosphorylation containing different R groups to effectively occupy this specific binding site (**Fig. 2g**). As shown in **Fig. 2h**, most of them showed good inhibitory activities toward Cdk5-mediated PPARγ phosphorylation except **8** containing hydrophilic piperazine moiety. In contrast, all of them showed no inhibitory effect on the phosphorylation of Rb peptide by Cdk5 (**Fig. 2i**). Taken together, *N*-(2-substituted phenyl)-2-chloro-5-nitrobenzamides having hydrophobic moieties efficiently blocked Cdk5-mediated PPARγ phosphorylation at Ser273 and the occupation of R substituents at the hydrophobic region between H3 and β3–β4 of PPARγ seems to be sufficient to reduce the dynamic configuration of this region, which inhibits the *in vitro* phosphorylation of PPARγ by Cdk5.

## 2.3. Structure-guided optimization and evaluation of covalent inhibitors for *in vivo* analysis

Among *N*-(2-substituted phenyl)-2-chloro-5-nitrobenzamides, we selected SB1405 (**2**) for the further *in vivo* study because of its excellent inhibition potency in *in vitro* Cdk5 assay (**Fig. 2h**) and a perfect occupancy of its benzyl moiety at the specific binding site (**Fig. 2e**). However, we concerned that *in vivo* evaluation of SB1405 might be limited due to its poor solubility. To solve this problem, we decided to modify the structure of SB1405, but we had to preserve 2-chloro-5-nitrobenzamide moiety to make a covalent bond with Cys313 of PPARγ and hydrophobic benzyl moiety to bind to the specific site for phosphorylation inhibition. Thus, we introduced additional moiety on the benzyl moiety of SB1405 to occupy remaining empty hydrophobic space (brown) and the subsequent hydrophilic space (blue) (**Fig. 3a**). On the basis of crystal structure of SB1405–PPARγ LBD, we designed and synthesized SB1451 (**9**) and SB1453 (**10**) containing hydrophilic piperazine moiety attached to additional benzene ring to improve its solubility (**Fig. 3b**).

After synthesis of SB1451 and SB1453, we examined their inhibitory activity toward PPARγ phosphorylation at Ser273 in a dose-dependent manner and confirmed their excellent potency in *in vitro* Cdk5 assay (**Fig. 3c**). This inhibitory potency of SB1451 and SB1453 in PPARγ phosphorylation was also conserved in the cellular system, which was

similar to that of rosiglitazone (**Fig. 3e**). However, they did not inhibit the basic kinase function of Cdk5 monitored by western blot analysis of Rb peptide phosphorylation *in vitro* (**Fig. 3d**).

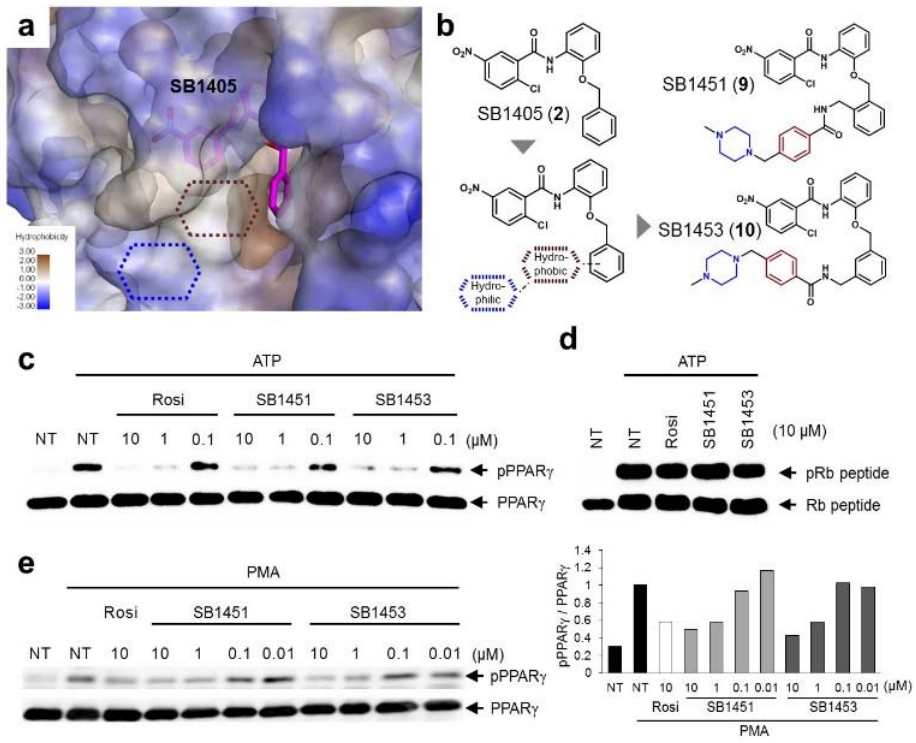


**Figure 3 | Rational optimization of covalent PPARγ-phosphorylation inhibitors for *in vivo* analysis.** (**a, b**) Structure-guided rational design of the covalent inhibitors SB1451 and SB1453 to improve the solubility of SB1405. (**c, d**) *In vitro* Cdk5 assay of PPARγ or the Rb peptide after treatment with rosiglitazone, SB1451, or SB1453. NT, no treatment; pPPARγ, phosphorylated PPARγ; pRb peptide, phosphorylated Rb peptide. (**e**) PMA-induced phosphorylation of PPARγ in HEK-293 cells expressing PPARγ after treatment with rosiglitazone, SB1451, or SB1453.

## 2.4. Covalent PPARγ phosphorylation inhibitors exert anti-diabetic effects *in vivo* without promoting adipogenesis

To examine the agonistic activity in PPARγ-mediated transcription, we conducted two cellular assays. First, using a luciferase reporter gene assay in HEK-293T cells with tandem PPAR-response elements, we confirmed that SB1451 and SB1453 have almost no classical transcriptional agonism compared to that of rosiglitazone (**Fig. 4a**). Secondly, we tested whether these covalent inhibitors stimulate the adipogenesis by monitoring cellular lipid accumulation in 3T3-L1 cells with Oil Red-O staining[20,21]. As shown in **Fig. 4b**, the treatment of rosiglitazone (10 μM) fully stimulated the adipocyte differentiation but that of SB1451 or SB1453 (10 μM) did not trigger adipogenesis in 3T3-L1 cells, which confirms no transactivation of these inhibitors. Even though we observed the slight increases in PPARγ's transcriptional activity upon treatment with SB1453 at 10 μM in the luciferase assay, this concentration was not sufficient enough to stimulate the differentiation of pre-adipocytes into mature adipocytes.

We evaluated anti-diabetic activity of SB1451 and SB1453 in animal models using high-fat diet-induced obese (DIO) mice that are insulin-resistant with the increased level of phosphorylated PPARγ[5]. *In vivo* experiments were performed by Dr. Sun-Sil Choi in Prof. Jang Hyun Choi's group at Ulsan National Institute of Science and Technology. As shown in **Fig. 4c**, SB1453 effectively decreases the phosphorylation level of PPARγ at Ser273 in white adipose tissue of DIO mice at the similar level of rosiglitazone. SB1451 was less potent in *in vivo* reduction of PPARγ phosphorylation and the subsequent anti-diabetic activity compared to SB1453. Previous studies clearly

demonstrated that SR1664, a selective inhibitor of PPARγ phosphorylation without classical agonism, shows *in vivo* anti-diabetic effects in obese animals[12,14]. Similar to SR1664, SB1453 altered the expression of 10 of the 17 genes regulated by PPARγ phosphorylation (**Fig. 4e**), but we did not observe any stimulation of the "agonist" gene set by SB1453 in white adipose tissue of DIO mice (**Fig. 4d**). This indicated that SB1453 effectively inhibited the PPARγ phosphorylation while not promoting adipogenesis in *in vivo* systems. Furthermore, the intraperitoneal injection of SB1453 at 10 mg/kg/day for 7 days improved glucose tolerance of DIO mice although this effect was moderate compared to rosiglitazone (**Fig. 4f**).

We also investigated several adverse effects, including fluid retention and cardiac hypertrophy, which have been observed following treatment with glitazones[8,22]. As shown in **Supplementary Fig. 7a**, rosiglitazone treatment caused hemodilution, whereas SB1453 treatment had no detectable changes compared with vehicle. Furthermore, the expressions of natriuretic peptide type B (BNP), the marker gene of heart failure, or myosin heavy chain β (β-MHC), the marker gene of hypertrophy, were significantly increased in only rosiglitazone-treated mice without changes in heart weight (**Supplementary Fig. 7b** and **c**). These results strongly suggest that SB1453 does not induce adverse effects associated with *in vivo* treatment of glitazones.

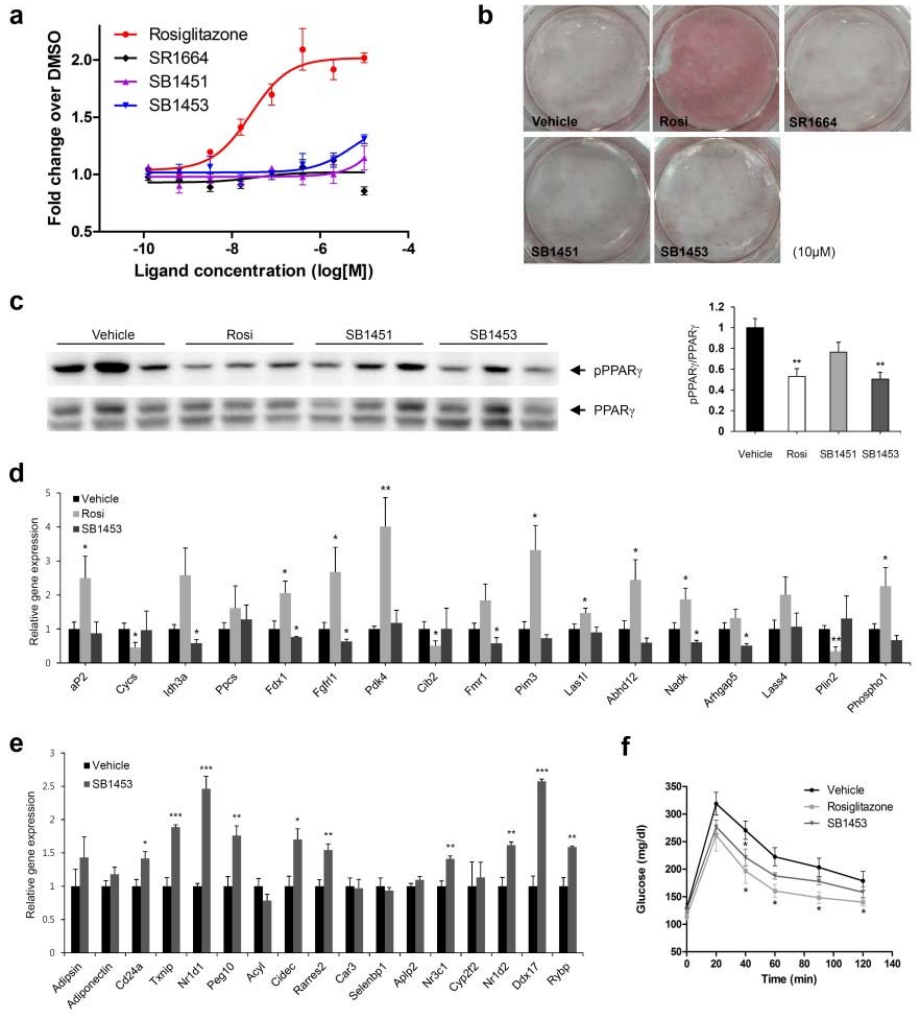


**Figure 4 | Anti-diabetic activity of SB1453 in DIO mice without promoting adipogenesis.** (**a**) Transcriptional activity of a PPAR-derived reporter gene in HEK-293T cells after 24 h of treatment with rosiglitazone, SR1664, SB1451 or SB1453 ($n$ = 3). (**b**) Oil Red O staining of accumulated lipids in 3T3-L1 cells treated with rosiglitazone, SR1664, SB1451, or SB1453. (**c**) Phosphorylation of PPARγ in WAT of DIO mice after 7 days of treatment with vehicle, rosiglitazone, SB1451, or SB1453 (10 mg/kg/day). (**d**) Expression of the agonist gene set in WAT. (**e**) Expression of the gene set regulated by PPARγ phosphorylation in WAT. (**f**) Glucose-tolerance test in DIO mice treated with vehicle, rosiglitazone, or SB1453 (7 days, 10 mg/kg/day) (n = 6). Error bars denote SEM. * $P < 0.05$, ** $P < 0.01$, *** $P < 0.001$.

## 2.5. Covalent inhibitor selectively binds to PPARγ

Lastly, we confirmed the target selectivity of SB1453 by using target identification probe. Prior to the probe design, we resolved the crystal structure of PPARγ complexed with SB1453 (resolution, 2.30 Å) to gain more information about its binding mode (**Fig. 5a**). As expected, SB1453 covalently bound to Cys313 on H3 and occupied the hydrophobic region between H3 and β3–β4. In addition, its piperazine moiety was positioned at the entrance of PPARγ binding pocket. Based on this structural information, we designed the target identification probe 11 containing terminal acetylene group on the piperazine moiety to enable the fluorescence labeling of target proteins via a bioorthogonal Click reaction (**Fig. 5b**). Despite the structural change, probe 11 retained its phosphorylation inhibitory effect, indicating that this probe probably made covalent bonding with Cys313 on H3 of PPARγ (**Fig. 5c**). Then, probe 11 was incubated with the proteome of differentiated 3T3-L1 cells, followed by copper-catalyzed Click reaction with an azide-containing Cy5 to visualize proteins complexed with probe 11. The resulting proteome was separated by gel electrophoresis, and target proteins were visualized via fluorescence scanning. Interestingly, the predominant bands were appeared on the fluorescent gel in a dose-dependent manner without any difference in protein expression pattern (**Fig. 5d** and **e**). These labeled proteins were identified as PPARγ1 (53kDa) and PPARγ2 (57kDa) by Western blot analysis (**Fig. 5f**). In fact, they are two isoforms of PPARγ and have common LBD to which SB1453 binds. This result demonstrated that our covalent inhibitor SB1453 selectively binds to PPARγ.

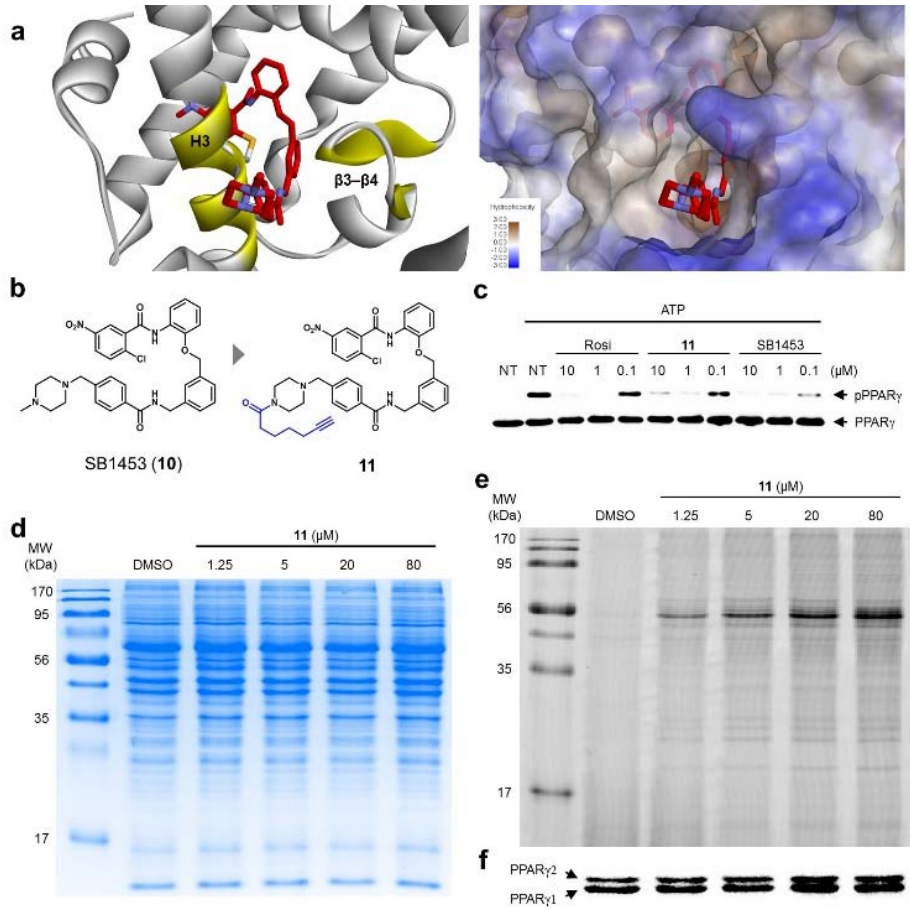


**Figure 5** | (**a**) X-ray co-crystal structure of SB1453–PPARγ LBD reveals the exposure of piperidine moiety at the entrance of PPARγ binding pocket. (b) Structure-guided rational design of the target identification probe 11 to demonstrate the target selectivity. (c) In vitro Cdk5 assay of PPARγ on treatment with rosiglitazone, 11, or SB1453 in a dose-dependent manner. (d, e) Coomassie staining and fluorescence scanning patterns of SDS-PAGE of lysates from differentiated 3T3-L1 adipose cells treated with probe 11 in various concentrations. (f) Western blot against the same gel in (e) to confirm PPARγ as the target proteins labeled by 11.

## 3. Conclusion

In this study, we identified that the alternate site binding of SR1664 effectively blocked the phosphorylation of PPARγ at Ser273 and by comparing this binding mode with that of a conventional PPARγ ligand rosiglitazone, we found a hydrophobic region between H3 and β3-β4, which is closely related to the inhibition of phosphorylation. To determine the functional effect of PPARγ ligands binding at the specific site, we rationally designed and synthesized irreversible covalent inhibitors as chemical tools. Based on the *in vitro* PPARγ phosphorylation assay using Cdk5, we found that the occupation of the specific binding site in PPARγ by small-molecule ligands is directly correlated with the inhibitory effects on the phosphorylation of PPARγ at Ser273. This structural insight led us to rationally design the improved covalent inhibitors, SB1451 and SB1453, which effectively inhibit the phosphorylation of PPARγ at Ser273 *in vitro* and in adipose cells. We also demonstrated that SB1453 shows anti-diabetic effects in DIO mice by reducing the level of phosphorylated PPARγ in white adipose tissue. Lastly, through fluorescence-based visualization of target proteins complexed with the covalent probe **11** containing a bioorthogonal functional handle, we confirmed that our covalent inhibitor selectively binds to PPARγ.

This study provided a useful guideline when designing a SPPARγM which effectively inhibits the phosphorylation of Ser273 for the development of anti-diabetic PPARγ ligands. It can be expected that new classes of PPARγ-targeting drugs will be developed in accordance with this guideline. An exquisitely designed *N*-(2-substituted phenyl)-2-chloro-5-nitrobenzamide such as SB1453 has a potential to be developed as a PPARγ-targeting anti-diabetic drug,

assuming it is completely free from the general concerns regarding the safety of irreversible covalent inhibitors[23].

## 4. Experimental Methods

**Chemical synthesis.** The synthesis of compounds is described in detail in the **Supplementary Note**.

**Reagents.** SR1664 (SML0636, Sigma), GW9662 (M6191, Sigma), and rosiglitazone (R0106, TCI) were purchased from commercial venders and used without further purification. Cell culture reagents, including serum, medium, and antibiotic-antimycotic solution, were obtained from Gibco, Invitrogen.

**Protein expression and purification.** The human PPARγ LBD construct (residues 195–477 in PPARγ1) was PCR-amplified and cloned into the expression vector pET-28b(+) [Novagen, USA]. This construct of the recombinant protein encodes a 21-residue *N*-terminal tail (MGSSHHHHHH SSGLVPRGSH M) containing a $His_6$ tag and a thrombin cleavage site in front of the starting residue Ala195. The recombinant human PPARγ LBD was overexpressed in *Escherichia coli* Rosetta 2(DE3) cells using the Luria Broth culture medium. Protein expression was induced by 0.5 mM isopropyl β-D-thiogalactopyranoside and the cells were incubated for additional 24 h at 18 °C following growth to mid-log phase at 37 °C. The cells were lysed by sonication in buffer A (20 mM Tris-HCl at pH 8.5, 150 mM NaCl, 10% (v/v) glycerol and 0.1 mM tris(2-carboxyethyl) phosphine hydrochloride) containing 5 mM imidazole and 1 mM phenylmethylsulfonyl fluoride. The crude lysate was centrifuged at 36,000 g for 1 h. The supernatant was applied to a HiTrap Chelating HP affinity chromatography column [GE Healthcare, UK], which was previously equilibrated with buffer A containing 5 mM imidazole. Upon eluting with a gradient of imidazole in the same buffer, the human PPARγ LBD

was eluted at 45–100 mM imidazole concentration. The eluted protein was desalted in buffer A by HiPrep 26/10 desalting column [GE Healthcare, UK] to remove imidazole, and the protein was cleaved with 2 U/mg thrombin protease [Sigma Aldrich, USA] at 4 °C overnight. The *N*-terminal fusion tag and uncleaved material were removed by rechromatography with a HiTrap Chelating HP affinity chromatography column. The flow-through was applied to a HiLoad XK-16 Superdex 200 prep-grade column [GE Healthcare, UK], which was previously equilibrated with buffer A. Fractions containing the human PPARγ LBD were pooled and concentrated to 15.4 mg/mL using an Amicon Ultra-15 Centrifugal Filter Unit [Millipore, USA].

**Crystallization.** Before crystallization, the purified PPARγ LBD and a LXXLL motif-containing peptide derived from human steroid receptor coactivator-1 (SRC1) (residues 685–700, ERHKILHRLLQEGSPS) were mixed in a ratio of 1:2, with a 10-fold molar excess of the PPARγ ligands. After overnight incubation, the protein was crystallized by the sitting-drop vapor diffusion method using the Mosquito robotic system [TTP Labtech, UK] at 23 °C by mixing 0.2 μL of the protein solution and 0.2 μL of the reservoir solution. Crystals of PPARγ LBD in complex with various ligands and the SRC1 peptide were obtained with a reservoir solution of 2.2 M sodium malonate (pH 7.0), except for crystals of PPARγ LBD in complex with SB1451. The PPARγ·SB1451·SRC1 crystals were obtained with a reservoir solution of 100 mM sodium cacodylate (pH 6.5), 190 mM sodium acetate and 26% (w/v) PEG 8000. All structures were deposited in the protein data bank: SR1664 (PDB: 5DWL), SB1404 (PDB: 5DV6), SB1405 (PDB: 5DV3), SB1406 (PDB: 5DSH), SB1451 (PDB: 5DV8) and SB1453 (PDB: 5DVC).

**X-ray data collection.** X-ray diffraction data were collected at 100 K using a Quantum 270 CCD detector system [Area Detector Systems Corporation, USA] at the BL-7A experimental station of Pohang Light Source, Korea. Raw X-ray diffraction data were processed and scaled using the program suit HKL2000[24]. Data collection statistics are summarized in **Supplementary Table 1**. All structures were solved by molecular replacement with the program *MolRep*[25] using the previously published PPARγ LBD structure (PDB: 3VN2)[26] as a search model. Subsequent model building was done manually using the program *COOT*[27] and the models were refined with the program *REFMAC5*[28], including the bulk solvent correction. A total of 5% of the data was randomly set aside as test data for the calculation of $R_{free}$[29]. The stereochemistry of the refined models was assessed by *MolProbity*[30]. Refinement statistics are summarized in **Supplementary Table 1**.

**Cell culture.** HEK-293, HEK-293T and 3T3-L1 cells were obtained from American Type Culture Collection and cultured in Dulbecco's modified Eagle's medium (DMEM) supplemented with 1% (v/v) antibiotic-antimycotic solution and 10% fetal bovine serum (FBS). 3T3-L1 preadipocytes were grown in 6-well plates to 100% confluency and induced by treating the cells with 1 μM dexamethasone, 850 nM insulin, and 10 μM compound in DMEM containing 10% FBS for 2 days, and the cell culture was subsequently maintained by replacing the medium with fresh DMEM containing 10% FBS and 850 nM insulin. At day 8, accumulated lipid in the 3T3-L1 cells was detected by Oil Red O staining.

***In vitro* kinase assay.** *In vitro* Cdk5 assay was conducted according to the manufacturer's instructions [Cell Signaling Technology, USA]. Briefly, 0.5 μg

of purified PPARγ LBD was incubated with active Cdk5/p35 [Millipore, USA] in assay buffer (25 mM Tris-HCl, pH 7.5, 5 mM β-glycerophosphate, 2 mM DTT, 0.1 mM $Na_3VO_4$, 10 mM $MgCl_2$) containing 25 μM ATP for 30 min at 30 °C. Compounds were pre-incubated with PPARγ LBD for 30 min at 30 °C before performing the assay. Rb peptide [residues 773–928, Millipore] was also used as a substrate of Cdk5 to know whether the compounds affect the fundamental kinase function of Cdk5 or not. Phosphorylation of substrates was analyzed by western blotting with anti-Cdk substrate antibody to detect phospho-Ser in a K/R-S-P-K/R motif, which is the consensus motif for Cdk substrates [Cell Signaling Technology, USA].

**Cell-based luciferase reporter gene assay.** HEK-293T cells were seeded in 96-well plates at a density of 7000 cells per well a day prior to transfection. The cells were transfected with pDR-1 luciferase reporter plasmid, PPARγ, RXRα, and pRL-renillin using the calcium phosphate transfection protocol. Following an overnight transfection, the cells were treated with rosiglitazone, SR1664, BH251, or BH253 for 24 h. The cells were harvested and reporter gene assay were performed by using the Dual-luciferase kit [Promega, USA]. Luciferase activity was measured using Bio-Tek microplate reader [ELx800TM, Bio-Tek Instruments Inc., USA] and normalized to Renilla activity. Fold change of treated cells over DMSO-treated control cells were plotted in triplicates.

**Target identification using fluorescence labeling.** Differentiated 3T3-L1 cells were scrapped with cold phosphate buffered saline (PBS) and centrifuged. The supernatant was discarded and cell pellet was resuspended in PBS containing protease inhibitor cocktail. The cells were lysed by freeze-thaw cycles, and the cell lysate was centrifuged at 4 °C, 13000 rpm for 15 min. The mixture of

proteome and **11** was incubated at 30 °C for 1 h. Click chemistry was performed to the mixture with Cy5-azide [Lumiprobe, USA] (80 μM), TBTA (100 μM), CuSO4 (1 mM), TCEP (2 mM) and tBuOH (5%) for 1.5 h. The resulting proteome was separated by gel electrophoresis and scanned with Typhoon Trio [GE Healthcare, UK]. The in-gel fluorescence signal was visualized at the Cy5 (633 nm excitation) channel by Typhoon Trio and analyzed by ImageQuant TL program [Amersham Bioscience, USA]. The fluorescence labeled protein was identified by western blotting with anti-PPARγ antibody [Cell Signaling Technology, USA].

**Preparation of cell or tissue lysates and immunoblotting.** HEK-293 cells expressing PPARγ were treated with phorbol 12-myristate 13-acetate (PMA) (0.5 μM) for 30 min and total cell lysates were incubated with FLAG M2 agarose [Sigma Aldrich, USA] at 4 °C. For tissue lysates, WAT from mice was homogenized in RIPA buffer (50 mM Tris, pH7.5, 150 mM NaCl, 1% NP-40, 0.5% sodium deoxycholate, 0.1% SDS with protease and phosphatase inhibitors). Immunoprecipitates, total cell lysates or tissue lysates were analyzed with phospho-specific antibody against PPARγ Ser273 or anti-PPARγ antibody [Santa Cruz Biotechnology, Inc., USA].

**Gene expression analysis.** Total RNA was isolated from cells or tissues using Trizol reagents [Invitrogen, CA, USA]. The RNA was reverse-transcribed using ABI reverse transcription kit. Quantitative PCR reactions were performed with SYBR green fluorescent dye using an ABI9300 PCR machine. Relative mRNA expression was determined by the ΔΔ-Ct method normalized to TATA-binding protein (TBP) levels.

**Animals.** All animal experiments were performed according to procedures approved by Ulsan National Institute of Science and Technology's Institutional Animal Care and Use Committee. 5-week-old male C57BL/6J mice [DBL, Korea] were fed a high fat diet [60% kcal fat, D12492, Research Diets Inc., NJ, USA] for 10 weeks. For glucose tolerant tests (GTTs), mice were intraperitoneally injected daily 10 mg/kg rosiglitazone, SB1451, SB1453, or vehicle for 7 days, and fasted overnight prior to injection of 1.5 g/kg D-glucose. Glucose was measured in tail vain blood at intervals after glucose injection using a Truetrack glucometer [Nipro Diagnostics, Japan]. For analysis of adverse effects, mice were intraperitoneally injected daily 10 mg/kg rosiglitazone, SB1453, or vehicle for 14 days. The packed cell volume (PCV) was determined by dividing the volume of packed red blood cells by the total volume of blood followed by centrifuging whole blood in a capillary tube.

**Statistical analysis.** Data are presented as means ± standard errors of the means (SEMs) as indicated in the figure legends. Comparisons between two groups were made by unpaired two-tailed Student's *t*-tests. P values of $<0.05$ were considered statistically significant. Microsoft Excel was used for statistical calculations.

## 5. References


1. Saltiel, A.R. & Kahn, C.R. Insulin siganlling and the regulation of glucose and lipid metabolism. *Nature* **414**, 799–806 (2001).

2. Lehmann, J. M. *et al.* An antidiabetic thiazolidinedione is a high affinity ligand for peroxisome proliferator-activated receptor γ (PPARγ). *J. Biol. Chem.* **270**, 12953–12956 (1995).

3. Lehrke, M. & Lazar, M.A. The many faces of PPARγ. *Cell* **123**, 993–999 (2005).

4. Soccio, R.E., Chen, E.R. & Lazar, M.A. Thiazolidinediones and the promise of insulin sensitization in type 2 diabetes. *Cell metab.* **20**, 573–591 (2014).

5. Choi, J.H. *et al.* Anti-diabetic drugs inhibit obesity-linked phosphorylation of PPARγ by Cdk5. *Nature* **466**, 451–456 (2010).

6. Banks, A.S. *et al.* An ERK/Cdk5 axis controls the diabetogenic actions of PPARγ. *Nature* **517**, 391–395 (2015).

7. Choi, J.H *et al*. Thrap3 docks on phosphoserine 273 of PPARγ and controls diabetic gene programming. *Genes and Development* **28**, 2361–2369 (2014).

8. Nesto, R.W. *et al*. Thiazolidinedione use, fluid retention, and congestive heart failure: a consensus statement from the American Heart Association and American Diabetes Association. *Diabetes Care* **27**, 256–263 (2004).

9. Ahmadian, M. *et al.* PPARγ signaling and metabolism: the good, the bad and the future. *Nat. Med.* **19**, 557–566 (2013).

10. Rangwala, S.M. & Lazar, M.A. The dawn of the SPPARMs? *Sci. STKE* **2002**, pe9 (2002).

11. Acton, 3rd J.J. *et al.* Benzoyl 2-methyl indoles as selective PPARγ modulators. *Bioorg. Med. Chem. Lett.* **15**, 357–362 (2005).

12. Choi, S. *et al.* A novel non-agonist peroxisome proliferator-activated receptor γ (PPARγ) ligand UHC1 blocks PPARγ phosphorylation by cyclin-dependent kinase 5 (CDK5) and improves insulin sensitivity. *J. Biol. Chem.* **289**, 26618–26629 (2014).

13. Higgins, L.S. & Depaoli, A.M. Selective peroxisome proliferator-activated receptor γ (PPARγ) modulation as a strategy for safer therapeutic PPARγ activation. *Am. J. Clin. Nutr*. **91**, 267S–272S (2010)

14. Choi, J.H. *et al.* Antidiabetic actions of a non-agonist PPARγ ligand blocking Cdk5-mediated phosphorylation. *Nature* **477**, 477–481 (2011).

15. Nolte, R.T. *et al.* Ligand binding and co-activator assembly of the peroxisome proliferator-activated receptor-γ. *Nature* **395**, 137–143 (1988).

16. Hughes, T.S. *et al.* An alternate binding site for PPARγ ligands. *Nat. Comm.* **5**, 3571 (2014).

17. Marciano, D.P. *et al.* Pharmacological repression of PPARγ promotes

osteogenesis. *Nat. Comm*. **6**, 7443 (2015).

18. Leesnitzer, L.M. *et al.* Functional consequences of cysteine modification in the ligand binding sites of peroxisome proliferator activated receptors by GW9662. *Biochemistry* **41**, 6640–6650 (2002).

19. Grana, X. *et al.* PITALRE, a nuclear CDC2-related protein kinase that phosphorylates the retinoblastoma protein in vitro. *Proc. Natl Acad. Sci. USA* **91**, 3834–3838 (1994).

20. Tontonoz, P., Hu, E. & Spiegelman, B.M. Stimulation of adipogenesis in fibroblasts by PPARγ2, a lipid-activated transcription factor. *Cell* **79**, 1147–1156 (1994).

21. Chawla, A., Schwarz, E.J., Dimaculangan, D.D. & Lazar, M.A. Peroxisome proliferator-activated receptor (PPAR) gamma: adipose-predominant expression and induction early in adipocyte differentiation. *Endocrinology* **135**, 798–800 (1994).

22. Hannan, R.D., Jenkins, A., Jenkins, A.K. & Brandenburger, Y. Cardiac hypertrophy: a matter of translation. *Clin. Exp. Pharmacol. Physiol.* **30**, 517–527 (2003).

23. Singh, J., Petter, R.C., Baillie, T.A. & Whitty, A. The resurgence of covalent drugs. *Nat. Rev. Drug Discov.* **10**, 307–317 (2011).

24. Amano, Y. *et al.* Structural basis for telmisartan-mediated partial activation of PPAR gamma. *Hypertens. Res.* **35**, 715–719 (2012).

25. Brünger, A.T. Free R value: a novel statistical quantity for assessing

the accuracy of crystal structures. *Nature* **355**, 472–474 (1992).

26. Chen, V.B. *et al.* MolProbity: all-atom structure validation for macromolecular crystallography. *Acta Cryst. D* **66**, 12–21 (2010).

27. Emsley, P., Lohkamp, B., Scott, W.G. & Cowtan, K. Features and development of Coot. *Acta Cryst. D* **66**, 486–501 (2010).

28. Murshudov, G.N., Vagin, A.A. & Dodson, E.J. Refinement of Macromolecular Structures by the Maximum-Likelihood Method. *Acta Cryst. D* **53**, 240–255 (1997).

29. Otwinowski, Z. & Minor, W. Processing of X-ray diffraction data collected in oscillation mode. *Methods Enzymol.* **276**, 307–326 (1997).

30. Vagin, A. & Teplyakov, A. Molecular replacement with MOLREP. *Acta Cryst. D* **66**, 22–25 (2010).

# 6. Supplementary Information

## 6.1. Supplementary Results

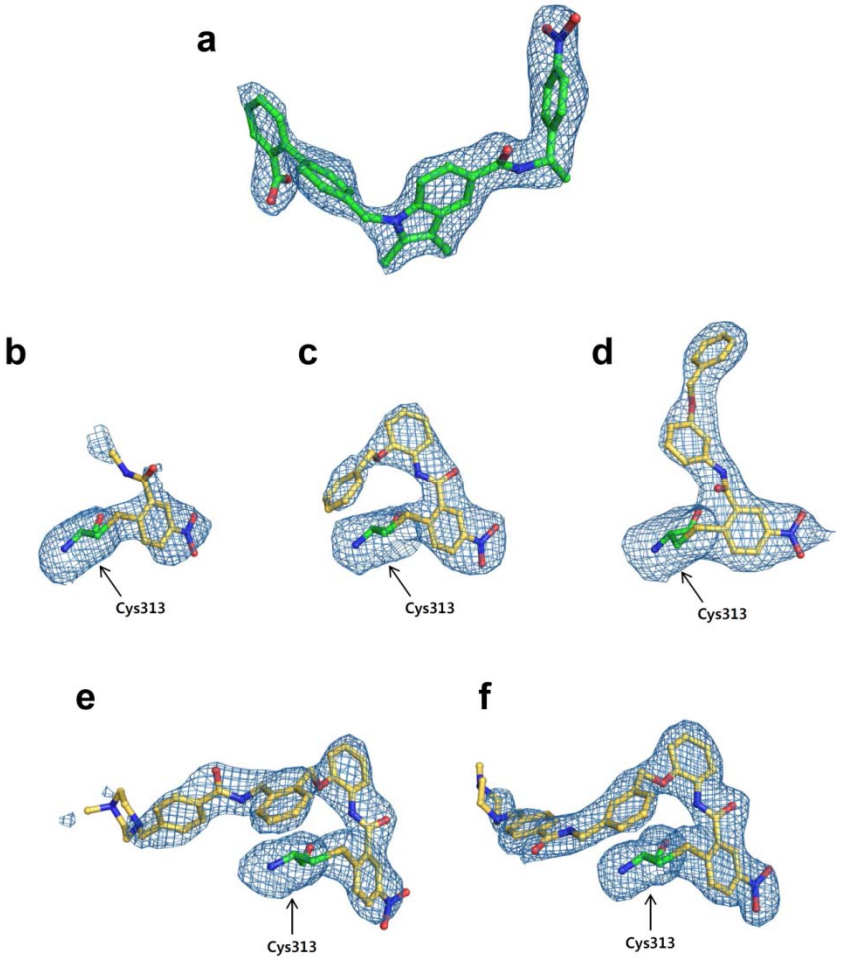


**Supplementary Figure 1. Electron density maps for compounds.** Electron density is shown from the $F_O$-$F_C$ omit maps (contoured at 2.5σ). (**a**) SR1664 (PDB: 5DWL). (**b**) SB1404 (PDB: 5DV6). (**c**) SB1405 (PDB: 5DV3). (**d**) SB1406 (PDB: 5DSH). (**e**) SB1451 (PDB: 5DV8). (**f**) SB1453 (PDB: 5DVC).

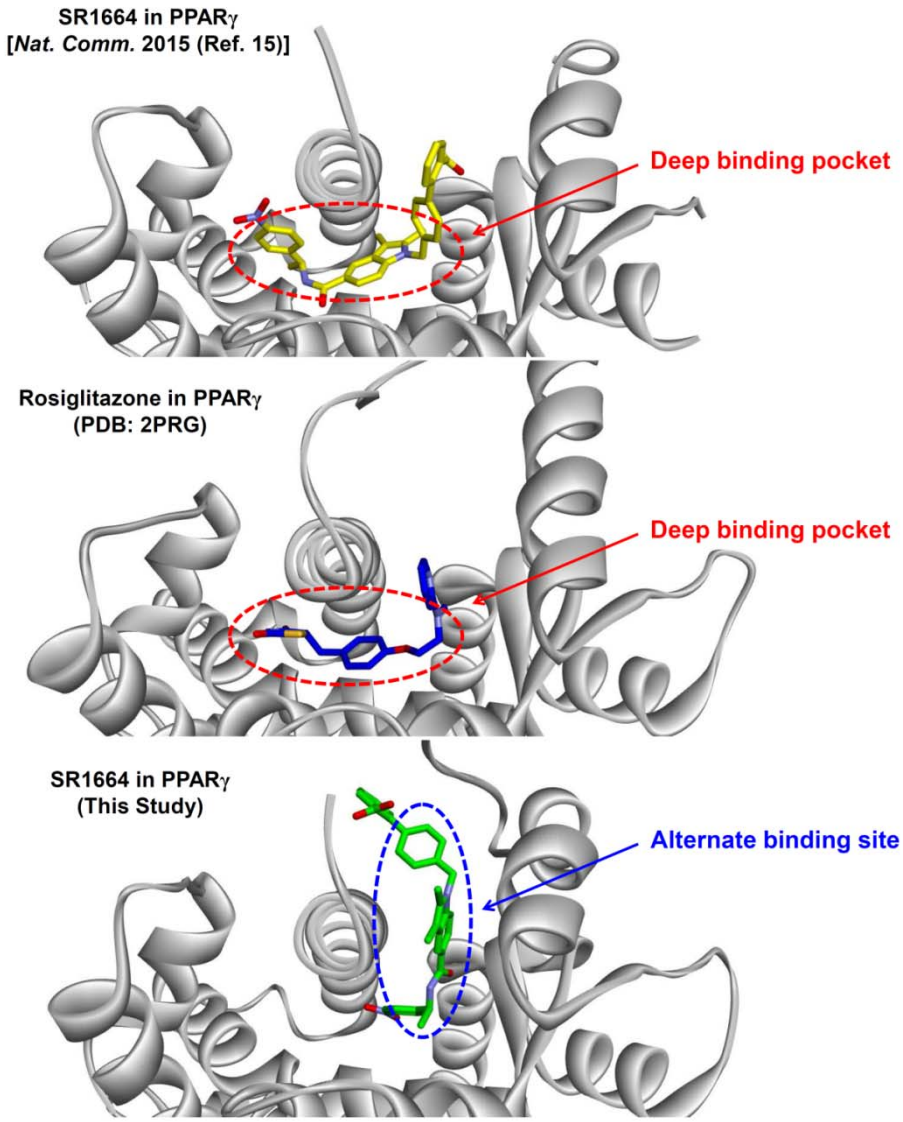


**Supplementary Figure 2. Two different observations of binding modes of SR1664 in PPARγ.** In previously reported SR1664–PPARγ LBD co-crystal structure (PDB: 4R2U), SR1664 (yellow) occupies the deep binding pocket as rosiglitazone does (blue) shown in rosiglitazone–PPARγ LBD X-ray co-crystal structure (PDB: 2PRG). However, SR1664 (green) binds to the alternate site in our SR1664–PPARγ LBD X-ray co-crystal structure.

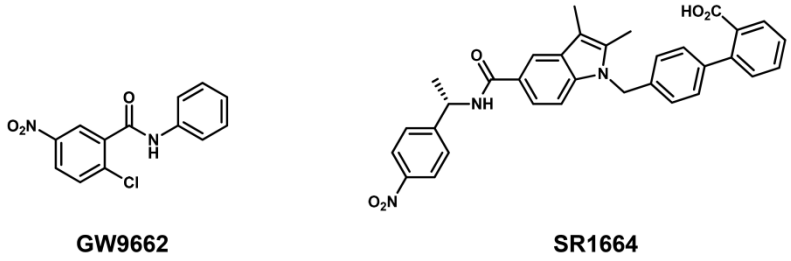


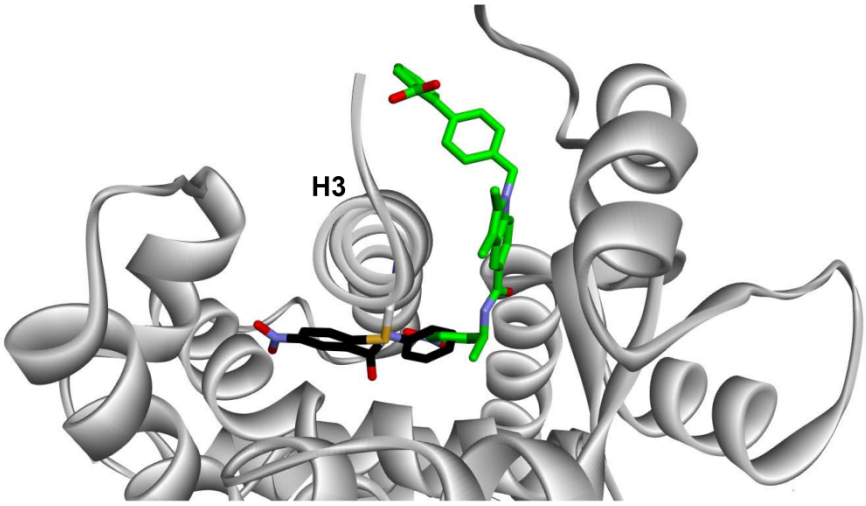


**Supplementary Figure 3. Alignment of the SR1664–PPARγ LBD and GW9662–PPARγ LBD (PDB: 3B0R) X-ray co-crystal structures.** SR1664 (green) exhibits a steric clash with phenyl group of GW9662 (black) which is covalently bound to Cys313 on H3 of PPARγ.

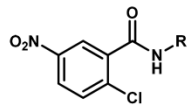


R = phenyl ▶ GW9662

R = methyl ▶ SB1404

2-chloro-5-nitrobenzamide

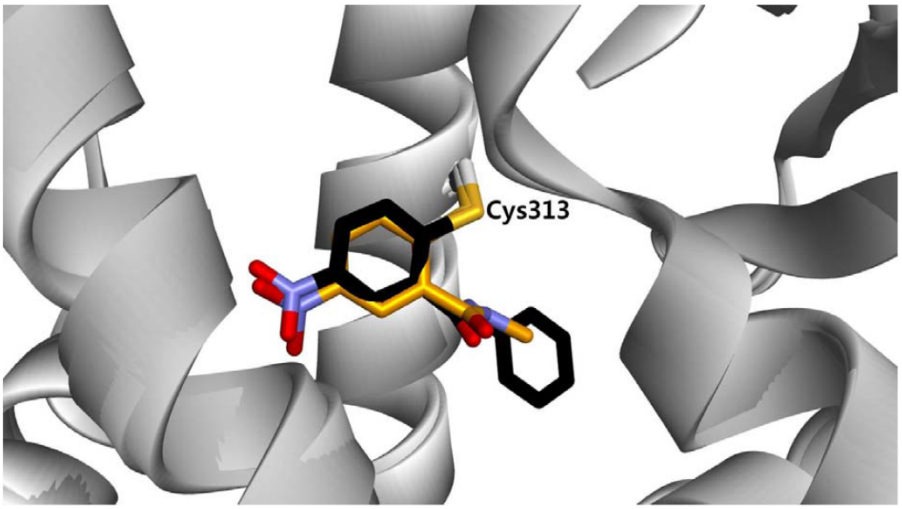


**Supplementary Figure 4. Alignment of the SB1404–PPARγ LBD and GW9662–PPARγ LBD (PDB: 3B0R) X-ray co-crystal structures.** Like GW9662 (black), SB1404 (orange) makes covalent bonding with Cys313 on H3 of PPARγ, indicating that 2-chloro-5-nitrobenzamide moiety can serve as an electrophile and covalently trap Cys313 regardless of functional groups attached to amide.

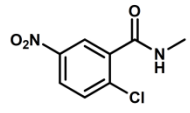


SB1404

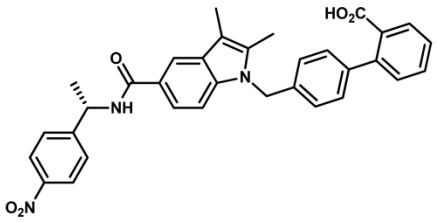


SR1664

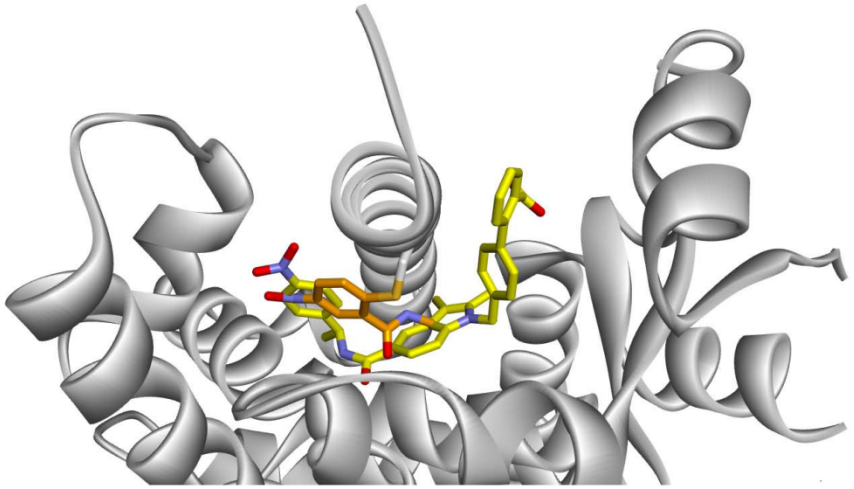

**Supplementary Figure 5. Alignment of the previously reported SR1664–PPARγ LBD (PDB: 4R2U) and SB1404–PPARγ LBD X-ray co-crystal structures.** SR1664 (yellow) overlaps with SB1404 (orange) complexed with PPARγ LBD, indicating SR1664 cannot coexist with SB1404 in the deep binding pocket of PPARγ through the previously reported binding mode [*Nat. Comm.* **2015** (Ref. 15)].

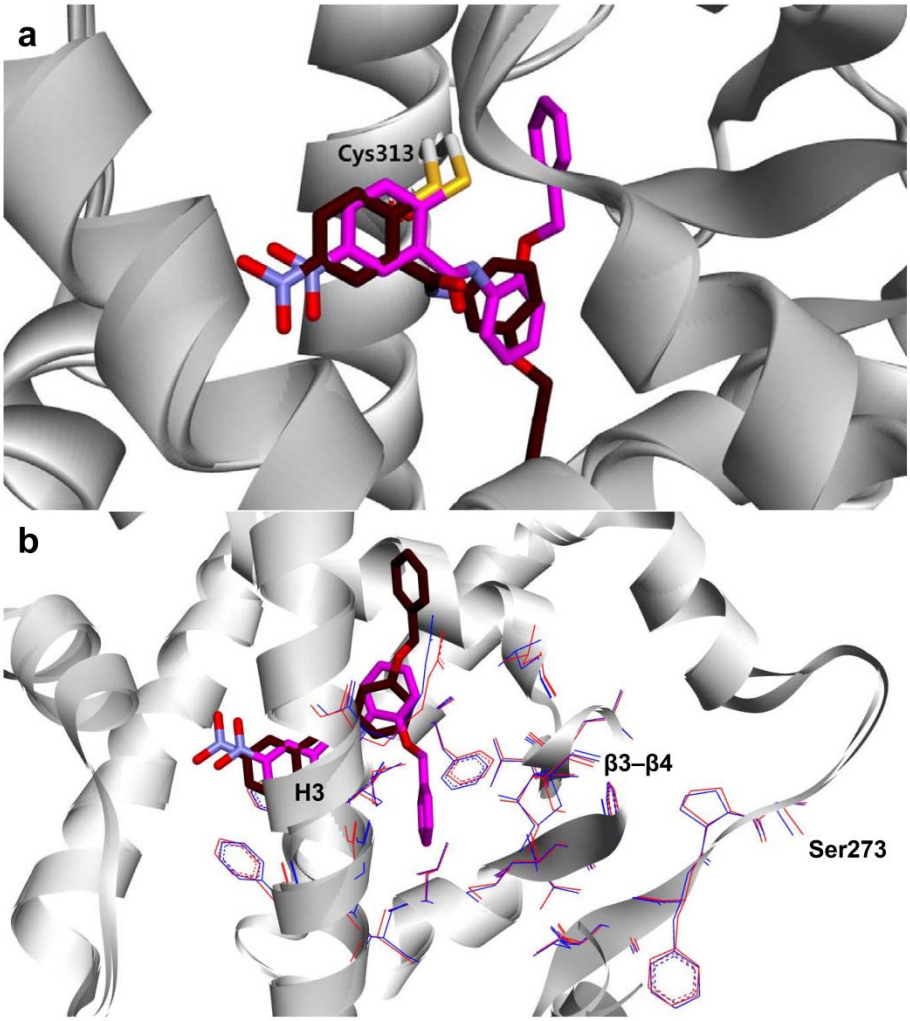


**Supplementary Figure 6. Alignment of the SB1405–PPARγ LBD and SB1406–PPARγ LBD X-ray co-crystal structures.** (**a**) Both SB1405 (pink) and SB1406 (brown) covalently bind to Cys313 on H3 of PPARγ, but they have different binding modes. (**b**) There is no significant difference between residues' positioning of SB1405–PPARγ LBD co-crystal structure (red) and that of SB1405–PPARγ LBD co-crystal structure (blue) around the specific binding site.

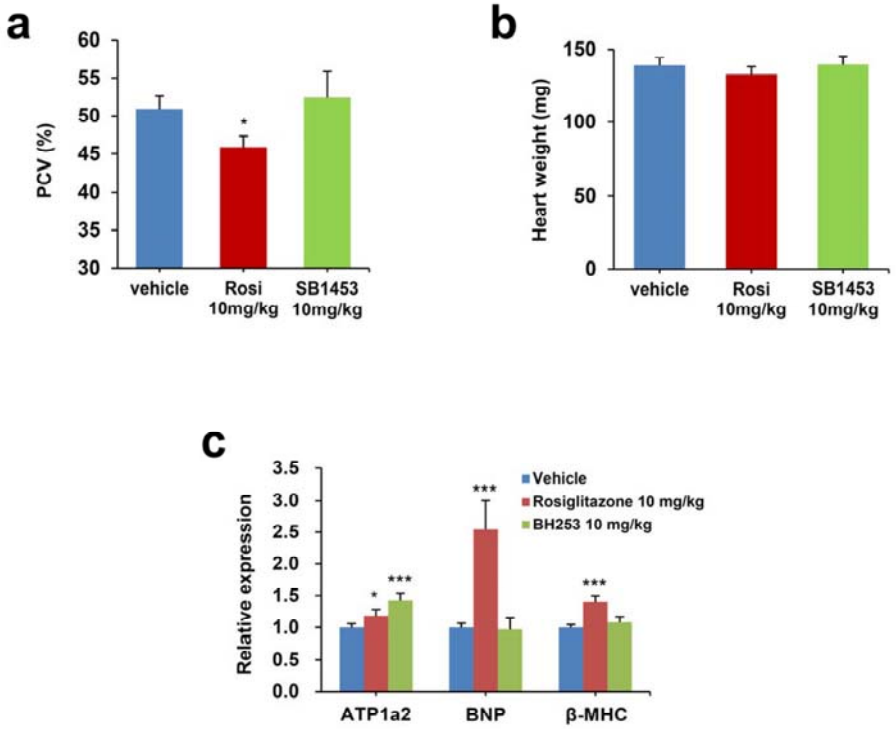


**Supplementary Figure 7. Adverse effects upon treatment with rosiglitazone or SB1453 *in vivo*.** Packed cell volume (PCV) in whole blood (**a**), heart weight (**b**), and the expression of marker genes for heart failure and cardiac hypertrophy in heart (**c**) were determined in high-fat diet-induced obese mice treated with rosiglitazone or SB1453 (14 days, 10 mg/kg/day) (*n*=*6*). All of represented error bars are S.E.M. (*n*=*6*). *p<0.05, ***p<0.001 compared with vehicle.

| Supplementary Table 1. Statistics on data collection and refinement | | | | | | |
|---|---|---|---|---|---|---|
| | **SB1404** | **SB1405** | **SB1406** | **SB1451** | **SB1453** | **SR1664** |
| ***A. Data collection*** | | | | | | |
| Beamline source[a] | PLS BL-7A | PLS BL-7A | PLS BL-7A | PLS BL-7A | PLS BL-7A | PLS BL-7A |
| Space group | $P2_12_12$ | $P2_12_12$ | $P2_12_12$ | $P2_12_12$ | $P2_12_12$ | $P2_12_12$ |
| Unit cell parameters | | | | | | |
| *a* (Å) | 53.38 | 53.95 | 53.33 | 55.27 | 54.86 | 53.08 |
| *b* (Å) | 130.85 | 130.89 | 131.33 | 131.30 | 130.28 | 130.87 |
| *c* (Å) | 53.27 | 52.59 | 52.85 | 51.97 | 52.25 | 53.06 |
| $\alpha = \beta = \gamma$ (°) | 90 | 90 | 90 | 90 | 90 | 90 |
| X-ray wavelength (Å) | 0.97934 | 0.97935 | 0.97934 | 0.97933 | 0.97935 | 0.97934 |
| Resolution range (Å) | 50.0–2.80 (2.85–2.80)[b] | 50.0–2.75 (2.80–2.75)[b] | 50.0–2.95 (3.00–2.95)[b] | 50.0–2.75 (2.80–2.75)[b] | 50.0–2.30 (2.34–2.30)[b] | 50.0–2.20 (2.24–2.20)[b] |
| Total / unique reflections | 53,885 / 9,648 | 51,736 / 10,385 | 56,026 / 8,258 | 51,628 / 10,377 | 101,485 / 17,551 | 135,258 / 19,374 |
| Completeness (%) | 98.5 (99.0)[b] | 99.5 (100.0)[b] | 99.3 (100.0)[b] | 99.7 (100.0)[b] | 99.7 (100.0)[b] | 99.2 (100.0)[b] |
| $\langle I \rangle / \langle \sigma I \rangle$ | 34.0 (4.0)[b] | 30.3 (5.0)[b] | 38.2 (4.6)[b] | 25.2 (4.0)[b] | 36.9 (5.2)[b] | 42.3 (4.3)[b] |
| $R_{merge}$[c] (%) | 6.1 (52.8)[b] | 7.6 (41.6)[b] | 6.4 (57.8)[b] | 8.9 (64.9)[b] | 7.2 (47.2)[b] | 7.2 (55.9)[b] |
| ***B. Model refinement*** | | | | | | |
| Resolution range (Å) | 30.0–2.80 | 30.0–2.75 | 30.0–2.95 | 30.0–2.75 | 30.0–2.30 | 30.0–2.20 |
| $R_{work}$ / $R_{free}$[d] (%) | 20.8 / 24.4 | 20.2 / 23.0 | 20.5 / 25.7 | 19.2 / 24.3 | 19.6 / 24.1 | 20.6 / 23.8 |
| No. of non-hydrogen atoms | | | | | | |
| Protein | 2189 | 2201 | 2154 | 2247 | 2252 | 2264 |
| Ligand | 13 | 26 | 26 | 44 | 44 | 41 |
| Water oxygen | 32 | 25 | 25 | 39 | 87 | 73 |
| Wilson *B* factor (Å$^2$) | 75.0 | 66.6 | 78.6 | 55.1 | 45.7 | 48.8 |
| Average *B* factor (Å$^2$) | | | | | | |
| Protein | 83.3 | 78.5 | 86.2 | 59.7 | 58.4 | 65.4 |
| Ligand | 98.6 | 78.3 | 84.5 | 59.4 | 60.0 | 64.9 |
| Water oxygen | 81.0 | 69.0 | 65.0 | 50.1 | 59.6 | 62.6 |
| R.m.s. deviations from ideal geometry | | | | | | |
| Bond lengths (Å) | 0.011 | 0.009 | 0.009 | 0.010 | 0.010 | 0.013 |
| Bond angles (°) | 1.48 | 1.45 | 1.47 | 1.43 | 1.50 | 1.49 |
| Ramachandran plot[e] | | | | | | |
| Favored / Outliers (%) | 97.0 / 0.0 | 97.4 / 0.0 | 97.3 / 0.0 | 97.1 / 0.0 | 98.5 / 0.0 | 98.2 / 0.0 |
| Poor rotamers (%) | 0.00 | 0.00 | 0.00 | 0.00 | 0.00 | 0.00 |

[a] PLS stands for Pohang Light Source, Korea.

[b] Values in parentheses refer to the highest resolution shell.

[c] $R_{merge} = \Sigma_h\Sigma_i \mid I(h)_i - \langle I(h) \rangle \mid / \Sigma_h\Sigma_i I(h)_i$, where $I(h)$ is the intensity of reflection $h$, $\Sigma_h$ is the sum over all reflections, and $\Sigma_i$ is the sum over i measurements of reflection $h$.

[d] $R_{work} = \Sigma \mid |F_{obs}| - |F_{calc}| \mid / \Sigma |F_{obs}|$, where $R_{free}$ is calculated for a randomly chosen 5% of reflections, which were not used for structure refinement and $R_{work}$ is calculated for the remaining reflections.

[e] Values obtained using *MolProbity*.

| Supplementary table 2. Primer sequences used for qPCR | | |
|---|---|---|
| **Gene** | **Forward primer** | **Reverse primer** |
| *aP2* | AAGGTGAAGAGCATCATAACCCT | TCACGCCTTTCATAACACATTCC |
| *Adiponectin* | TGTTCCTCTTAATCCTGCCCA | CCAACCTGCACAAGTTCCCTT |
| *Adipsin* | CATGCTCGGCCCTACATGG | CACAGAGTCGTCATCCGTCAC |
| *Cyp2f2* | GTCGGTGTTCACGGTGTACC | AAAGTTCCGCAGGATTTGGAC |
| *Rarres2* | GCCTGGCCTGCATTAAAATGG | CTTGCTTCAGAATTGGGCAGT |
| *Selenbp1* | ATGGCTACAAAATGCACAAAGTG | CCTGTGTTCCGGTAAATGCAG |
| *Car3* | TGACAGGTCTATGCTGAGGGG | CAGCGTATTTTACTCCGTCCAC |
| *Peg10* | TGCTTGCACAGAGCTACAGTC | AGTTTGGGATAGGGGCTGCT |
| *Cidec* | ATGGACTACGCCATGAAGTCT | CGGTGCTAACACGACAGGG |
| *Cd24a* | GTTGCACCGTTTCCCGGTAA | CCCCTCTGGTGGTAGCGTTA |
| *Acyl* | CAGCCAAGGCAATTTCAGAGC | CTCGACGTTTGATTAACTGGTCT |
| *Nr1d2* | TGAACGCAGGAGGTGTGATTG | GAGGACTGGAAGCTATTCTCAGA |
| *Ddx17* | TCTTCAGCCAACAATCCCAATC | GGCTCTATCGGTTTCACTACG |
| *Aplp2* | GTGGTGGAAGACCGTGACTAC | TCGGGGGAACTTTAACATCGT |
| *Nr3c1* | AGCTCCCCCTGGTAGAGAC | GGTGAAGACGCAGAAACCTTG |
| *Rybp* | CGACCAGGCCAAAAAGACAAG | CACATCGCAGATGCTGCATT |
| *Txnip* | TCTTTTGAGGTGGTCTTCAACG | GCTTTGACTCGGGTAACTTCACA |
| *Nr1d1* | TACATTGGCTCTAGTGGCTCC | CAGTAGGTGATGGTGGGAAGTA |
| *Cycs* | CCAAATCTCCACGGTCTGTTC | ATCAGGGTATCCTCTCCCCAG |
| *Ppcs* | CGCTTTCTGGACAACTTCAGT | GGGAGCGCATTCTCTTCGG |
| *Fdx1* | CAAGGGGAAAATTGGCGACTC | TTGGTCAGACAAACTTGGCAG |
| *Fgfrl1* | ATGGCCGCACAATCCACAG | TGGTGGCCTTGCACACATAAA |
| *Idh3a* | TGGGTGTCCAAGGTCTCTC | CTCCCACTGAATAGGTGCTTTG |
| *Abhd12* | GTCACCTTGGAGCATGAGC | GCAATGTAGAACCCCAGAACAC |
| *Nadk* | TCATGGGGATGAGACCTGGAG | ACAAGCACACTCTTGGGAGAC |
| *Arhgap5* | TTGGACTCTCTGGGACTGAAA | AGCACAGAAGTATGCTCTGGA |
| *Pdk4* | AGGGAGGTCGAGCTGTTCTC | GGAGTGTTCACTAAGCGGTCA |
| *Las1l* | GGAGGTGAACATTCCAGACTG | CTCATCCAACTCCCAGGTTTC |
| *Cib2* | GACAACTACCAGGACTGCACT | CCATCCTCGGAGAAAGCCTC |
| *Fmr1* | CAATGGCGCTTTCTACAAGGC | TCTGGTTGCCAGTTGTTTTCA |
| *Pim3* | AAGGACACGGTCTACACTGAC | GACACCACTCAATAAGCTGCT |
| *Phospho1* | CTCACCTTCGACTTCGATGAGA | CCCAGGTACTTAAAGACTCGTTG |
| *Plin2* | GACCTTGTGTCCTCCGCTTAT | CAACCGCAATTTGTGGCTC |
| *Lass4* | TACCCACATCAGACCCTGAAT | TCATGGGGATGAGACCTGGAG |

## 6.2. Supplementary Note

The section below describes the synthesis of compounds which are used in this study.

**General information**

All chemicals and solvents were purchased from commercial venders and used without further purification unless noted otherwise. Analytical thin layer chromatography (TLC) was performed on pre-coated glass-backed plates (silica gel 60; $F_{254}$ 0.25 mm) with visualization by ultraviolet (UV) irradiation at 254 nm and/or staining with ninhydrin solution. The products were purified by flash column chromatography on silica gel (230–400 mesh). $^{1}H$ and $^{13}C$ NMR spectra were recorded on Bruker DRX-300 [Bruker Biospin, Germany], Agilent 400-MR DD2 [Agilent, USA] or Varian Inova-500 [Varian Assoc., Palo Alto, USA]. $^{1}H$ chemical shifts are reported in ppm from tetramethylsilane (TMS) as internal standard. Multiplicity was indicated as follows: s (singlet), d (doublet), t (triplet), q (quartet), p (pentet), m (multiplet), dd (doublet of doublet), dt (doublet of triplet), td (triplet of doublet), brs (broad singlet), etc. Coupling constants are reported in Hertz (Hz). $^{13}C$ chemical shifts are reported in ppm relative to chloroform-*d* (δ 77.16, triplet) or DMSO-$d_6$ (δ 39.52, septet). Mass spectrometric analysis was performed with Finnigan Surveyor MSQ Plus LC/MS [Thermo Electron Corp., USA] or LCMS-2020 [Shimadzu Corp., JAPAN] using electrospray ionization (ESI).

**General procedure for synthesis of compounds 1–4 and 6**

To a solution of 2-chloro-5-nitrobenzoyl chloride (500 mg, 2.3 mmol) and amine (1.5 equiv.) in dichloromethane (20 mL), triethylamine (2.5 equiv.) was added and the mixture was stirred at room temperature for 1 h. After removal of solvent and triethylamine under the reduced pressure, the residue was dissolved with 1N HCl and dichloromethane. The organic layer was separated and the aqueous layer was extracted two times with dichloromethane. The combined organic layer was dried over anhydrous $Na_2SO_4$(s) and filtered through a celite-packed glass filter. The filtrate was concentrated under the reduced pressure and purified by silica-gel flash column chromatography (1:5~1:2 = ethyl acetate:*n*-hexane, v/v) to obtain the desired product.

**Compound 1 (SB1404)**, 2-chloro-*N*-methyl-5-nitrobenzamide

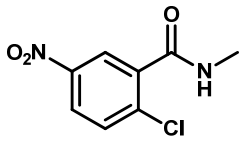

Yield: 68% as white solid; $^1$H NMR (400 MHz, $CDCl_3$) δ 8.51 (d, *J* = 2.8 Hz, 1H), 8.21 (dd, *J* = 8.4, 2.8 Hz, 1H), 7.60 (d, *J* = 8.8 Hz, 1H), 6.23 (brs, 1H), 3.07 (d, *J* = 4.8 Hz, 1H); $^{13}$C NMR (100 MHz, $CDCl_3$) δ 165.0, 146.7, 137.7, 136.6, 131.6, 125.8, 125.4, 27.2; LRMS (ESI) *m/z* calcd for $C_8H_8ClN_2O_3$ $[M+H]^+$: 215.02; Found: 215.06.

**Compound 2 (SB1405)**, *N*-(2-(benzyloxy)phenyl)-2-chloro-5-nitrobenzamide

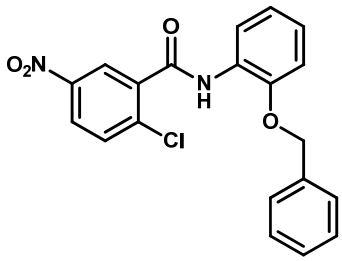

Yield: 98% as light yellow solid; $^1$H NMR (400 MHz, $CDCl_3$) δ 8.78 (brs, 1H), 8.64 (d, *J* = 2.8 Hz, 1H), 8.48 (dd, *J* = 7.6, 1.2 Hz, 1H), 8.16 (dd, *J* = 8.8, 2.4 Hz, 1H), 7.48 (d, *J* = 8.8 Hz, 1H), 7.41–7.34 (m, 5H), 7.10 (d, *J* = 7.6, 1.6 Hz, 1H),

7.05–7.00 (m, 2H), 5.11 (s, 2H); $^{13}$C NMR (100 MHz, $CDCl_3$) δ 161.5, 147.8, 146.7, 137.5, 136.2, 136.0, 131.7, 128.8, 128.6, 128.0, 127.3, 126.1, 125.9, 125.0, 121.6, 120.6, 111.8, 71.2; LRMS (ESI) *m/z* calcd for $C_{20}H_{16}ClN_2O_4$ $[M+H]^+$: 383.08; Found: 382.91.

**Compound 3 (SB1406)**, *N*-(3-(benzyloxy)phenyl)-2-chloro-5-nitrobenzamide

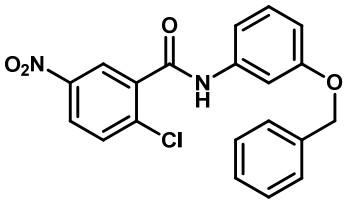


Yield: 98% as white solid; $^1$H NMR (400 MHz, $CDCl_3$) δ 8.58 (d, *J* = 2.4 Hz, 1H), 8.23 (dd, J = 8.8, 2.4 Hz, 1H), 7.84 (s, 1H), 7.64 (d, J = 8.8 Hz, 1H), 7.45–7.24 (m, 7H), 7.09 (d, J = 8.4 Hz, 1H), 6.81 (dd, J = 8.4, 2.0 Hz, 1H), 5.07 (s, 2H); $^{13}$C NMR (100 MHz, $CDCl_3$) δ 162.4, 159.5, 146.7, 138.2, 137.7, 136.8, 136.6, 131.7, 130.1, 128.7, 128.2, 127.7, 126.1, 125.3, 112.8, 112.2, 107.2 70.2; LRMS (ESI) *m/z* calcd for $C_{20}H_{16}ClN_2O_4$ $[M+H]^+$: 383.08; Found: 382.87.

**Compound 4**, 2-chloro-5-nitro-*N*-(2-phenoxyphenyl)benzamide

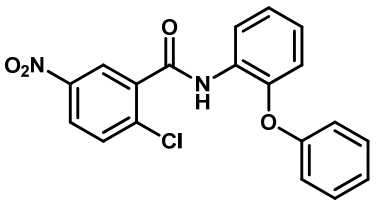


Yield: 94% as off-white solid; $^1$H NMR (500 MHz, $CDCl_3$) δ 8.63 (s, 1H), 8.60 (d, *J* = 2.5 Hz, 1H), 8.58 (dd, *J* = 7.5, 1.5 Hz, 1H), 8.23 (dd, *J* = 7.5, 2.5 Hz, 1H), 7.60 (d, *J* = 8.5 Hz, 1H), 7.38–7.35 (m, 2H), 7.21–7.10 (m, 3H), 7.02 (d, *J* = 9.0 Hz, 2H), 6.92 (dd, *J* = 8.0, 1.5 Hz, 1H); $^{13}$C NMR (100 MHz, $CDCl_3$) δ 161.9, 156.4, 146.8, 146.2, 137.5, 136.4, 131.7, 130.1, 129.1, 126.0, 125.8, 125.3, 124.3, 124.2, 121.4, 118.6, 118.1; LRMS (ESI) *m/z* calcd for $C_{19}H_{14}ClN_2O_4$ $[M+H]^+$: 369.06; Found: 369.05.

**Compound 6**, 2-chloro-*N*-(2-ethoxyphenyl)-5-nitrobenzamide

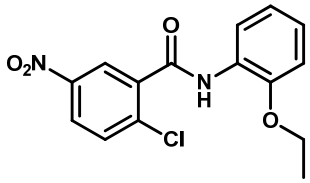

Yield: 95% as off-white solid; $^{1}$H NMR (400 MHz, $CDCl_3$) δ 8.77 (brs, 1H), 8.72 (d, *J* = 2.8 Hz, 1H), 8.50 (dd, *J* = 8.0, 1.2 Hz, 1H), 8.25 (dd, *J* = 8.8, 2.8 Hz, 1H), 7.66 (d, *J* = 8.8 Hz, 1H), 7.13 (td, *J* = 8.0, 1.2 Hz, 1H), 7.02 (t, *J* = 8.0 Hz, 1H), 6.92 (d, *J* = 8.0 Hz, 1H), 4.14 (q, *J* = 6.8 Hz, 2H), 1.45 (t, *J* = 6.8 Hz, 3H); $^{13}$C NMR (100 MHz, $CDCl_3$) δ 161.5, 147.7, 146.9, 137.5, 136.5, 131.9, 127.1, 126.2, 126.0, 125.0, 121.2, 120.3, 111.1, 64.4, 15.0; LRMS (ESI) *m/z* calcd for $C_{15}H_{14}ClN_2O_4$ $[M+H]^+$: 321.06; Found: 321.15.

**General procedure for synthesis of compounds 5 and 7**

*N*-Boc-2-aminophenol (100 mg, 0.48 mmol), alkyl bromide (2.0 equiv.), and $K_2CO_3$ (1.5 equiv.) were dissolved in anhydrous DMF (15 mL) under argon atmosphere. The reaction mixture was stirred at 80 °C for 12 h, and the crude mixture was diluted with deionized water. The aqueous layer was extracted three times with ethyl acetate. The combined organic layer was dried over anhydrous $Na_2SO_4$(s) and filtered through a celite-packed glass filter. The filtrate was concentrated under the reduced pressure and purified by silica-gel flash column chromatography (1:10 = ethyl acetate:*n*-hexane, v/v) to obtain *N*-Boc-2-substituted aniline. After Boc-deprotection with 10% trifluoroacetic acid in dichloromethane (10 mL) at room temperature for 1 h, the reaction mixture was washed with saturated aqueous $NaHCO_3$ three times, and concentrated

under the reduced pressure to provide 2-substituted aniline. To a solution of 2-substituted aniline in dichloromethane (10 mL), 2-chloro-5-nitrobenzoyl chloride (1.5 equiv.) and triethylamine (2.0 equiv.) were added and the mixture was stirred at room temperature for 1 h. After removal of solvent and triethylamine under the reduced pressure, the residue was purified by silica-gel flash column chromatography (1:5 = ethyl acetate:*n*-hexane, v/v) to obtain the desired product.

**Compound 5**, 2-chloro-5-nitro-*N*-(2-phenethoxyphenyl)benzamide

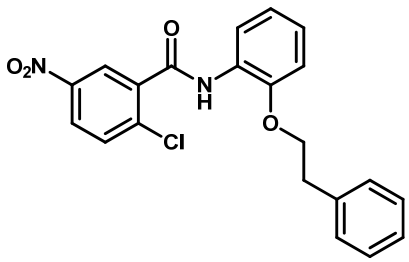


Yield: 63% as light yellow solid; $^{1}$H NMR (300 MHz, $CDCl_3$) δ 8.54 (d, *J* = 5.7 Hz, 1H), 8.46 (dd, *J* = 8.1, 1.8 Hz, 1H), 8.36 (s, 1H), 8.26 (dd, *J* = 8.7, 2.7 Hz, 1H), 7.64 (d, *J* = 8.7 Hz, 1H), 7.16–7.08 (m, 6H), 7.04 (td, *J* = 7.8, 1.5 Hz, 1H), 6.95 (dd, *J* = 7.8, 1.5 Hz, 1H), 4.30 (t, *J* = 6.6 Hz, 2H), 3.10 (t, *J* = 6.6 Hz, 2H); $^{13}$C NMR (75 MHz, $CDCl_3$) δ 161.7, 147.4, 146.8, 137.8, 137.7, 136.9 131.7, 128.8, 128.6, 127.3, 126.7, 125.9, 125.5, 125.0, 121.6, 120.4, 111.6, 69.1, 35.6; LRMS (ESI) *m/z* calcd for $C_{21}H_{18}ClN_2O_4$ $[M+H]^+$: 397.10; Found: 397.15.

**Compound 7**, 2-chloro-*N*-(2-(hexyloxy)phenyl)-5-nitrobenzamide

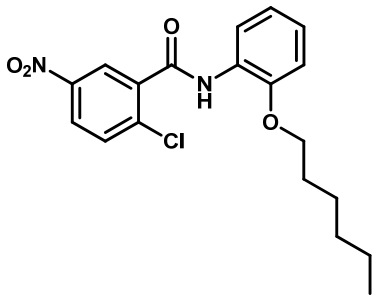

Yield: 50% as white solid; $^{1}$H NMR (400 MHz, $CDCl_3$) δ 8.76 (brs, 1H), 8.72 (d, *J* = 2.8 Hz, 1H), 8.50 (dd, *J* = 8.0, 1.2 Hz, 1H), 8.25 (dd, *J* = 8.8, 2.8 Hz, 1H), 7.66 (d, *J* = 8.8 Hz, 1H), 7.13 (t, *J* = 8.0, 1H), 7.02 (t, *J* = 8.0 Hz, 1H), 6.92 (d, *J* = 8.0 Hz, 1H), 4.06 (t, *J* = 6.8 Hz, 2H), 1.81 (m, 2H), 1.45 (m, 2H), 1.32 (m, 4H), 0.87 (t, *J* = 6.8 Hz, 3H); $^{13}$C NMR (100 MHz, $CDCl_3$) δ 161.5, 147.9, 146.9, 137.5, 136.5, 131.8, 127.1, 126.2, 126.0, 125.0, 121.2, 120.3, 111.1, 68.9, 31.6, 29.3, 25.9, 22.7, 14.1; LRMS (ESI) *m/z* calcd for $C_{19}H_{22}ClN_2O_4$ $[M+H]^+$: 377.13; Found: 377.20.

**Synthesis of compound 8**, 2-chloro-*N*-(2-(2-(4-methylpiperazin-1-yl)ethoxy) phenyl)-5-nitrobenzamide

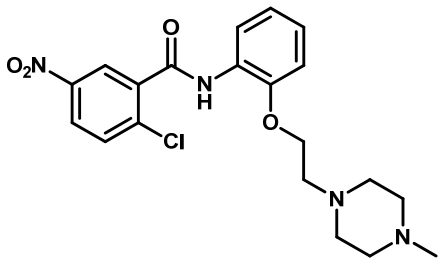

*N*-Boc-2-aminophenol (290 mg, 1.4 mmol), 4-methylpiperazine-1-ethanol (200 mg, 1.4 mmol), triphenylphosphine (550 mg, 2.1 mmol) were dissolved in anhydrous THF (20 mL) under argon atmosphere and diethyl azodicarboxylate (360 mg, 2.1 mmol) was added slowly. The reaction mixture was stirred at room temperature for 12 h, and concentrated under the reduced pressure. The residue was purified by silica-gel flash column chromatography (1:20 = methanol:dichloromethane, v/v) to obtain tert-butyl (2-(2-(4-methylpiperazin-1-yl)ethoxy)phenyl)carbamate. After Boc-deprotection with 10% trifluoroacetic acid in dichloromethane (10

mL) at room temperature for 1 h, the reaction mixture was washed with saturated aqueous $NaHCO_3$ three times, and concentrated under the reduced pressure to provide 2-(2-(4-methylpiperazin-1-yl)ethoxy)aniline. To a solution of 2-(2-(4-methylpiperazin-1-yl)ethoxy)aniline in dichloromethane (10 mL), 2-chloro-5-nitrobenzoyl chloride (460 mg, 2.1 mmol) and triethylamine (0.39 mL, 2.8 mmol) were added and the mixture was stirred at room temperature for 1 h. After removal of solvent and triethylamine under the reduced pressure, the residue was purified by silica-gel flash column chromatography (1:10 = MeOH:$CH_2Cl_2$, v/v) to obtain **8** (260 mg). Yield: 45% as light yellow solid; $^1$H NMR (400 MHz, $CDCl_3$) δ 9.31 (brs, 1H), 8.64 (d, *J* = 2.8 Hz, 1H), 8.45 (td, *J* = 8.0, 1.6 Hz, 1H), 8.26 (td, *J* = 8.4, 2.8 Hz, 1H), 7.66 (d, *J* = 8.4 Hz, 1H), 7.13 (dd, *J* = 8.0, 1.6 Hz, 1H), 7.08 (dd, *J* = 8.0, 1.2 Hz, 1H), 6.98 (dd, *J* = 8.0, 1.2 Hz, 1H), 4.19 (t, *J* = 5.6 Hz, 2H), 2.72 (t, J = 5.6 Hz, 2H), 2.50–2.43 (m, 8H), 2.16 (s, 3H); $^{13}$C NMR (100 MHz, $CDCl_3$) δ 161.9, 147.9, 146.5, 137.8, 137.0, 131.5, 128.0, 125.7, 125.5, 125.1, 121.9, 121.0, 113.2, 66.7, 57.0, 54.6, 53.1, 45.8; LRMS (ESI) *m/z* calcd for $C_{20}H_{24}ClN_4O_4$ $[M+H]^+$: 419.15; Found: 419.06.

**Procedure for synthesis of compound 9 (SB1451)**

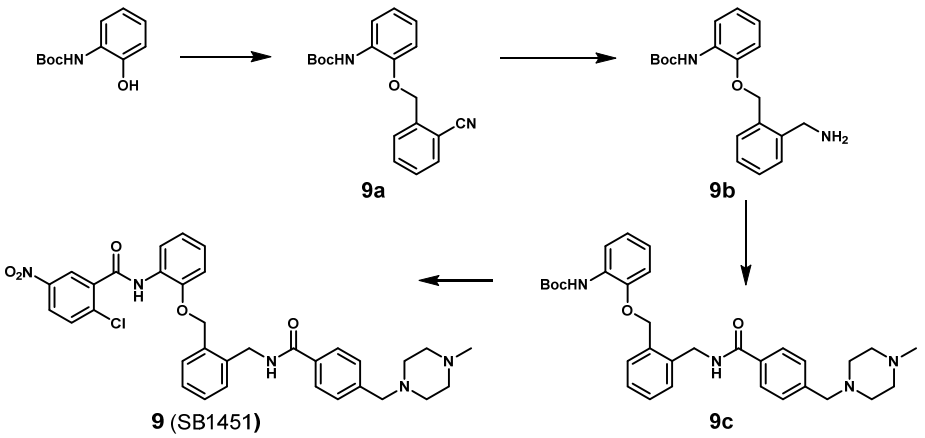


**Synthesis of 9a,** *tert*-butyl (2-((2-cyanobenzyl)oxy)phenyl)carbamate

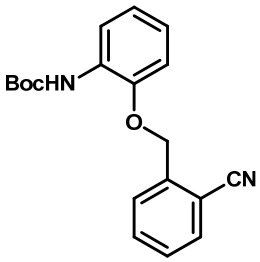


*N*-Boc-2-aminophenol (800 mg, 3.8 mmol), 2-(bromomethyl) benzonitrile (1.5 g, 7.6 mmol) and $K_2CO_3$ (790 mg, 5.7 mmol) were dissolved in anhydrous DMF (30 mL) under argon atmosphere. The reaction mixture was stirred at 80 °C for 12 h, and the crude mixture was diluted with deionized water. The aqueous layer was extracted three times with ethyl acetate. The combined organic layer was dried over anhydrous $Na_2SO_4$(s) and filtered through a celite-packed glass filter. The filtrate was concentrated under the reduced pressure and purified by silica-gel flash column chromatography (1:5 = ethyl acetate:*n*-hexane, v/v) to obtain **9a** (1.23 g). Yield: 99% as off-white solid; $^1$H NMR (400 MHz, $CDCl_3$) δ 8.09 (d, *J* = 6.8 Hz, 1H), 7.73 (d, *J* = 8.0 Hz, 1H), 7.64 (t, *J* = 7.6 Hz, 1H), 7.59 (d, *J*

=7.2 Hz, 1H), 7.46 (t, $J$ = 7.2 Hz, 1H), 7.09 (s, 1H), 7.00–6.92 (m, 2H), 6.89 (d, $J$ = 8.0 Hz, 1H), 5.33 (s, 2H), 1.53 (s, 9H); $^{13}$C NMR (100 MHz, $CDCl_3$) δ 152.9, 146.2, 140.2, 133.30, 133.25, 128.9, 128.7, 128.6, 122.4, 122.3, 119.0, 117.2, 111.9, 111.5, 80.6, 68.4, 28.5; LRMS (ESI) *m/z* calcd for $C_{19}H_{21}N_2O_3$ $[M+H]^+$: 325.16; Found: 325.25.

**Synthesis of 9b,** *tert*-butyl (2-((2-(aminomethyl)benzyl)oxy)phenyl)carbamate

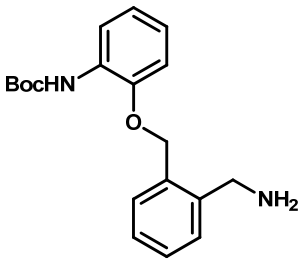


To a solution of **9a** (600 mg, 1.85 mmol) in anhydrous THF (15 mL) under argon atmosphere, $LiAlH_4$ (1.0 M in THF, 3.7ml) was added dropwise at 0 °C, and the mixture was warmed to room temperature. After 3 h, the reaction mixture was cooled to 0 °C and quenched with deionized water (3 mL). The crude mixture was worked up with ethyl acetate and saturated aqueous sodium potassium tartrate, and the organic layer was washed by brine. The combined organic layer was dried over anhydrous $Na_2SO_4$(s) and filtered through a celite-packed glass filter. The filtrate was concentrated under the reduced pressure and purified by silica-gel flash column chromatography (1:10 = MeOH:$CH_2Cl_2$, v/v) to obtain **9b** (360 mg). Yield: 59% as yellow oil; $^1$H NMR (500 MHz, $CDCl_3$) δ 8.13 (s, 1H), 7.85 (s, 1H), 7.44–7.38 (m, 3H), 7.31 (t, $J$ = 7.0 Hz, 1H), 7.02-6.96 (m, 3H), 5.15 (s, 2H), 3.96 (s, 2H), 1.77 (brs, 2H), 1.52 (s, 9H); $^{13}$C NMR (100 MHz, $CDCl_3$) δ 153.1, 147.1, 140.4, 134.4, 129.9, 129.24, 129.20, 129.0, 127.7, 122.5, 121.9, 118.9, 112.5, 80.2, 69.6, 43.4, 28.5; LRMS (ESI) *m/z* calcd for $C_{19}H_{25}N_2O_3$ $[M+H]^+$: 329.19; Found:329.25.

**Synthesis of 9c,** *tert*-butyl (2-((2-((4-((4-methylpiperazin-1-yl)methyl) benzamido)methyl)benzyl)oxy)phenyl)carbamate

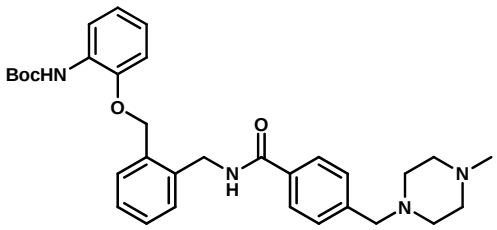


To a solution of **9b** (140 mg, 0.43 mmol) in dichloromethane (10 mL), 4-((4-methyl-1-piperazinyl)methyl)benzoic acid dihydrochloride (160 mg, 0.52 mmol), 1-ethyl-3-(3-dimethyl aminopropyl)carbodiimide hydrochloride (100 mg, 0.52 mmol), triethylamine (0.24 mL, 1.7 mmol), and 4-dimethylaminopyridine (5.3 mg, 0.043 mmol) were added, and the mixture was stirred at room temperature for 12 h. The crude mixture was worked up with dichloromethane and saturated aqueous $NaHCO_3$, and the organic layer was washed by brine. The combined organic layer was dried over anhydrous $Na_2SO_4$(s) and filtered through a celite-packed glass filter. The filtrate was concentrated under the reduced pressure and purified by silica-gel flash column chromatography (1:5 = MeOH:$CH_2Cl_2$, v/v) to obtain **9c** (170 mg). Yield: 74% as yellow oil; $^1$H NMR (400 MHz, $CDCl_3$) δ 8.04 (s, 1H), 7.63 (d, J = 8.4 Hz, 2H), 7.46–7.34 (m, 4H), 7.33 (d, J = 9.2 Hz, 2H), 6.99 (s, 1H), 6.97–6.90 (m, 3H), 6.61 (t, J = 4.8 Hz, 1H), 5.18 (s, 2H), 4.73 (d, J = 5.6 Hz, 2H), 3.49 (s, 2H), 2,34 (brs, 8H), 2.29 (s, 3H), 1.47 (s, 9H); $^{13}$C NMR (100 MHz, $CDCl_3$) δ 167.0, 152.8, 146.7, 142.4, 137.0, 134.7, 132.9, 130.0, 129.7, 120.24, 129.22, 128.5, 128.3, 127.0, 122.6, 122.0, 118.7, 112.3, 80.6, 69.3, 62.5, 55.1, 53.0, 46.0, 41.6, 28.4; LRMS (ESI) *m/z* calcd for $C_{32}H_{41}N_4O_4$ $[M+H]^+$: 545.31; Found:545.35.

**Synthesis of 9 (SB1451),** 2-chloro-*N*-(2-((2-((4-((4-methylpiperazin-1-yl)methyl)benzamido)methyl)benzyl)oxy)phenyl)-5-nitrobenzamide

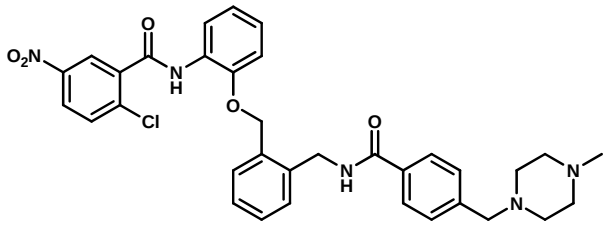

After **9c** (110 mg, 0.20 mmol) was treated with 10% trifluoroacetic acid in dichloromethane (10 mL) at room temperature for 1 h, the reaction mixture was washed with saturated aqueous $NaHCO_3$ three times, and concentrated under the reduced pressure to provide *N*-(2-((2-aminophenoxy)methyl)benzyl)-4-((4-methylpiperazin-1-yl)methyl)benzamide. To a solution of *N*-(2-((2-aminophenoxy)methyl)benzyl)-4-((4-methylpiperazin-1-yl)methyl)benzamide in dichloromethane (10 mL), 2-chloro-5-nitrobenzoyl chloride (66 mg, 0.30 mmol) and triethylamine (56 μL, 0.40 mmol) were added and the mixture was stirred at room temperature for 1 h. After removal of solvent and triethylamine under the reduced pressure, the residue was purified by silica-gel flash column chromatography (1:5 = MeOH:$CH_2Cl_2$, v/v) to obtain **9** (85 mg). Yield : 68% as light yellow solid; $^1$H NMR (400 MHz, DMSO-$d_6$) δ 10.09 (s, 1H), 8.99 (t, *J* = 6.0 Hz, 1H), 8.38 (d, *J* = 2.8 Hz, 1H), 8.26 (dd, *J* = 8.8, 2.8 Hz, 1H), 7.87 (dd, *J* = 7.6, 1.2 Hz, 1H), 7.80 (d, *J* = 9.2, 1H), 7.75 (d, *J* = 7.6, 2H), 7.55 (d, *J* = 7.6, 1H), 7.39–7.20 (m, 7H), 7.01 (t, *J* = 7.6 Hz, 1H), 5.34 (s, 2H), 4.59 (d, *J* = 5.6 Hz, 2H), 3.84 (s, 2H), 2.34 (brs, 8H), 2.15 (s, 3H); $^{13}$C NMR (100 MHz, DMSO-$d_6$) δ 166.1, 163.1, 150.5, 146.0, 141.8, 137.9, 137.7, 137.2, 134.2, 132.8, 131.3, 128.5, 128.2, 128.1, 127.1, 126.8, 126.29, 126.26, 125.5, 124.7, 124.0, 120.5, 113.1, 67.9, 61.6, 54.7, 52.5, 45.7; LRMS (ESI) *m/z* calcd for $C_{34}H_{35}ClN_5O_5$ $[M+H]^+$: 628.23; Found: 628.30.

**Procedure for synthesis of compound 10 (SB1453)**

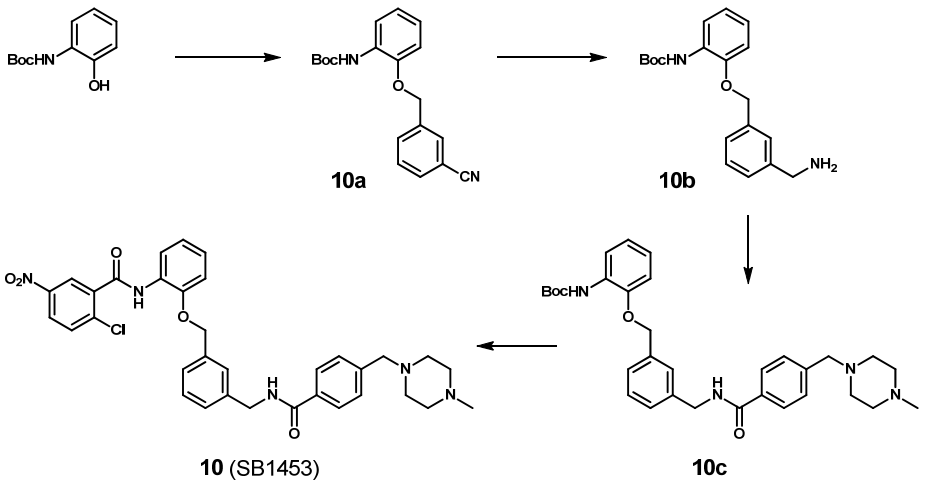


**Synthesis of 10a**, *tert*-butyl (2-((3-cyanobenzyl)oxy)phenyl)carbamate

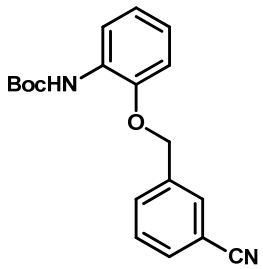


*N*-Boc-2-aminophenol (800 mg, 3.8 mmol), 3-(bromomethyl) benzonitrile (1.5 g, 7.6 mmol) and $K_2CO_3$ (790 mg, 5.7 mmol) were dissolved in anhydrous DMF (30 mL) under argon atmosphere. The reaction mixture was stirred at 80 °C for 12 h, and the crude mixture was diluted with deionized water. The aqueous layer was extracted three times with ethyl acetate. The combined organic layer was dried over anhydrous $Na_2SO_4$(s) and filtered through a celite-packed glass filter. The filtrate was concentrated under the reduced pressure and purified by silica-gel flash column chromatography (1:5 = ethyl acetate:*n*-hexane, v/v) to obtain **10a** (1.20 g). Yield: 97% as yellow oil; $^1$H NMR (400 MHz, $CDCl_3$) δ 8.10 (d, $J$ = 7.2 Hz, 1H), 7.71 (s, 1H), 7.64 (d, $J$ =8.0 Hz, 1H), 7.52 (t, $J$ = 8.0 Hz, 1H), 7.02

(s, 1H), 7.00–6.91 (m, 2H), 6.83 (dd, $J$ = 7.6, 1.2 Hz, 1H), 5.14 (s, 2H), 1.53 (s, 9H); $^{13}$C NMR (100 MHz, $CDCl_3$) δ 152.8, 146.3, 138.3, 132.0, 131.7, 130.9, 129.7, 128.5, 122.5, 122.1, 118.9, 118.6, 113.1, 111.7, 80.7, 69.6, 28.5; LRMS (ESI) *m/z* calcd for $C_{19}H_{21}N_2O_3$ $[M+H]^+$: 325.16; Found:325.20.

**Synthesis of 10b,** *tert*-butyl (2-((3-(aminomethyl)benzyl)oxy)phenyl) carbamate

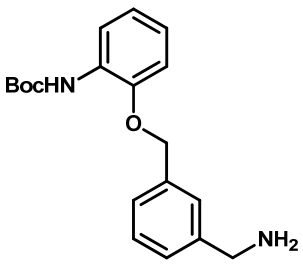


To a solution of **10a** (600 mg, 1.85 mmol) in anhydrous THF (15 mL) under argon atmosphere, $LiAlH_4$ (1.0 M in THF, 3.7 mL) was added dropwise at 0 °C, and the mixture was warmed to room temperature. After 3 h, the reaction mixture was cooled to 0 °C and quenched with deionized water (3 mL). The crude mixture was worked up with ethyl acetate and saturated aqueous sodium potassium tartrate, and the organic layer was washed by brine. The combined organic layer was dried over anhydrous $Na_2SO_4$(s) and filtered through a celite-packed glass filter. The filtrate was concentrated under the reduced pressure and purified by silica-gel flash column chromatography (1:10 = MeOH:$CH_2Cl_2$, v/v) to obtain **10b** (440 mg). Yield: 72% as off-white solid; $^1$H NMR (400 MHz, $CDCl_3$) δ 8.07 (brs, 1H), 7.40 (s, 1H), 7.38–7.29 (m, 3H), 7.12 (s, 1H), 6.97–6.87 (m, 3H), 5.08 (s, 2H), 3.91 (s, 2H), 2.81 (brs, 2H), 1.51 (s, 9H); $^{13}$C NMR (100 MHz, $CDCl_3$) δ 152.9, 146.8, 137.1, 129.1, 128.4, 127.4, 126.6, 126.4, 122.5, 121.6, 118.6, 111.8, 80.5, 70.8, 45.9, 28.5; LRMS (ESI) *m/z* calcd for $C_{19}H_{25}N_2O_3$ $[M+H]^+$: 329.19; Found: 329.22.

**Synthesis of 10c**, *tert*-butyl (2-((3-((4-((4-methylpiperazin-1-yl)methyl) benzamido)methyl)benzyl)oxy)phenyl)carbamate

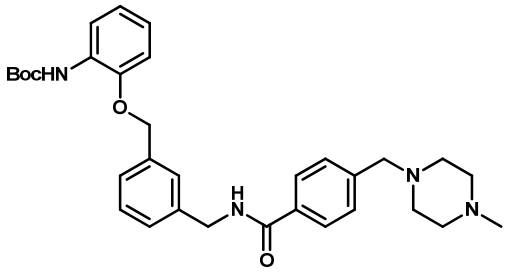


To a solution of **10b** (140 mg, 0.43 mmol) in dichloromethane (10 mL), 4-((4-methyl-1-piperazinyl)methyl)benzoic acid dihydrochloride (160 mg, 0.52 mmol), 1-ethyl-3-(3-dimethyl aminopropyl)carbodiimide hydrochloride (100 mg, 0.52 mmol), triethylamine (0.24 mL, 1.7 mmol), and 4-dimethylaminopyridine (5.3 mg, 0.043 mmol) were added, and the mixture was stirred at room temperature for 12 h. The crude mixture was worked up with dichloromethane and saturated aqueous $NaHCO_3$, and the organic layer was washed by brine. The combined organic layer was dried over anhydrous $Na_2SO_4$(s) and filtered through a celite-packed glass filter. The filtrate was concentrated under the reduced pressure and purified by silica-gel flash column chromatography (1:5 = MeOH:$CH_2Cl_2$, v/v) to obtain **10c** (230mg). Yield: 98% as yellow oil; $^1$H NMR (400 MHz, $CDCl_3$) δ 8.05 (s, 1H), 7.75 (d, *J* = 8.0 Hz, 2H), 7.38 (d, *J* = 8.0 Hz, 2H), 7.36–7.33 (m, 4H), 7.07 (brs, 1H), 6.93–6.86 (m, 3H), 6.66 (s, 1H), 5.09 (s, 2H), 4.65 (d, *J* = 5.6 Hz, 2H), 3.54 (s, 2H), 2.50 (brs, 8H), 2.31 (s, 3H), 1.53 (s, 9H); $^{13}$C NMR (100 MHz, $CDCl_3$) δ 167.4, 152.9, 146.7, 142.1, 139.0, 137.2, 133.2, 129.3, 128.5, 127.9, 127.1, 127.0, 126.8, 122.5, 121.6, 118.6, 112.0, 80.6, 70.8, 62.5, 55.0, 52.9, 45.9, 44.0, 28.4; LRMS (ESI) *m/z* calcd for $C_{32}H_{41}N_4O_4$ $[M+H]^+$: 545.31; Found: 545.40.

**Synthesis of 10 (SB1453),** 2-chloro-*N*-(2-((3-((4-((4-methylpiperazin-1-yl)methyl)benzamido)methyl)benzyl)oxy)phenyl)-5-nitrobenzamide

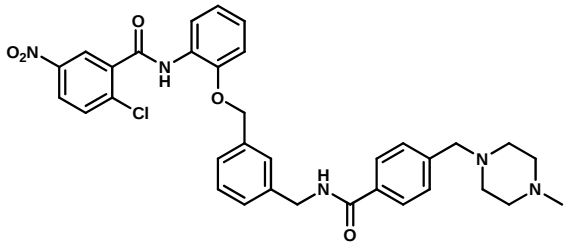

After **10c** (110 mg, 0.20 mmol) was treated with 10% trifluoroacetic acid in dichloromethane (10 mL) at room temperature for 1 h, the reaction mixture was washed with saturated aqueous $NaHCO_3$ three times, and concentrated under the reduced pressure to provide *N*-(3-((2-aminophenoxy)methyl)benzyl)-4-((4-methylpiperazin-1-yl)methyl)benzamide. To a solution of *N*-(3-((2-aminophenoxy)methyl)benzyl)-4-((4-methylpiperazin-1-yl)methyl)benzamide in dichloromethane (10 mL), 2-chloro-5-nitrobenzoyl chloride (66 mg, 0.30 mmol) and triethylamine (56 μL, 0.40 mmol) were added and the mixture was stirred at room temperature for 1 h. After removal of solvent and triethylamine under the reduced pressure, the residue was purified by silica-gel flash column chromatography (1:5 = MeOH:$CH_2Cl_2$, v/v) to obtain **10** (102 mg). Yield: 81% as light yellow solid; $^1$H NMR (400 MHz, DMSO-$d_6$) δ 10.07 (s, 1H), 8.98 (t, *J* = 6.0 Hz, 1H), 8.37 (d, *J* = 2.8 Hz, 1H), 8.29 (dd, *J* = 8.4, 2.8 Hz, 1H), 7.84–7.81 (m, 4H), 7.43–7.31 (m, 5H), 7.26 (d, *J* = 7.6 Hz, 1H), 7.15 (t, *J* = 5.2 Hz, 2H), 7.01 (t, *J* = 7.6 Hz, 1H), 5.19 (s, 2H), 4.47 (d, *J* = 6.0 Hz, 2H), 3.48 (s, 2H), 2.34 (brs, 8H), 2.14 (s, 3H); $^{13}$C NMR (100 MHz, DMSO-$d_6$) δ 166.0, 163.0, 150.6, 146.0, 141.8, 139.9, 137.7, 137.2, 137.0, 133.0, 131.3, 128.6, 128.4, 127.2, 126.6. 126.32, 126.27, 125.9, 125.6, 124.7, 124.1, 120.5, 113.2, 69.8, 61.6, 54.7, 52.6, 45.7, 42.5; LRMS (ESI) *m/z* calcd for $C_{34}H_{35}ClN_5O_5$ $[M+H]^+$: 628.23; Found: 628.41.

**Procedure for synthesis of compound 11**

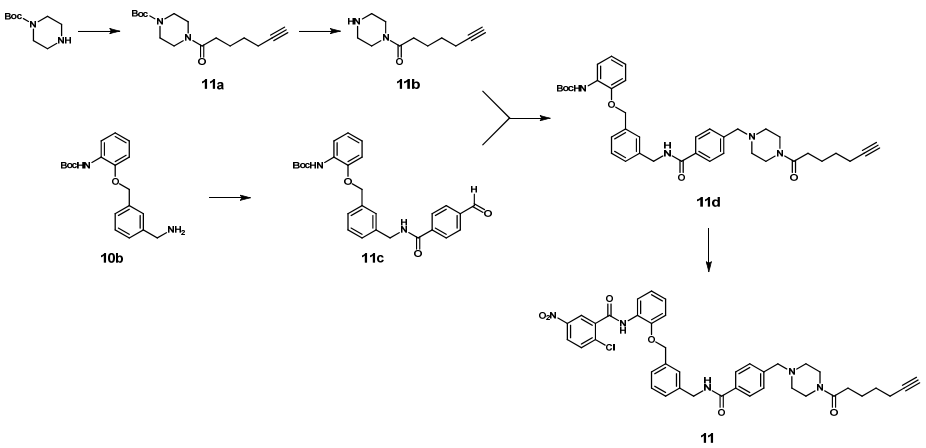


**Synthesis of 11a**, *tert*-butyl 4-(hept-6-ynoyl)piperazine-1-carboxylate

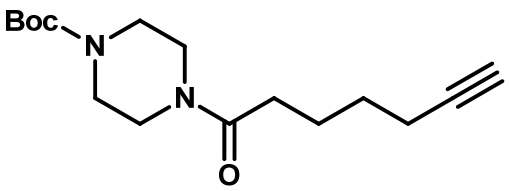

To a solution of 1-Boc-piperazine (1.00 g, 5.37 mmol) in dichloromethane (50 mL), 6-heptynoic acid (722 mg, 6.44 mmol), 1-ethyl-3-(3-dimethylaminopropyl)carbodiimide hydrochloride (1.23 g, 6.44 mmol), triethylamine (0.897 mL, 6.44 mmol), and 4-dimethylaminopyridine (65.6mg, 0.537 mmol) were added, and the mixture was stirred at room temperature for 12 h. The crude mixture was worked up with dichloromethane and saturated aqueous NaHCO3, and the organic layer was washed by brine. The combined organic layer was dried over anhydrous $Na_2SO_4$(s) and filtered through a celite-packed glass filter. The filtrate was concentrated under the reduced pressure and purified by silica-gel flash column

chromatography (1:10 = MeOH:$CH_2Cl_2$, v/v) to obtain **11a** (1.50 g). Yield: 95% as light yellow solid; $^1$H NMR (400 MHz, $CDCl_3$) δ 3.59 (t, *J* = 4.8 Hz, 2H), 3.45 (s, 4H), 3.40 (t, *J* = 4.8 Hz, 2H), 2.36 (t, *J* = 7.2 Hz, 2H), 2.23 (td, *J* = 7.2, 2.4 Hz, 2H), 1.95 (t, *J* = 2.8 Hz, 1H), 1.77 (p, *J* = 7.2 Hz, 2H), 1.59 (p, *J* = 7.2 Hz, 2H), 1.47 (s, 9H); $^{13}$C NMR (100 MHz, $CDCl_3$) δ 171.4, 154.8, 84.1, 80.4, 68.7, 45.5, 41.5, 32.9, 28.5, 28.1, 24.3, 18.3; LRMS (ESI) *m/z* calcd for $C_{16}H_{27}N_2O_3$ $[M+H]^+$: 295.20; Found: 295.20.

**Synthesis of 11b**, 1-(piperazin-1-yl)hept-6-yn-1-one

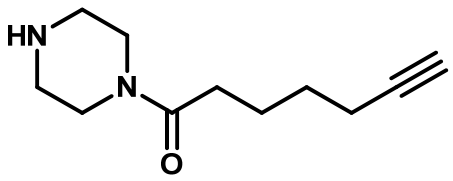


After **11a** (1.00 g, 3.40 mmol) was treated with 10% trifluoroacetic acid in dichloromethane (50 mL) at room temperature for 12 h, the reaction mixture was washed with saturated aqueous $NaHCO_3$ three times, and concentrated under the reduced pressure to obtain **11** (530 mg). Yield: 80% as yellow oil; $^1$H NMR (400 MHz, $CDCl_3$) $^1$H NMR (400 MHz, $CDCl_3$) δ 3.60 (t, *J* = 4.8 Hz, 2H), 3.46 (t, *J* = 4.8 Hz, 2H), 2.86 (m, 4H), 2.74(brs, 1H), 2.35 (t, *J* = 7.2 Hz, 2H), 2.23 (td, *J* = 7.2, 2.8 Hz 2H), 1.95 (t, *J* = 2.4 Hz, 1H), 1.76 (p, *J* = 7.2 Hz, 2H), 1.59 (p, *J* = 7.2 Hz, 2H); $^{13}$C NMR (100 MHz, $CDCl_3$) δ 171.1, 84.0, 68.6, 46.6, 46.2, 45.7, 42.4, 32.6, 28.0, 24.3, 18.2; LRMS (ESI) *m/z* calcd for $C_{11}H_{19}N_2O$ $[M+H]^+$: 195.15; Found: 195.20.

**Synthesis of 11c**, *tert*-butyl (2-((3-((4-formylbenzamido)methyl)benzyl)oxy) phenyl)carbamate

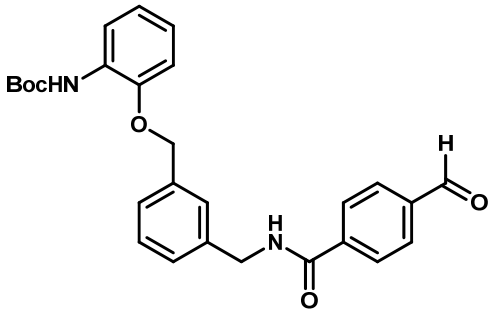


To a solution of **10b** (120 mg, 0.36 mmol) in dichloromethane (10 mL), 4-formyl benzoic acid (66 mg, 0.44 mmol), 1-ethyl-3-(3-dimethyl aminopropyl) carbodiimide hydrochloride (84 mg, 0.44 mmol), triethylamine (0.10 mL, 0.73 mmol), and 4-dimethylaminopyridine (4.5 mg, 0.036 mmol) were added, and the mixture was stirred at room temperature for 12 h. The crude mixture was worked up with dichloromethane and saturated aqueous $NaHCO_3$, and the organic layer was washed by brine. The combined organic layer was dried over anhydrous $Na_2SO_4$(s) and filtered through a celite-packed glass filter. The filtrate was concentrated under the reduced pressure and purified by silica-gel flash column chromatography (1:1 = ethyl acetate:*n*-hexane, v/v) to obtain **11c** (72 mg). Yield: 43% as off-white solid; $^1$H NMR (400 MHz, $CDCl_3$) δ 10.03 (s, 1H), 8.01 (s, 1H), 7.93 (d, $J$ = 8.4 Hz, 2H), 7.89 (d, $J$ = 8.4 Hz, 2H), 7.37–7.31 (m, 4H), 7.03 (s, 1H), 6.96–6.86 (m, 4H), 5.07 (s, 2H), 4.63 (d, $J$ = 5.6 Hz, 2H), 1.48 (s, 9H); $^{13}$C NMR (100 MHz, $CDCl_3$) δ 191.6, 166.4, 152.9, 146.8, 139.5, 138.5, 138.3, 137.2, 129.9, 129.3, 128.5, 127.93, 127.88, 127.1, 127.0, 122.6, 121.7, 118.7, 112.1, 80.6, 70.9, 44.2, 28.4; LRMS (ESI) *m/z* calcd for $C_{27}H_{29}N_2O_5$ $[M+H]^+$: 461.21; Found: 461.30.

**Synthesis of 11d**, *tert*-butyl (2-((3-((4-((4-(hept-6-ynoyl)piperazin-1-yl)methyl) benzamido)methyl)benzyl)oxy)phenyl)carbamate

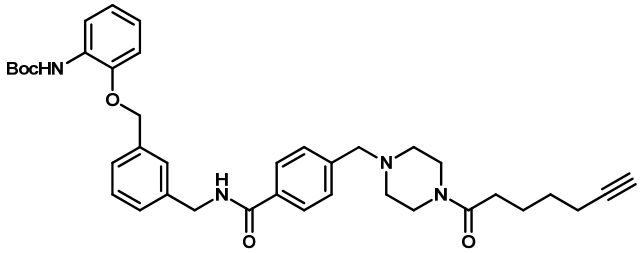


To a solution of **11b** (46 mg, 0.23 mmol) in dichloromethane (10 mL), **11c** (72 mg, 0.16 mmol), and sodium triacetoxyborohydride (33 mg, 0.16 mmol) were added, and the mixture was stirred under argon atmosphere at room temperature for 12 h. The crude mixture was worked up with dichloromethane and saturated aqueous $NaHCO_3$, and the organic layer was washed by brine. The combined organic layer was dried over anhydrous $Na_2SO_4$(s) and filtered through a celite-packed glass filter. The filtrate was concentrated under the reduced pressure and purified by silica-gel flash column chromatography (1:10 = MeOH:$CH_2Cl_2$, v/v) to obtain **11d** (95 mg). Yield: 95% as light yellow solid; $^1$H NMR (400 MHz, $CDCl_3$) δ 8.05 (s, 1H), 7.77 (d, *J* = 7.6 Hz, 2H), 7.39–7.32 (m, 6H), 7.06 (s, 1H), 6.92–6.85 (m, 3H), 6.82 (t, *J* = 5.2 Hz, 1H), 5.08 (s, 2H), 4.64 (d, *J* = 5.2 Hz, 2H), 3.60 (brs, 2H), 3.54 (s, 2H), 3.45 (brs, 2H), 2.42–2.38 (m, 4H), 2.32 (t, *J* = 7.6 Hz, 2H), 2.20 (td, *J* = 7.2, 2.8 Hz, 2H), 1.94 (t, *J* = 2.8 Hz, 1H), 1.74 (p, *J* = 7.2 Hz, 2H), 1.56 (p, *J* = 7.2 Hz, 2H), 1.50 (s, 9H); $^{13}$C NMR (100 MHz, $CDCl_3$) δ 171.2, 167.2, 152.8, 146.7, 141.7, 139.0, 137.1, 133.3, 129.17, 129.13, 128.5, 127.7, 127.2, 127.0, 126.7, 126.6, 122.4, 121.6, 118.5, 111.9, 84.1, 80.5, 70.8, 68.7, 62.4, 53.2, 52.8, 45.6, 43.9, 41.5, 32.7, 28.4, 28.1, 24.3, 18.2; LRMS (ESI) *m/z* calcd for $C_{38}H_{47}N_4O_5$ $[M+H]^+$: 639.35; Found: 639.40.

**Synthesis of 11**, 2-chloro-*N*-(2-((3-((4-((4-(hept-6-ynoyl)piperazin-1-yl)methyl) benzamido)methyl)benzyl)oxy)phenyl)-5-nitrobenzamide

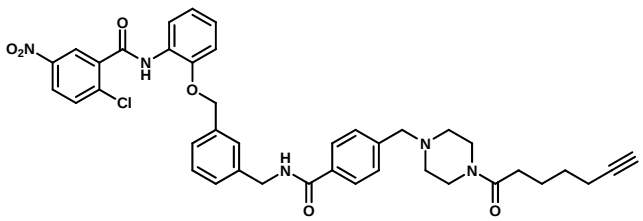

After **11d** (95 mg, 0.15 mmol) was treated with 10% trifluoroacetic acid in dichloromethane (10 mL) at room temperature for 1 h, the reaction mixture was washed with saturated aqueous $NaHCO_3$ three times, and concentrated under the reduced pressure to provide *N*-(3-((2-aminophenoxy)methyl)benzyl)-4-((4-(hept-6-ynoyl)piperazin-1-yl)methyl)benzamide. To a solution of *N*-(3-((2-aminophenoxy)methyl)benzyl)-4-((4-(hept-6-ynoyl)piperazin-1-yl)methyl) benzamide in dichloromethane (10 mL), 2-chloro-5-nitrobenzoyl chloride (39 mg, 0.18 mmol) and triethylamine (41 μL, 0.29 mmol) were added and the mixture was stirred at room temperature for 1 h. After removal of solvent and triethylamine under the reduced pressure, the residue was purified by silica-gel flash column chromatography (1:5 = MeOH:$CH_2Cl_2$, v/v) to obtain **11** (101 mg). Yield: 94% as light yellow solid; $^1$H NMR (500 MHz, $CDCl_3$) δ 8.71 (s, 1H), 8.63 (d, *J* = 2.0 Hz, 1H), 8.48 (dd, *J* = 8.0, 1.5 Hz, 1H), 8.18 (dd, *J* = 8.5, 2.5 Hz, 1H), 7.73 (d, *J* = 8.5 Hz, 2H), 7.55 (d, *J* = 9.0 Hz, 1H),7.40–7.33 (m, 6H), 7.12 (td, *J* = 7.5, 1.5 Hz, 1H), 7.07–7.00 (m, 2H), 6.54 (t, *J* = 6.0 Hz, 1H), 5.13 (s, 2H), 4.65 (d, *J* = 6.0 Hz, 2H), 3.62 (brs, 2H), 3.56 (s, 2H), 3.47 (brs, 2H), 2.42 (brs, 4H), 2.33 (t, *J* = 7.5 Hz, 2H), 2.22 (td, *J* = 7.0, 2.5 Hz, 2H), 1.94 (t, *J* = 2.5 Hz, 1H), 1.75 (p, *J* = 7.5 Hz, 2H), 1.58 (p, *J* = 7.5 Hz, 2H); $^{13}$C NMR (125 MHz, $CDCl_3$) δ 171.2, 167.2, 161.6, 147.8, 146.8, 139.2, 137.6, 136.7, 136.3, 131.9, 129.4, 129.3, 128.1, 127.4, 127.2, 126.0, 125.2, 121.8, 120.8, 112.0, 84.2,

71.1, 68.7, 62.4, 53.3, 52.9, 45.6, 43.9, 41.8, 32.8, 28.2, 24.4, 18.3; LRMS (ESI) *m/z* calcd for $C_{40}H_{41}ClN_5O_6$ $[M+H]^+$: 722.27; Found: 722.25.

# 국문초록

## 항당뇨성 퍼옥시좀 증식자 활성화 수용체 감마 리간드의 개발을 위한 공유결합성 저해제를 사용한 메카니즘적 설명

서울대학교 대학원

화학부 유기화학전공

배 환

퍼옥시좀 증식자 활성화 수용체 감마(PPARγ)는 지방생성, 지방대사 그리고 혈당항상성유지에 있어서 중요한 역할을 하고 있으며, 리간드에 의해 그 기능이 조절되는 전사인자이다. 몇몇 PPARγ 리간드는 항당뇨 효과를 지니고 있고, 그들은 공통적으로 273 번 세린 잔기(Ser273)의 인산화를 저해한다는 특징을 가지고 있다. 최근에 발표된 리간드인 SR1664 는 PPARγ 리간드들의 전형적인 특징인 전사촉진(transactivation)을 일으키지 않으면서도 Ser273 의 인산화만을 선택적으로 억제하는 독특한 특성을 가지고 있다. 또한 SR1664 가 항당뇨 효과를 가지고 있다는 사실은

인산화의 저해가 항당뇨 작용에 있어서 매우 중요할 수 있다는 것을 의미한다.

이 논문에서 우리는 SR1664 가 PPARγ 의 대안적 결합 자리(alternate binding site)에 붙는다는 것을 보였으며, 이러한 특이적인 결합이 Ser273 의 인산화를 직접적으로 저해한다는 것을 증명하였다. 그리고 합성한 공유결합성 저해제들을 화학적 도구로 사용함으로써, PPARγ 의 결합자리에 존재하는 Helix3 와 β3–β4 사이의 특정한 소수성 영역이 리간드에 의해 점유될 때 Ser273 의 인산화가 저해된다는 사실도 밝혀내었다. 또한 고지방식으로 비만을 유발시킨 쥐를 사용하여 동물실험을 진행하였고, 특정 소수성 영역에 효과적으로 결합하여 Ser273 의 인산화를 저해하도록 디자인한 공유결합성 저해제가 항당뇨 효과를 지니고 있음을 확인할 수 있었다. 마지막으로 형광 표지를 사용한 표적 단백질 동정을 통해 우리가 디자인한 공유결합성 저해제가 선택적으로 PPARγ 에 결합한다는 것을 증명할 수 있었다.

**주요어**: 퍼옥시좀 증식자 활성화 수용체 감마, Ser273 인산화, 대안적 결합 자리, 공유결합성 저해제, 합리적 디자인, 화학적 도구, 항당뇨 효과, 표적 단백질 동정

**학번**: 2013-22925

# Appendix

# (NMR Spectra)

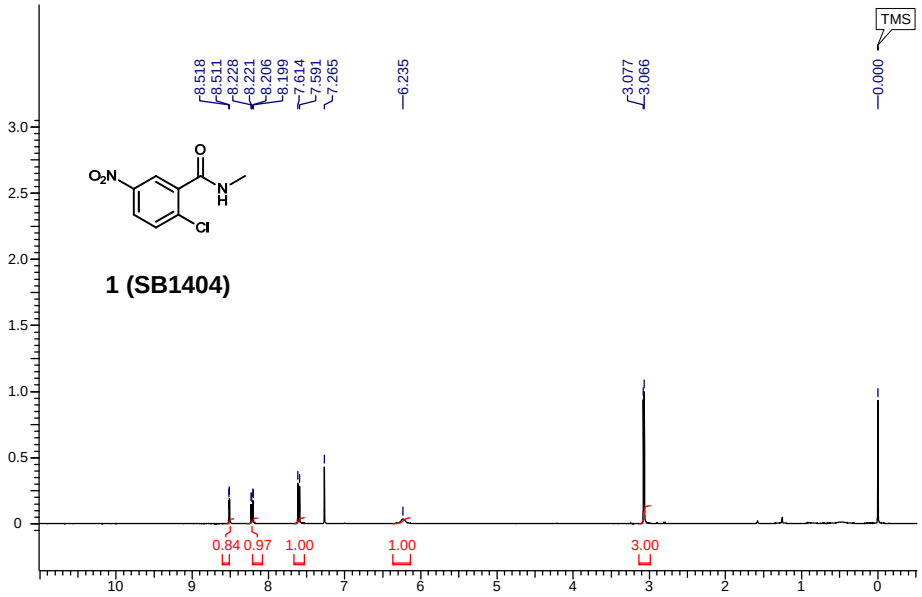
TMS
8.518
8.511
8.228
8.221
8.206
8.199
7.614
7.591
7.265
6.235
3.077
3.066
0.000
O2N
O
N
H
Cl
1 (SB1404)
0.84
0.97
1.00
1.00
3.00

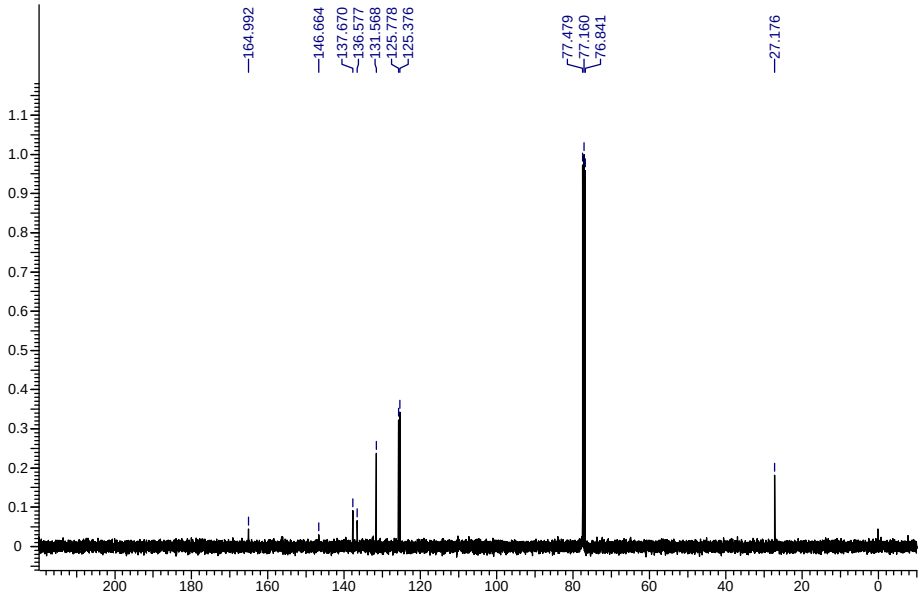
164.992
146.664
137.670
136.577
131.568
125.778
125.376
77.479
77.160
76.841
27.176

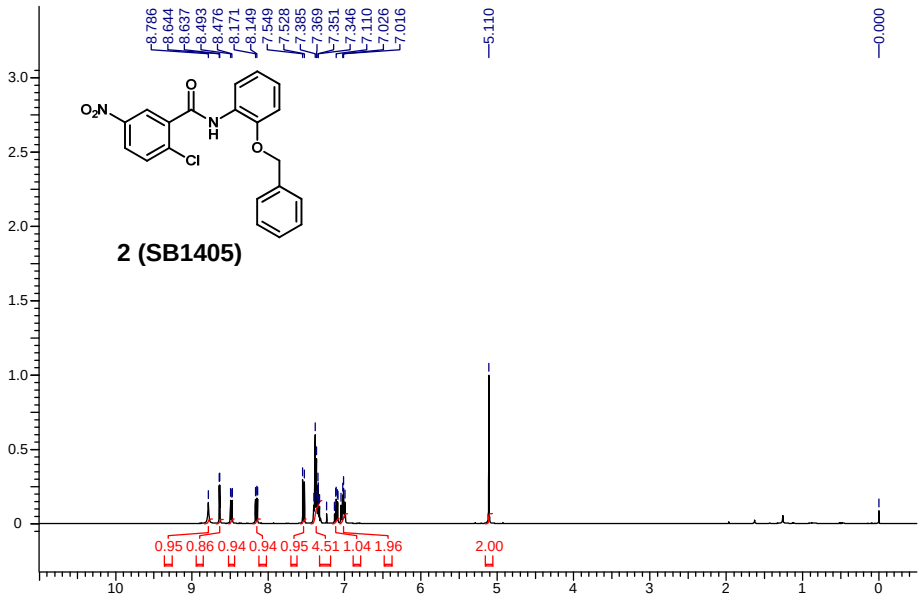
8.786
8.644
8.637
8.493
8.476
8.171
8.149
7.549
7.528
7.385
7.369
7.351
7.346
7.110
7.026
7.016
5.110
0.000
O2N
O
N
H
Cl
O
2 (SB1405)
0.95 0.86 0.94 0.94 0.95 4.51 1.04 1.96
2.00

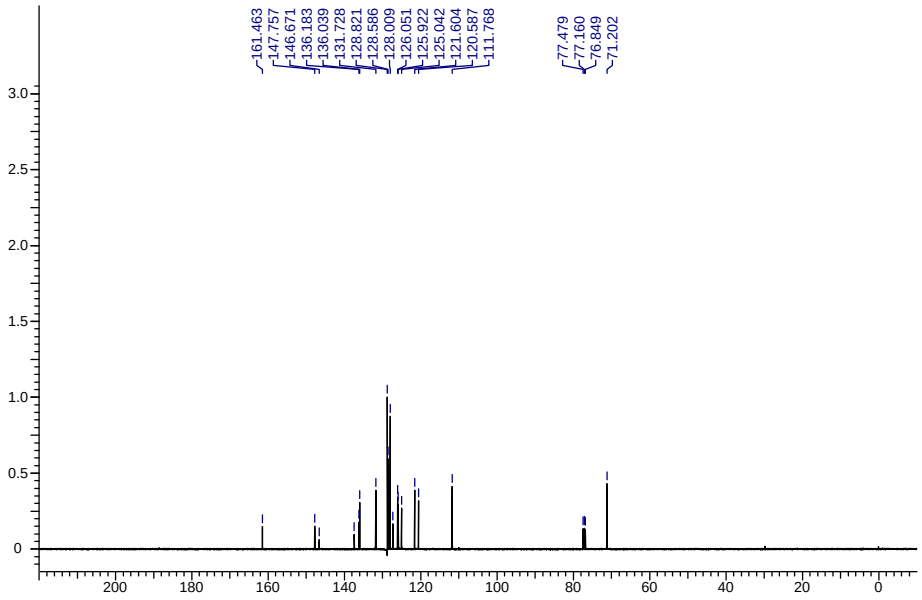
161.463
147.757
146.671
136.183
136.039
131.728
128.821
128.586
128.009
126.051
125.922
125.042
121.604
120.587
111.768
77.479
77.160
76.849
71.202

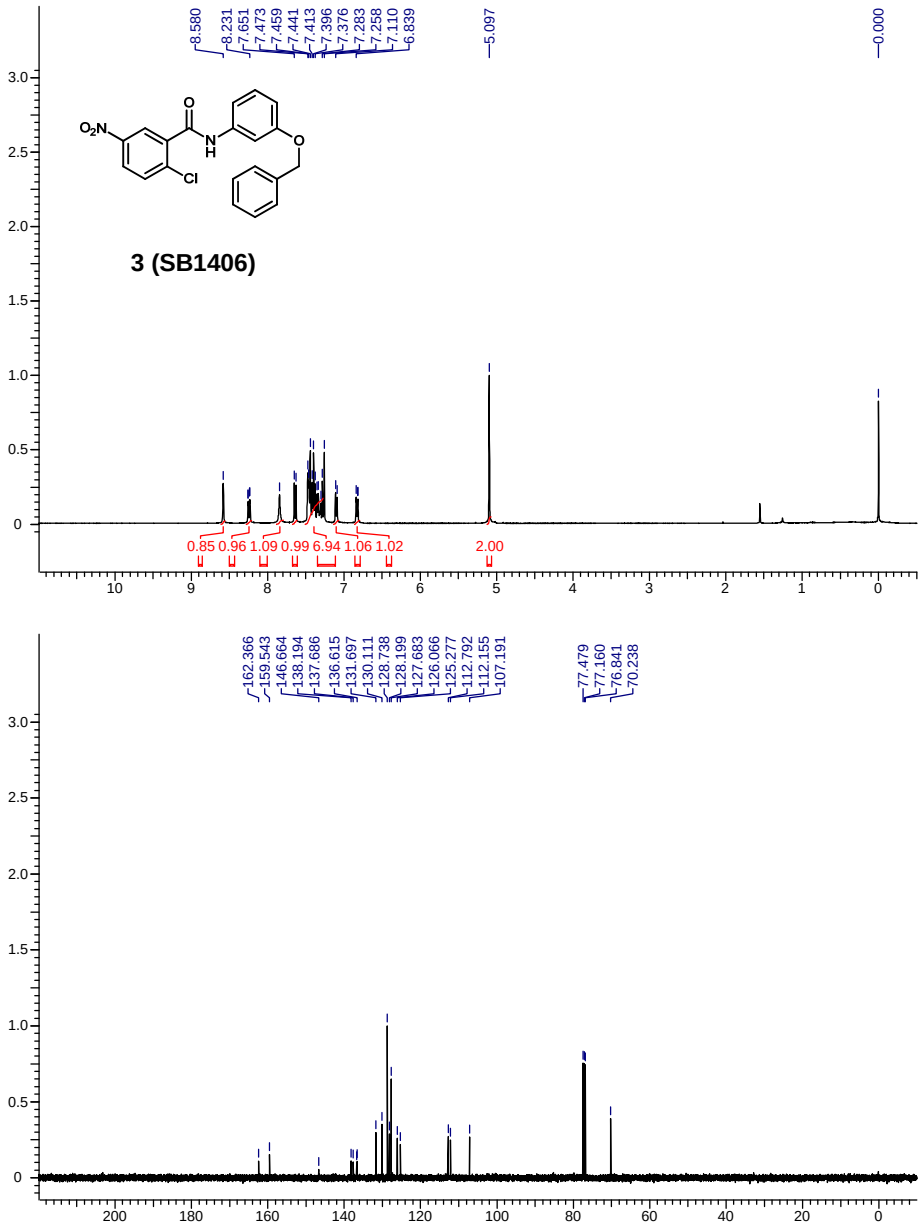
8.580
8.231
7.651
7.473
7.459
7.441
7.413
7.396
7.376
7.283
7.258
7.110
6.839
5.097
0.000
O2N
O
N
H
O
Cl
3 (SB1406)
0.85 0.96 1.09 0.99 6.94 1.06 1.02
2.00
162.366
159.543
146.664
138.194
137.686
136.615
131.697
130.111
128.738
128.199
127.683
126.066
125.277
112.792
112.155
107.191
77.479
77.160
76.841
70.238

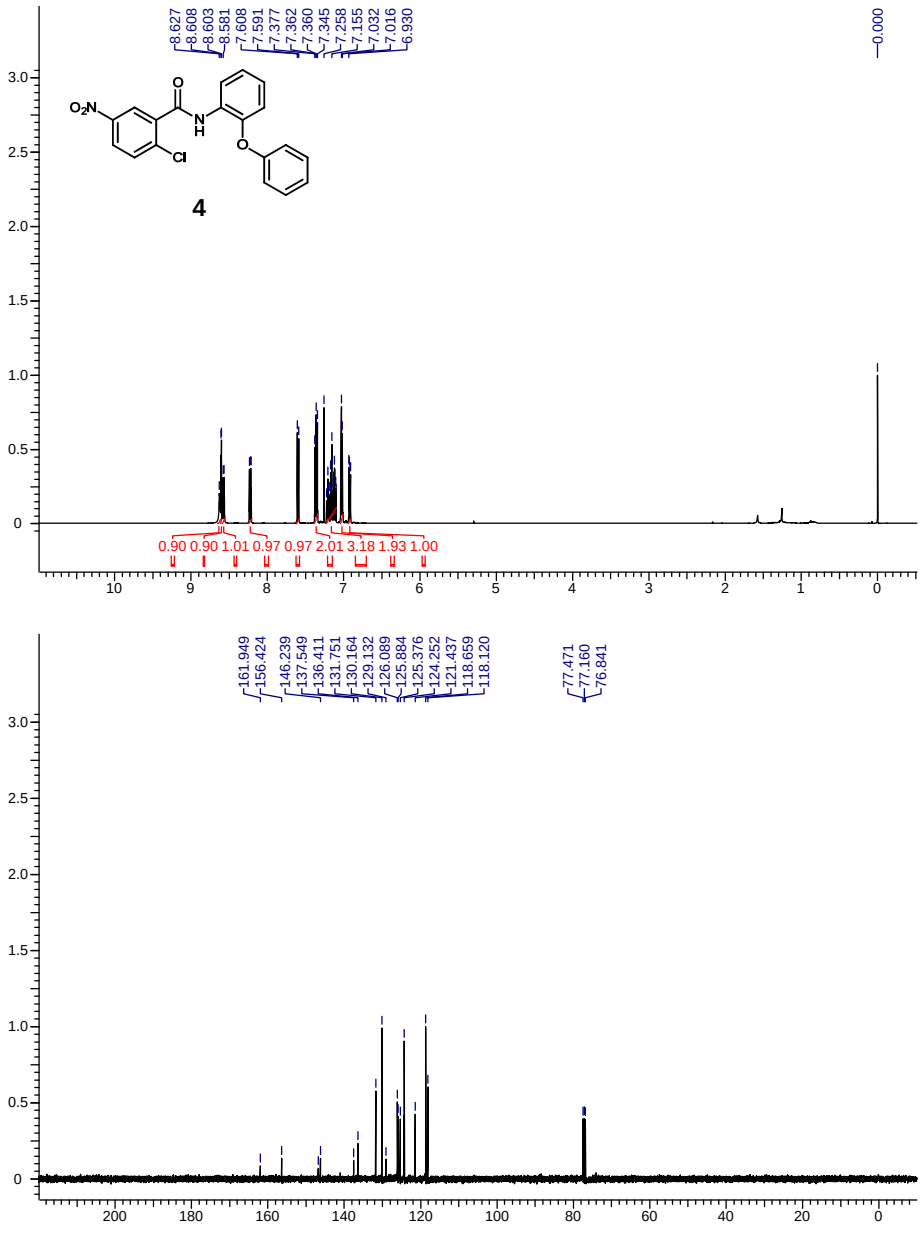
8.627
8.608
8.603
8.581
7.608
7.591
7.377
7.362
7.360
7.345
7.258
7.155
7.032
7.016
6.930
0.000
O2N
O
N
H
Cl
O
4
0.90 0.90 1.01 0.97 0.97 2.01 3.18 1.93 1.00
161.949
156.424
146.239
137.549
136.411
131.751
130.164
129.132
126.089
125.884
125.376
124.252
121.437
118.659
118.120
77.471
77.160
76.841

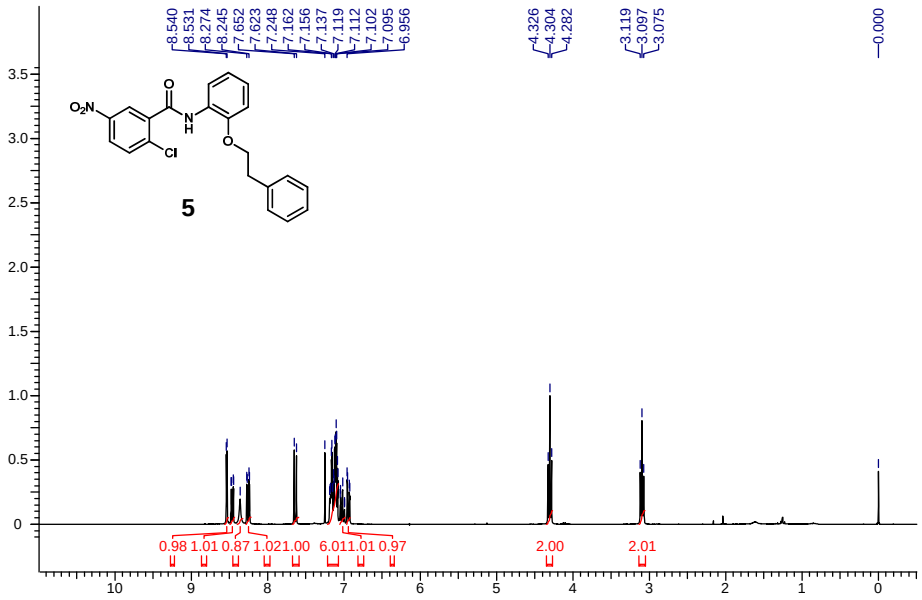
8.540
8.531
8.274
8.245
7.652
7.623
7.248
7.162
7.156
7.137
7.119
7.112
7.102
7.095
6.956
4.326
4.304
4.282
3.119
3.097
3.075
0.000
O2N
O
N
H
Cl
O
5
0.98 1.01 0.87 1.02 1.00 6.01 1.01 0.97
2.00
2.01

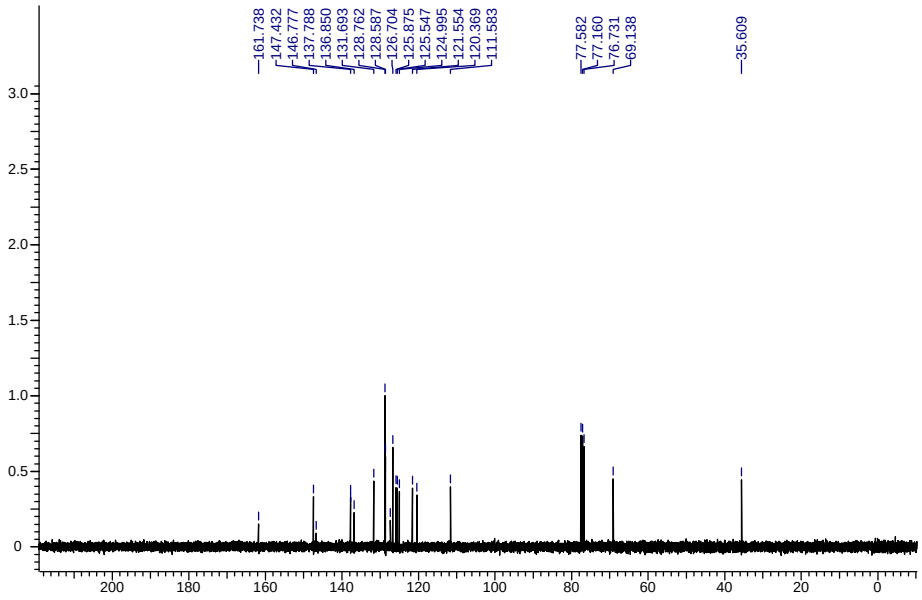
161.738
147.432
146.777
137.788
136.850
131.693
128.762
128.587
126.704
125.875
125.547
124.995
121.554
120.369
111.583
77.582
77.160
76.731
69.138
35.609

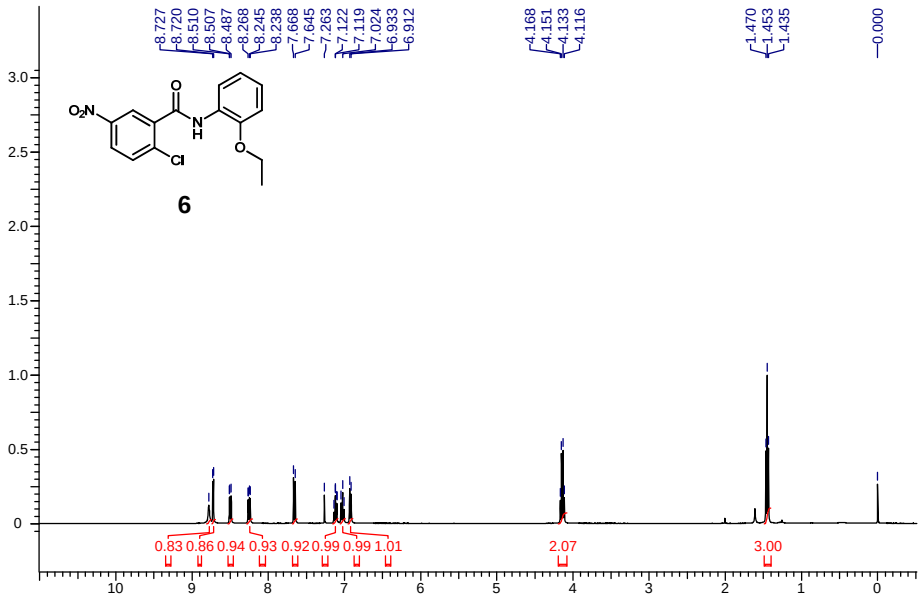
8.727
8.720
8.510
8.507
8.487
8.268
8.245
8.238
7.668
7.645
7.263
7.122
7.119
7.024
6.933
6.912
4.168
4.151
4.133
4.116
1.470
1.453
1.435
0.000
O2N
O
N
H
O
Cl
6
0.83 0.86 0.94 0.93 0.92 0.99 0.99 1.01
2.07
3.00

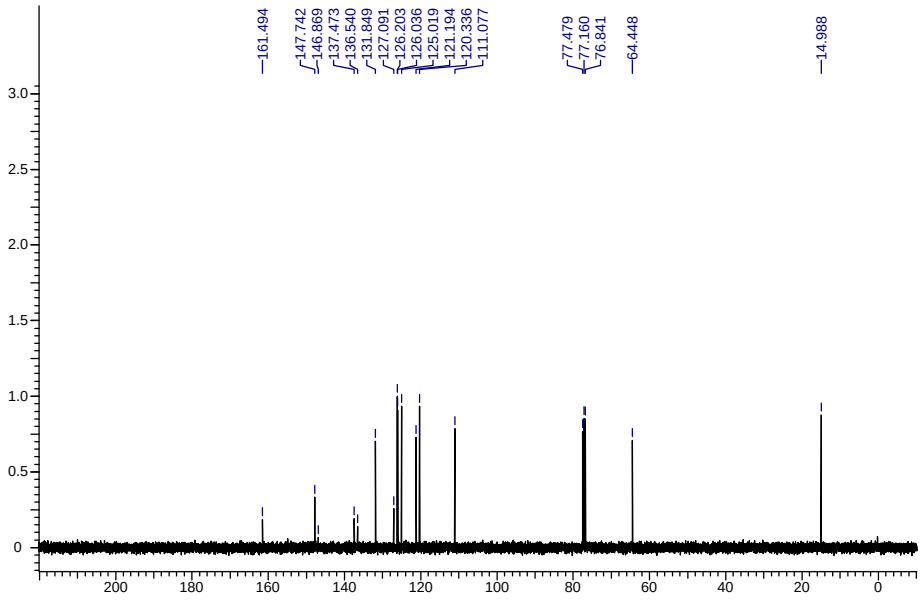
161.494
147.742
146.869
137.473
136.540
131.849
127.091
126.203
126.036
125.019
121.194
120.336
111.077
77.479
77.160
76.841
64.448
14.988

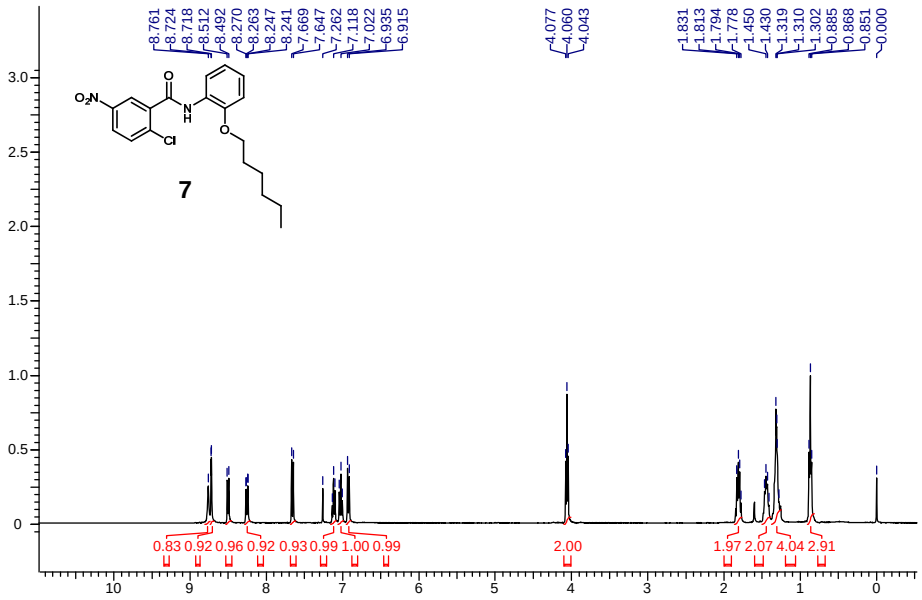
8.761
8.724
8.718
8.512
8.492
8.270
8.263
8.247
8.241
7.669
7.647
7.262
7.118
7.022
6.935
6.915
4.077
4.060
4.043
1.831
1.813
1.794
1.778
1.450
1.430
1.319
1.310
1.302
0.885
0.868
0.851
0.000
O2N
O
N
H
Cl
O
7
0.83 0.92 0.96 0.92 0.93 0.99 1.00 0.99
2.00
1.97 2.07 4.04 2.91

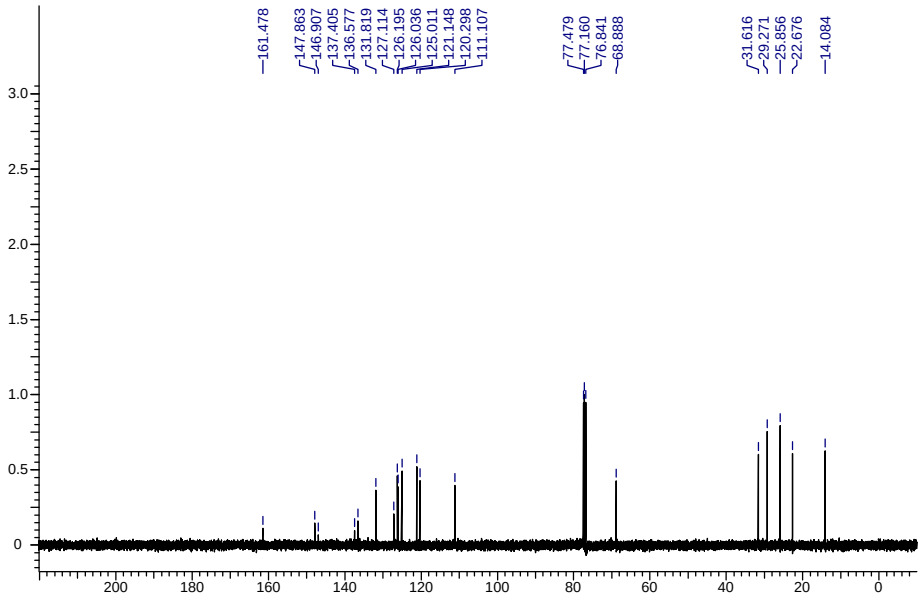
161.478
147.863
146.907
137.405
136.577
131.819
127.114
126.195
126.036
125.011
121.148
120.298
111.107
77.479
77.160
76.841
68.888
31.616
29.271
25.856
22.676
14.084

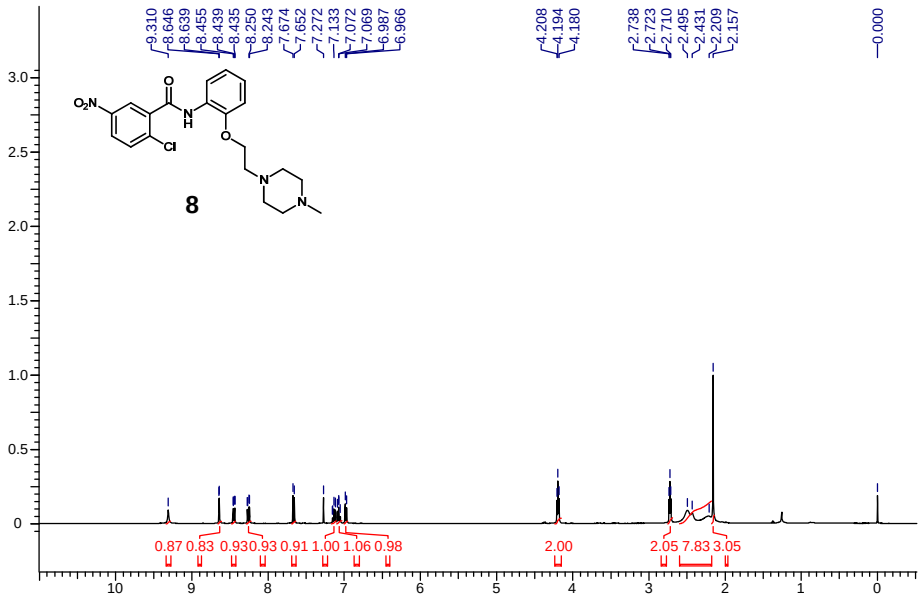
9.310
8.646
8.639
8.455
8.439
8.435
8.250
8.243
7.674
7.652
7.272
7.133
7.072
7.069
6.987
6.966
4.208
4.194
4.180
2.738
2.723
2.710
2.495
2.431
2.209
2.157
0.000
8
0.87 0.83 0.93 0.93 0.91 1.00 1.06 0.98
2.00
2.05 7.83 3.05

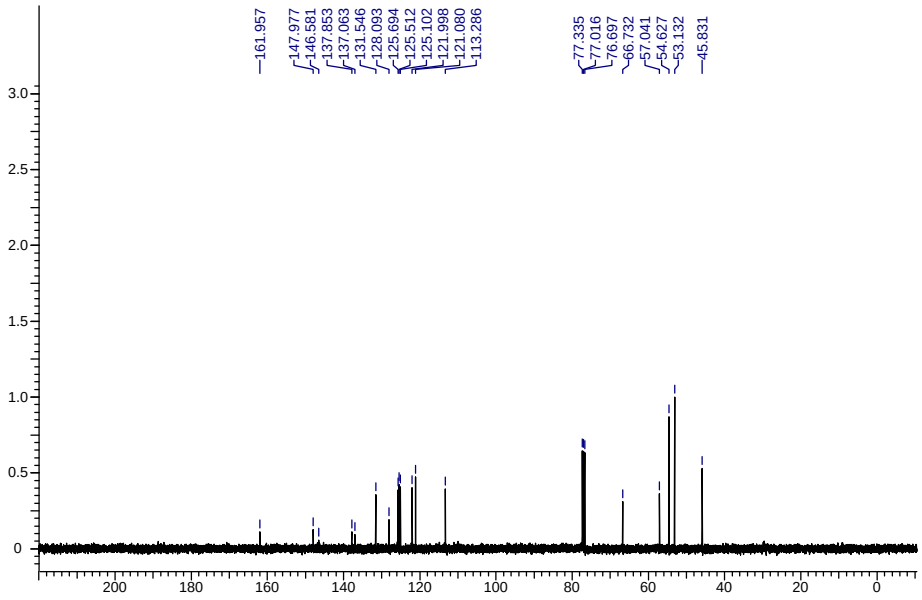
161.957
147.977
146.581
137.853
137.063
131.546
128.093
125.694
125.512
125.102
121.998
121.080
113.286
77.335
77.016
76.697
66.732
57.041
54.627
53.132
45.831

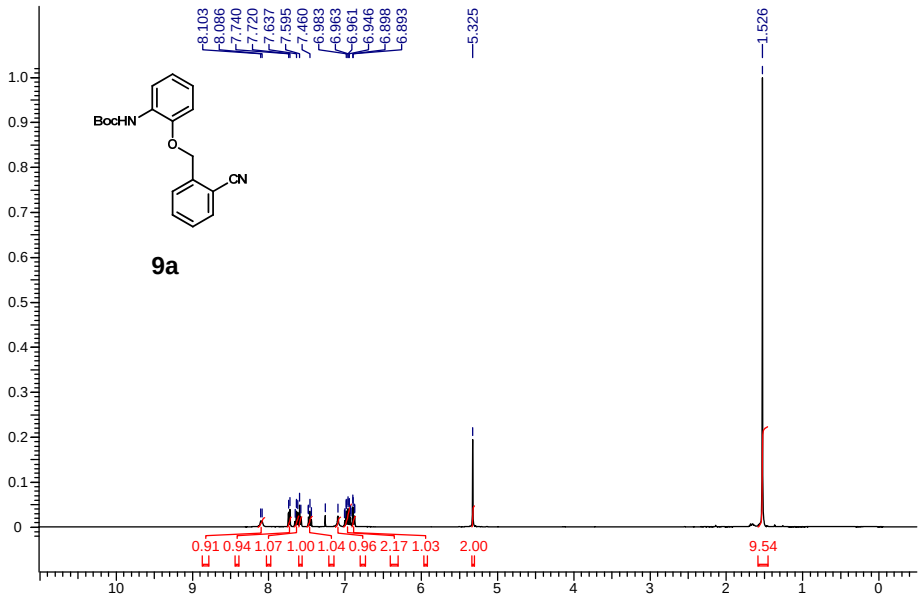
8.103
8.086
7.740
7.720
7.637
7.595
7.460
6.983
6.963
6.961
6.946
6.898
6.893
5.325
1.526
BocHN
O
CN
9a
0.91 0.94 1.07 1.00 1.04 0.96 2.17 1.03 2.00 9.54

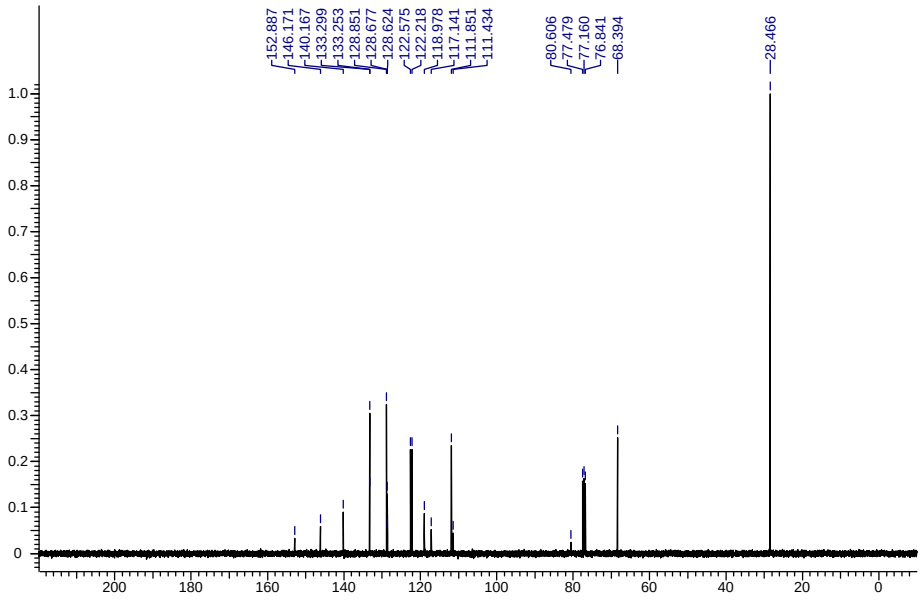
152.887
146.171
140.167
133.299
133.253
128.851
128.677
128.624
122.575
122.218
118.978
117.141
111.851
111.434
80.606
77.479
77.160
76.841
68.394
28.466

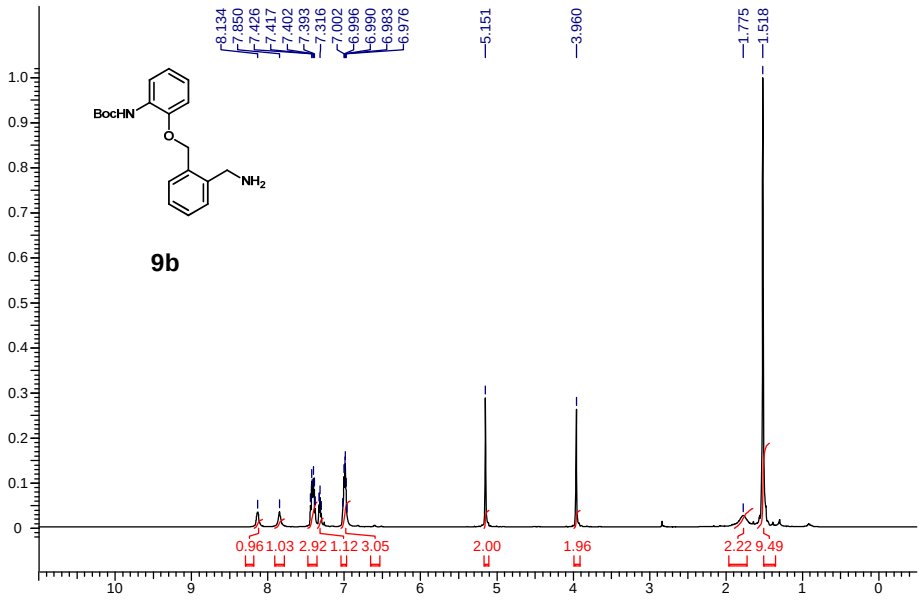
8.134
7.850
7.426
7.417
7.402
7.393
7.316
7.002
6.996
6.990
6.983
6.976
5.151
3.960
1.775
1.518
BocHN
O
NH2
9b
0.96 1.03 2.92 1.12 3.05
2.00
1.96
2.22 9.49

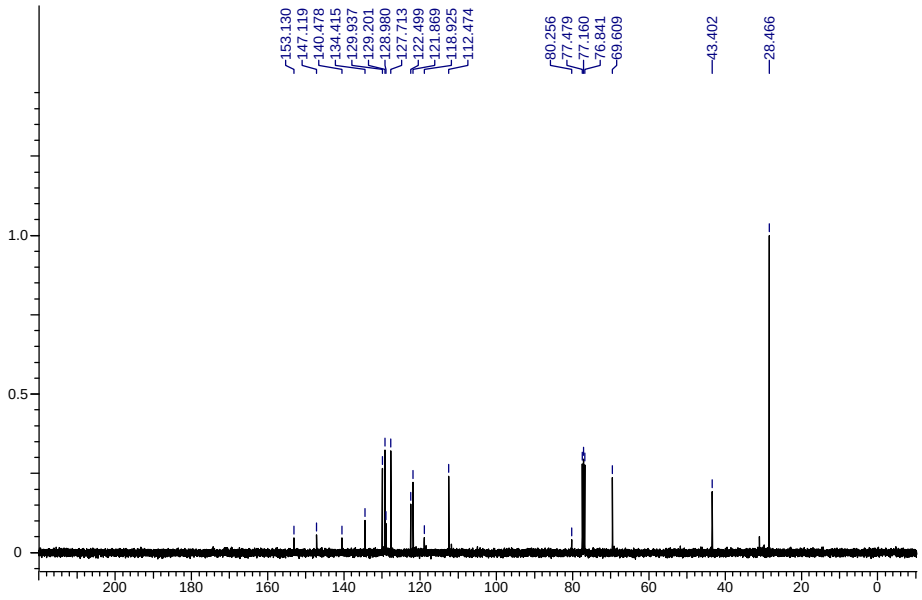
153.130
147.119
140.478
134.415
129.937
129.201
128.980
127.713
122.499
121.869
118.925
112.474
80.256
77.479
77.160
76.841
69.609
43.402
28.466

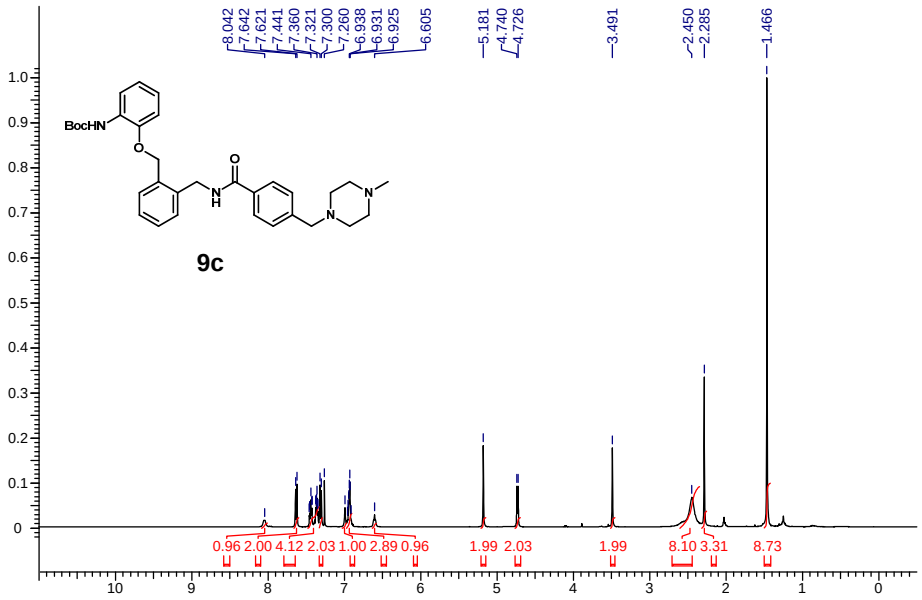
8.042
7.642
7.621
7.441
7.360
7.321
7.300
7.260
6.938
6.931
6.925
6.605
5.181
4.740
4.726
3.491
2.450
2.285
1.466
BocHN
O
N
H
O
N
N
9c
0.96 2.00 4.12 2.03 1.00 2.89 0.96
1.99 2.03
1.99
8.10 3.31
8.73

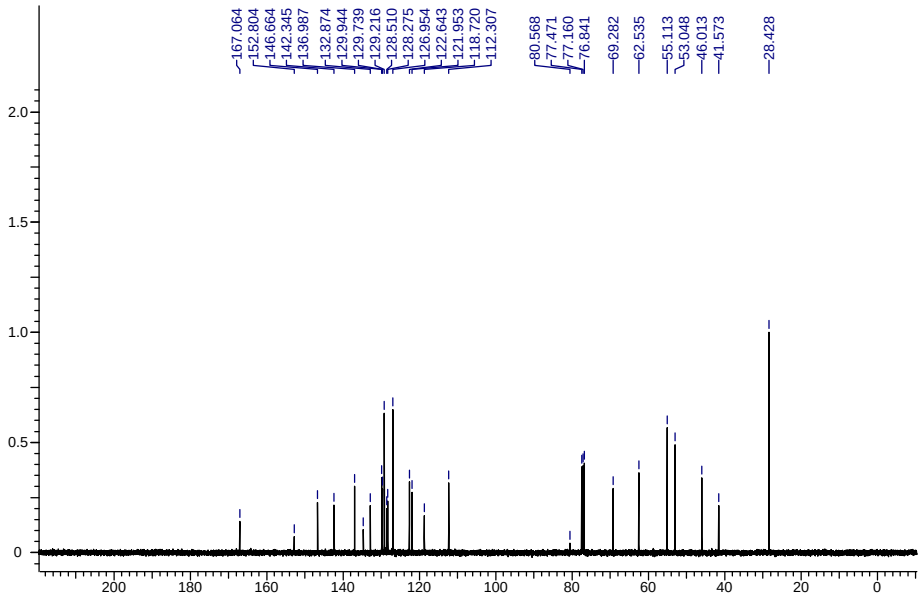
167.064
152.804
146.664
142.345
136.987
132.874
129.944
129.739
129.216
128.510
128.275
126.954
122.643
121.953
118.720
112.307
80.568
77.471
77.160
76.841
69.282
62.535
55.113
53.048
46.013
41.573
28.428

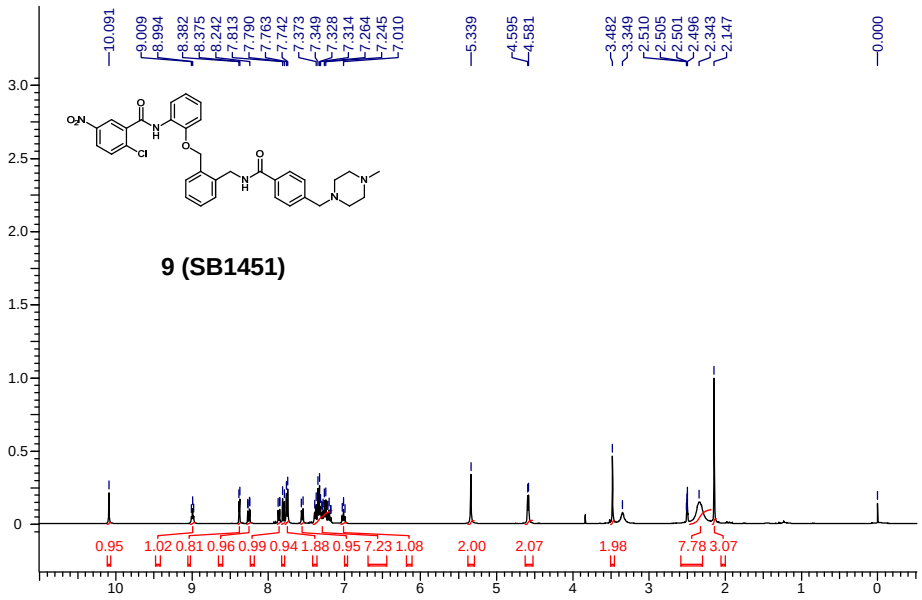
10.091
9.009
8.994
8.382
8.375
8.242
7.813
7.790
7.763
7.742
7.373
7.349
7.328
7.314
7.264
7.245
7.010
5.339
4.595
4.581
3.482
3.349
2.510
2.505
2.501
2.496
2.343
2.147
0.000
9 (SB1451)
0.95 1.02 0.81 0.96 0.99 0.94 1.88 0.95 7.23 1.08 2.00 2.07 1.98 7.78 3.07

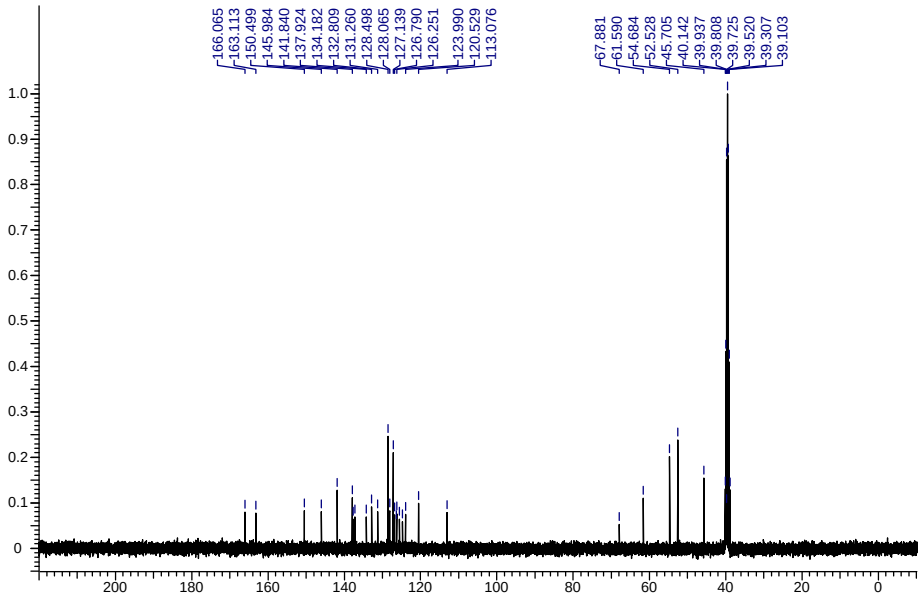
166.065
163.113
150.499
145.984
141.840
137.924
134.182
132.809
131.260
128.498
128.065
127.139
126.790
126.251
123.990
120.529
113.076
67.881
61.590
54.684
52.528
45.705
40.142
39.937
39.808
39.725
39.520
39.307
39.103

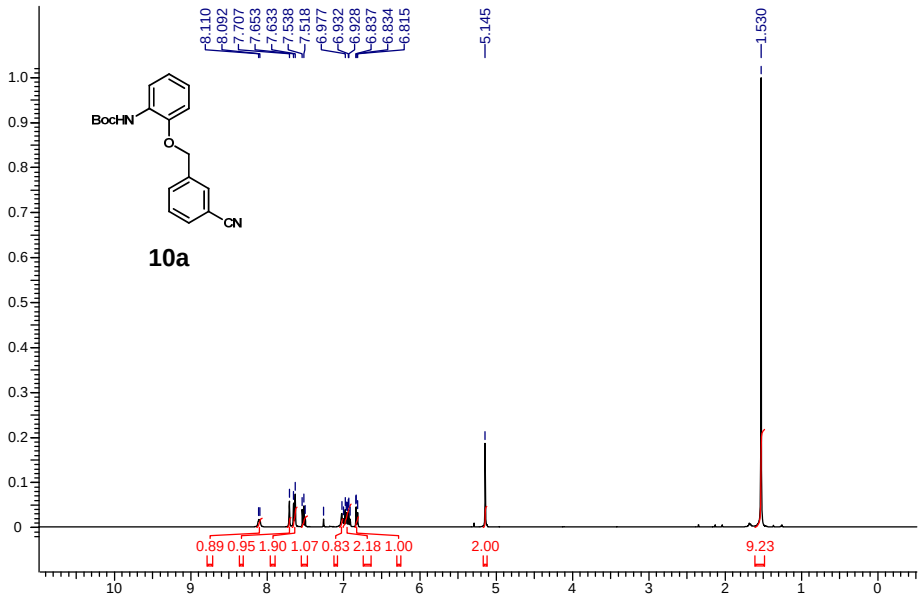
8.110
8.092
7.707
7.653
7.633
7.538
7.518
6.977
6.932
6.928
6.837
6.834
6.815
5.145
1.530
BocHN
O
CN
10a
0.89 0.95 1.90 1.07 0.83 2.18 1.00
2.00
9.23

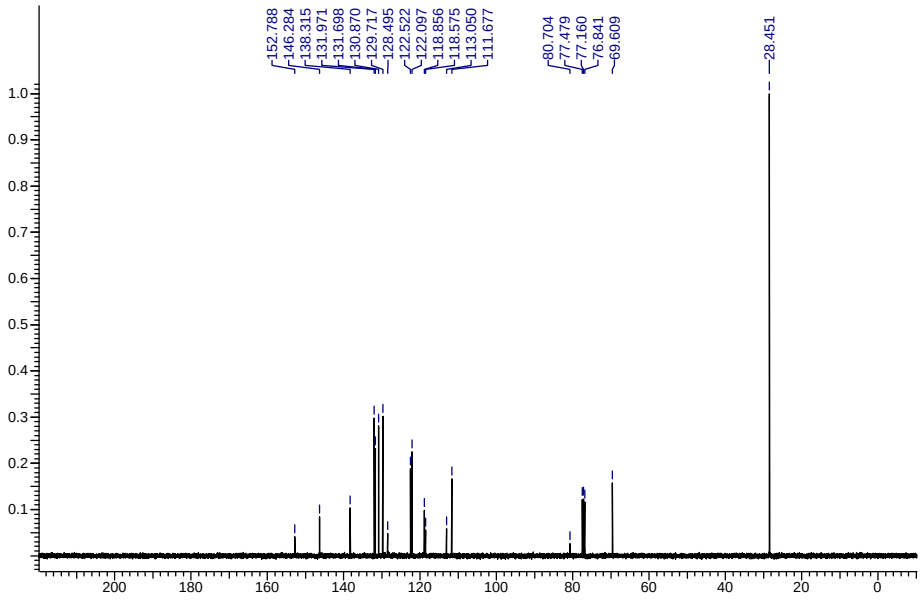
152.788
146.284
138.315
131.971
131.698
130.870
129.717
128.495
122.522
122.097
118.856
118.575
113.050
111.677
80.704
77.479
77.160
76.841
69.609
28.451

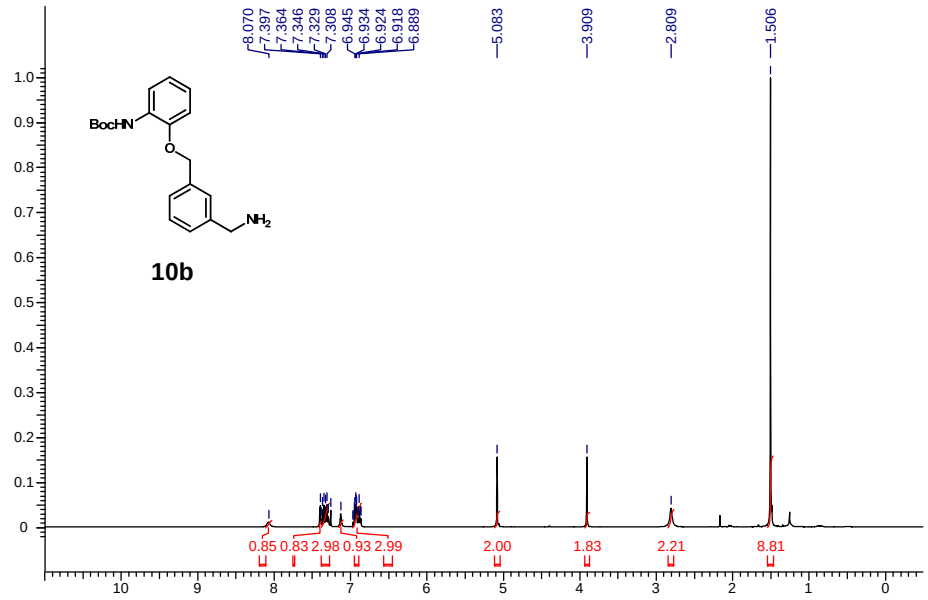
8.070
7.397
7.364
7.346
7.329
7.308
6.945
6.934
6.924
6.918
6.889
5.083
3.909
2.809
1.506
BocHN
O
NH2
10b
0.85 0.83 2.98 0.93 2.99
2.00
1.83
2.21
8.81

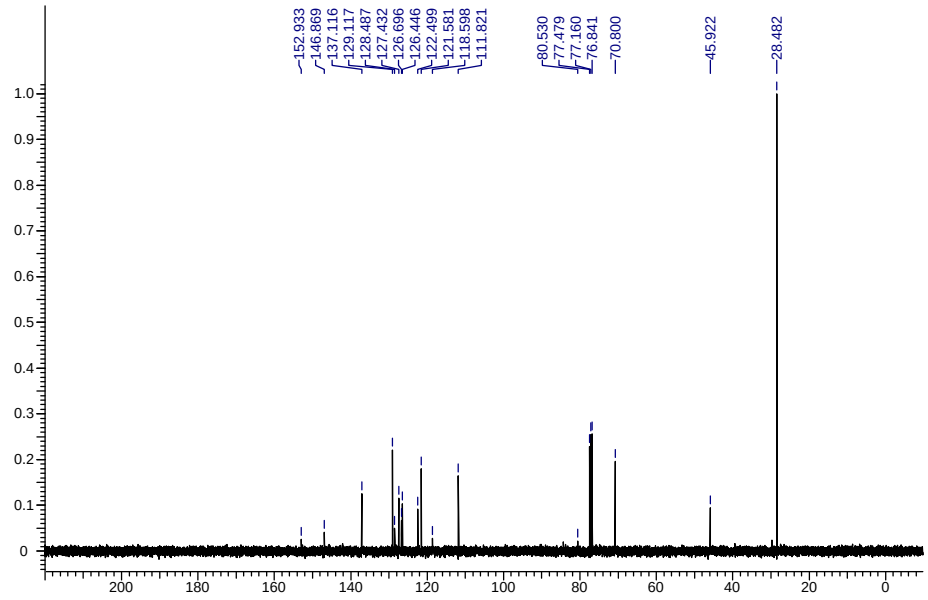
152.933
146.869
137.116
129.117
128.487
127.432
126.696
126.446
122.499
121.581
118.598
111.821
80.530
77.479
77.160
76.841
70.800
45.922
28.482

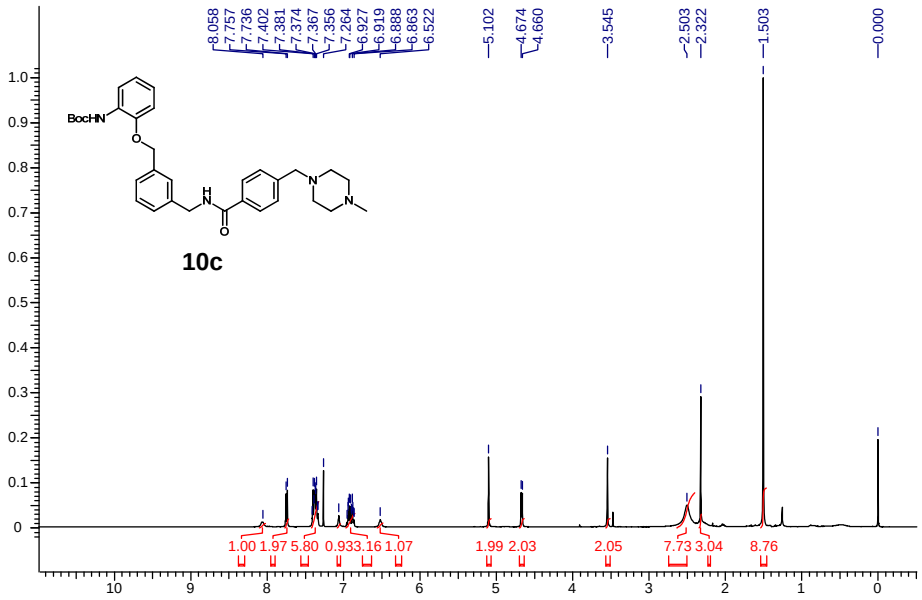
8.058
7.757
7.736
7.402
7.381
7.374
7.367
7.356
7.264
6.927
6.919
6.888
6.863
6.522
5.102
4.674
4.660
3.545
2.503
2.322
1.503
0.000
BocHN
O
H
N
N
N
O
10c
1.00 1.97 5.80 0.93 3.16 1.07
1.99 2.03
2.05
7.73 3.04
8.76

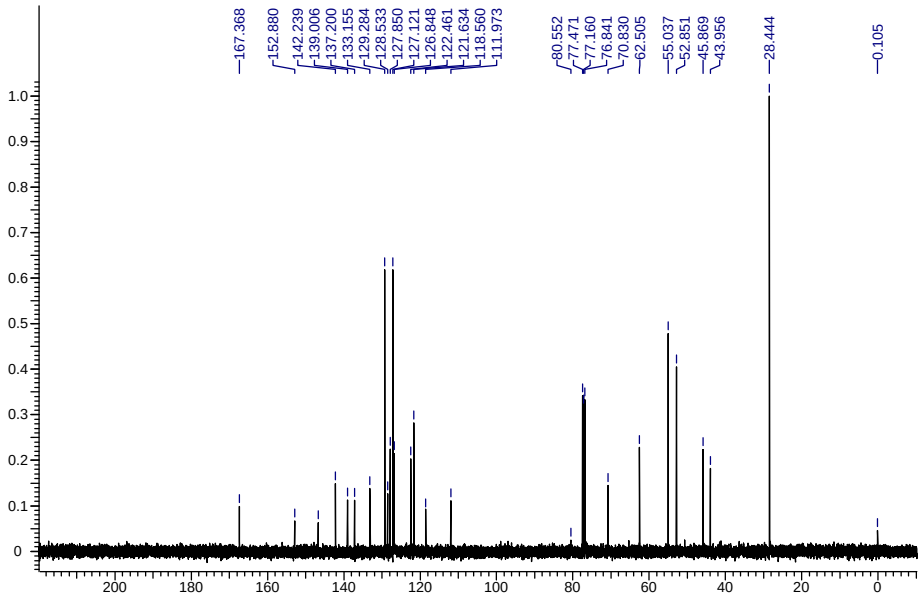
167.368
152.880
142.239
139.006
137.200
133.155
129.284
128.533
127.850
127.121
126.848
122.461
121.634
118.560
111.973
80.552
77.471
77.160
76.841
70.830
62.505
55.037
52.851
45.869
43.956
28.444
0.105

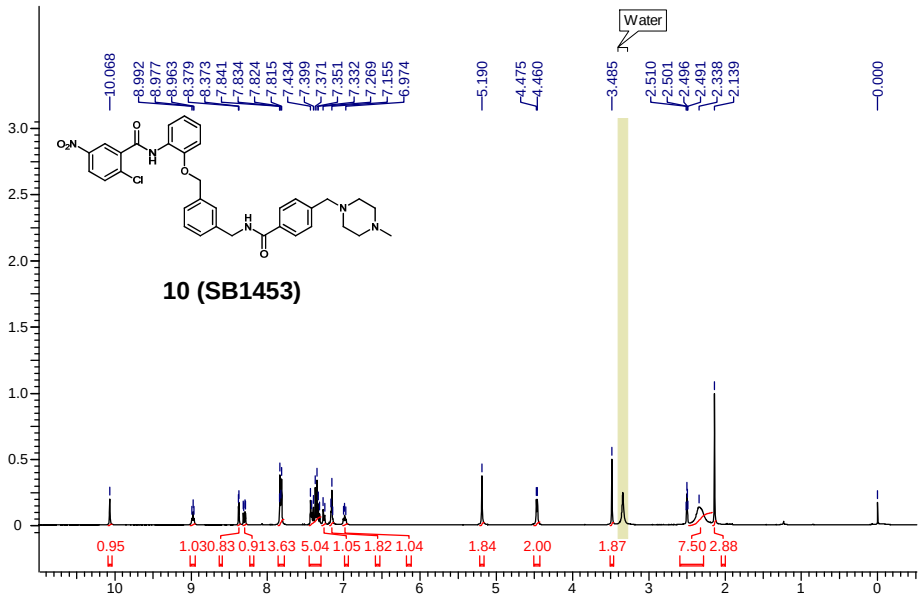
Water
10.068
8.992
8.977
8.963
8.379
8.373
7.841
7.834
7.824
7.815
7.434
7.399
7.371
7.351
7.332
7.269
7.155
6.974
5.190
4.475
4.460
3.485
2.510
2.501
2.496
2.491
2.338
2.139
0.000
10 (SB1453)
0.95
1.03
0.83
0.91
3.63
5.04
1.05
1.82
1.04
1.84
2.00
1.87
7.50
2.88

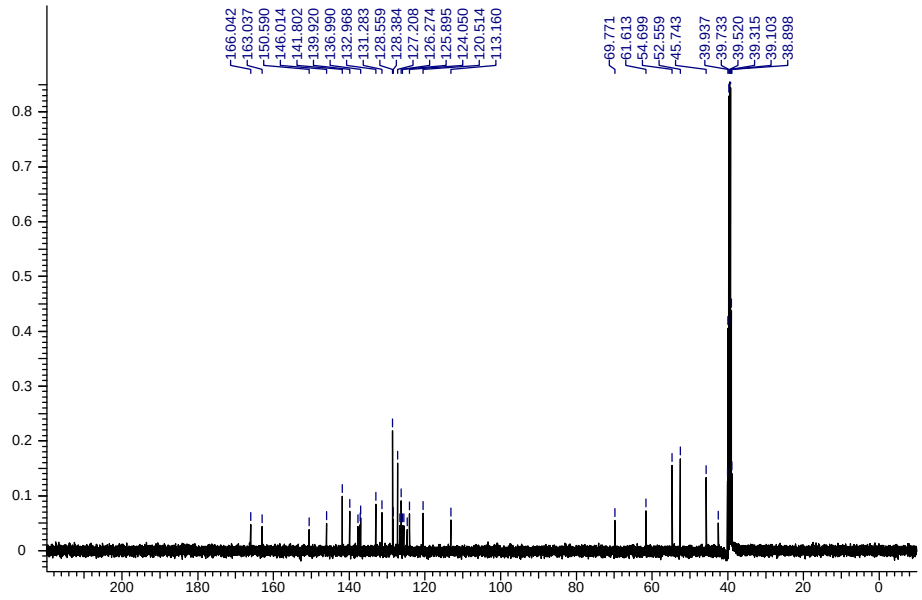
166.042
163.037
150.590
146.014
141.802
139.920
136.990
132.968
131.283
128.559
128.384
127.208
126.274
125.895
124.050
120.514
113.160
69.771
61.613
54.699
52.559
45.743
39.937
39.733
39.520
39.315
39.103
38.898

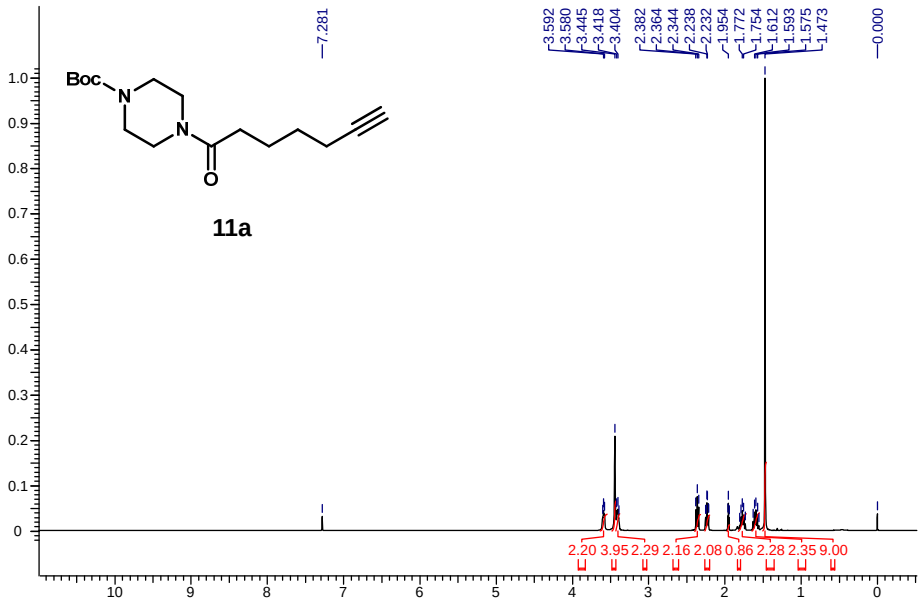
Boc
N
N
O
11a
7.281
3.592
3.580
3.445
3.418
3.404
2.382
2.364
2.344
2.238
2.232
1.954
1.772
1.754
1.612
1.593
1.575
1.473
0.000
2.20 3.95 2.29 2.16 2.08 0.86 2.28 2.35 9.00

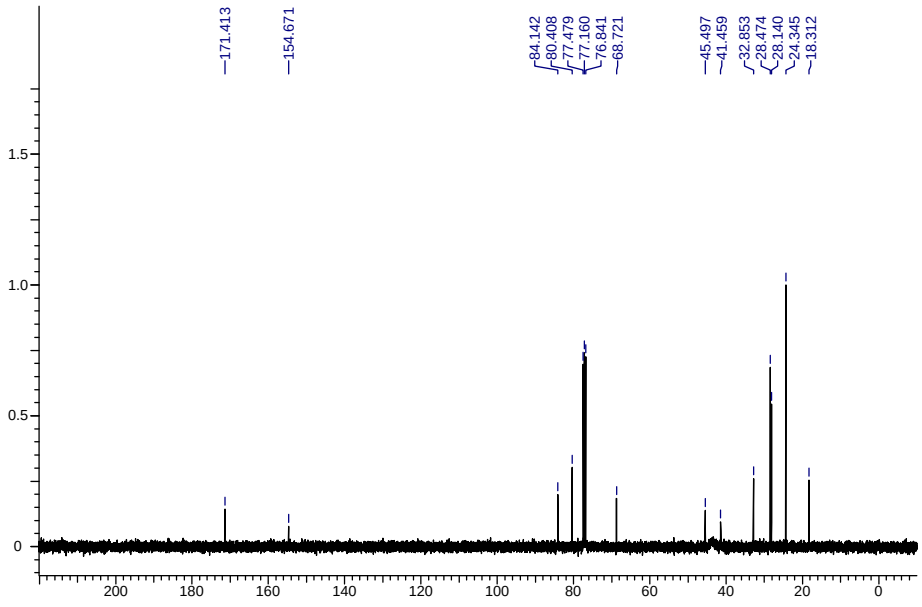
171.413
154.671
84.142
80.408
77.479
77.160
76.841
68.721
45.497
41.459
32.853
28.474
28.140
24.345
18.312

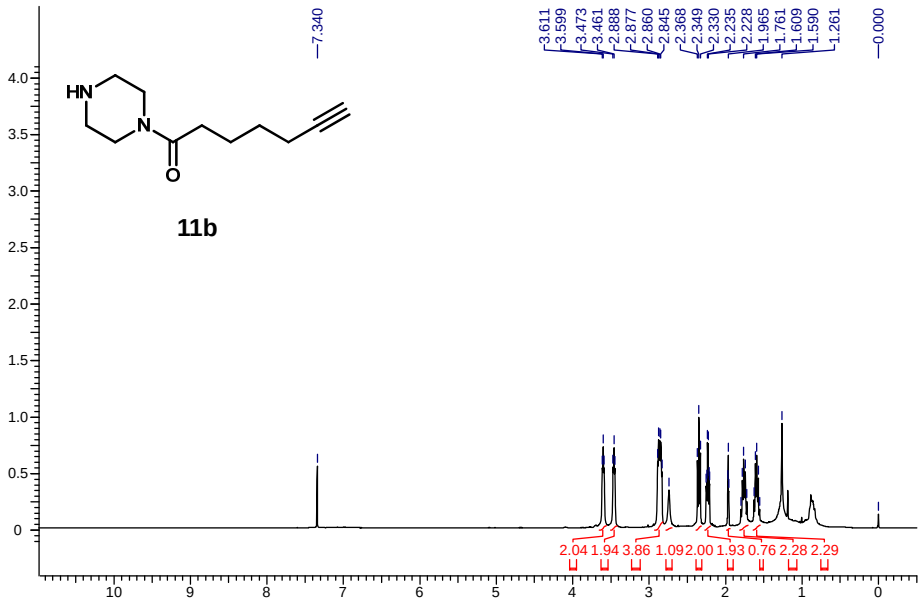
7.340
3.611
3.599
3.473
3.461
2.888
2.877
2.860
2.845
2.368
2.349
2.330
2.235
2.228
1.965
1.761
1.609
1.590
1.261
0.000
HN
N
O
11b
2.04 1.94 3.86 1.09 2.00 1.93 0.76 2.28 2.29

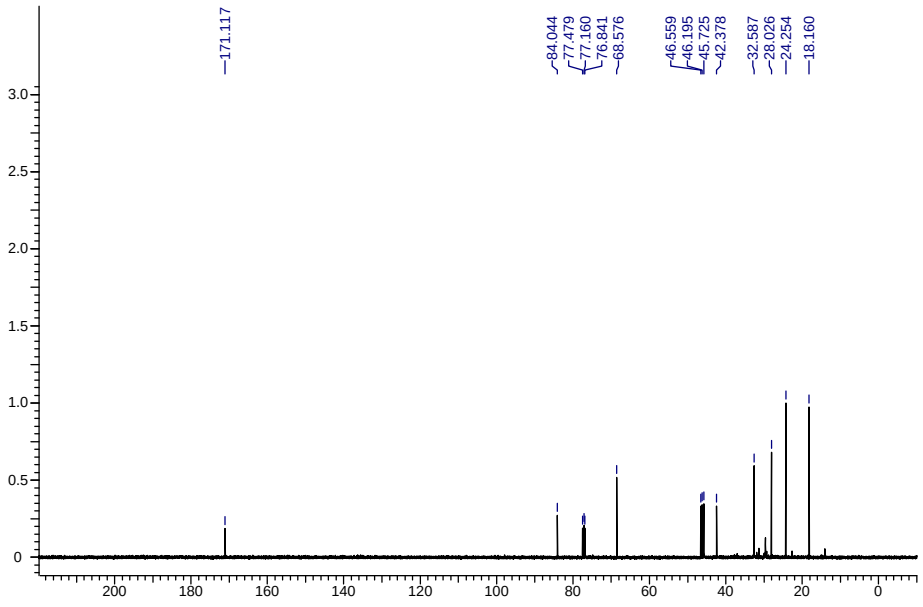
171.117
84.044
77.479
77.160
76.841
68.576
46.559
46.195
45.725
42.378
32.587
28.026
24.254
18.160

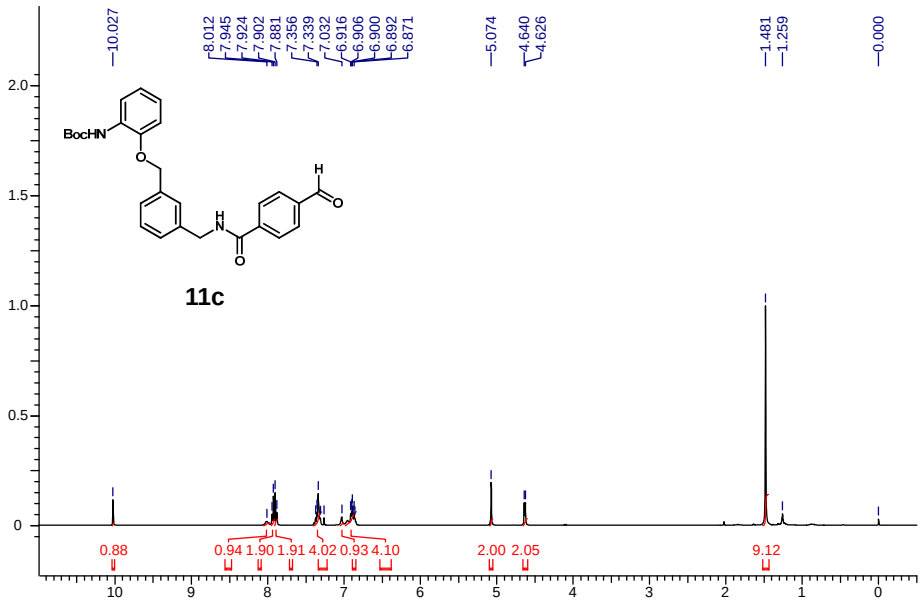
10.027
8.012
7.945
7.924
7.902
7.881
7.356
7.339
7.032
6.916
6.906
6.900
6.892
6.871
5.074
4.640
4.626
1.481
1.259
0.000
BocHN
O
H
N
O
O
11c
0.88
0.94
1.90
1.91
4.02
0.93
4.10
2.00
2.05
9.12

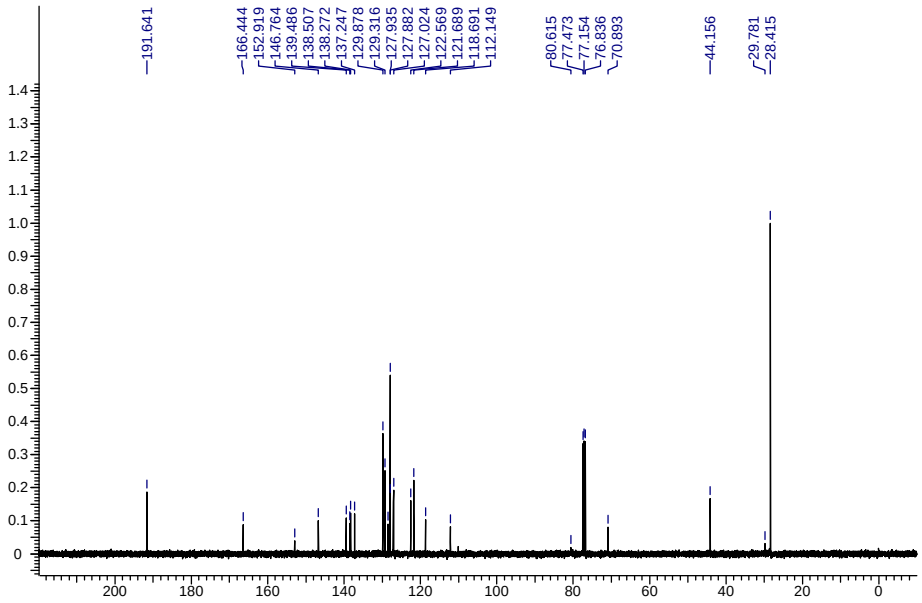
191.641
166.444
152.919
146.764
139.486
138.507
138.272
137.247
129.878
129.316
127.935
127.882
127.024
122.569
121.689
118.691
112.149
80.615
77.473
77.154
76.836
70.893
44.156
29.781
28.415

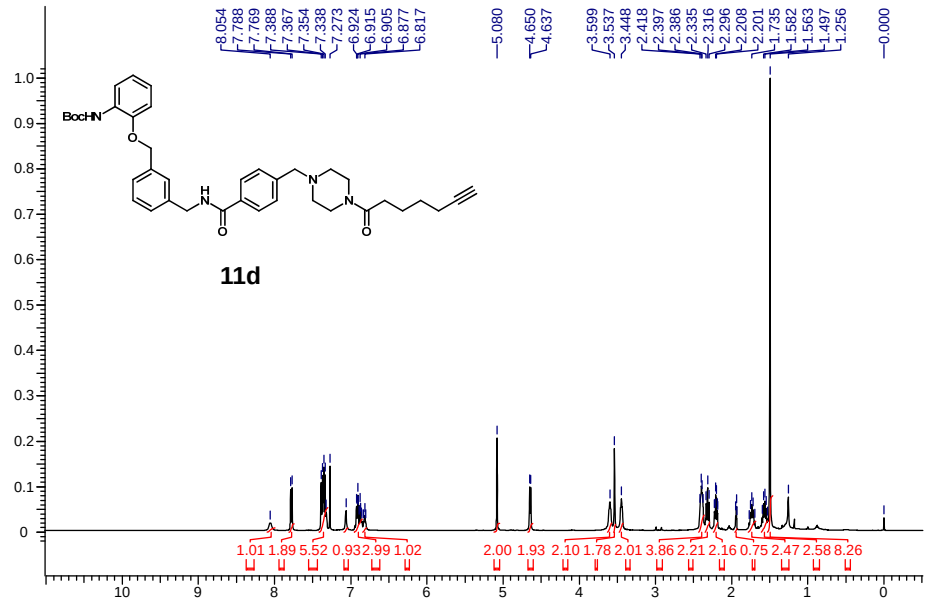
8.054
7.788
7.769
7.388
7.367
7.354
7.338
7.273
6.924
6.915
6.905
6.877
6.817
5.080
4.650
4.637
3.599
3.537
3.448
2.418
2.397
2.386
2.335
2.316
2.296
2.208
2.201
1.735
1.582
1.563
1.497
1.256
0.000
BocHN
11d
1.01 1.89 5.52 0.93 2.99 1.02
2.00 1.93 2.10 1.78 2.01 3.86 2.21 2.16 0.75 2.47 2.58 8.26

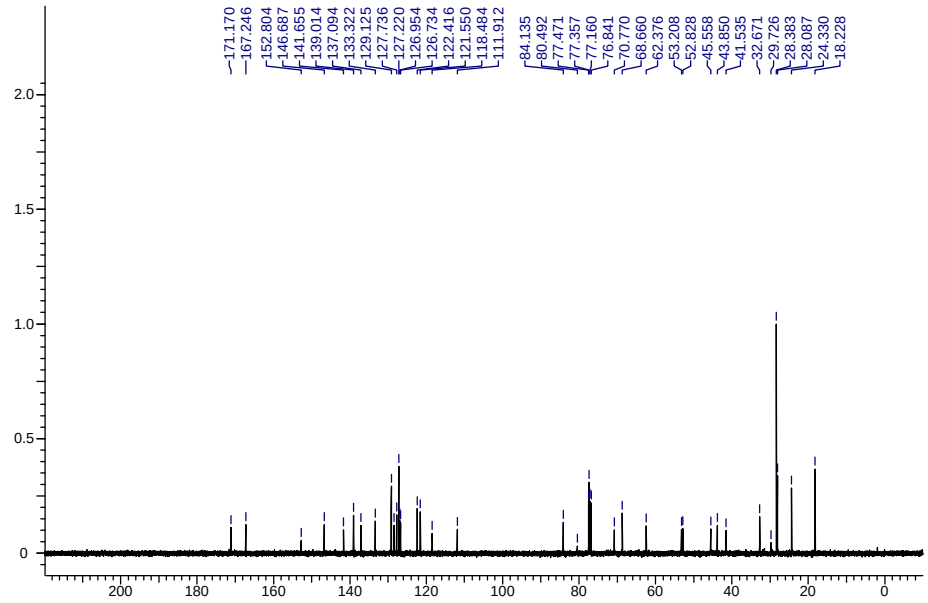
171.170
167.246
152.804
146.687
141.655
139.014
137.094
133.322
129.125
127.736
127.220
126.954
126.734
122.416
121.550
118.484
111.912
84.135
80.492
77.471
77.357
77.160
76.841
70.770
68.660
62.376
53.208
52.828
45.558
43.850
41.535
32.671
29.726
28.383
28.087
24.330
18.228

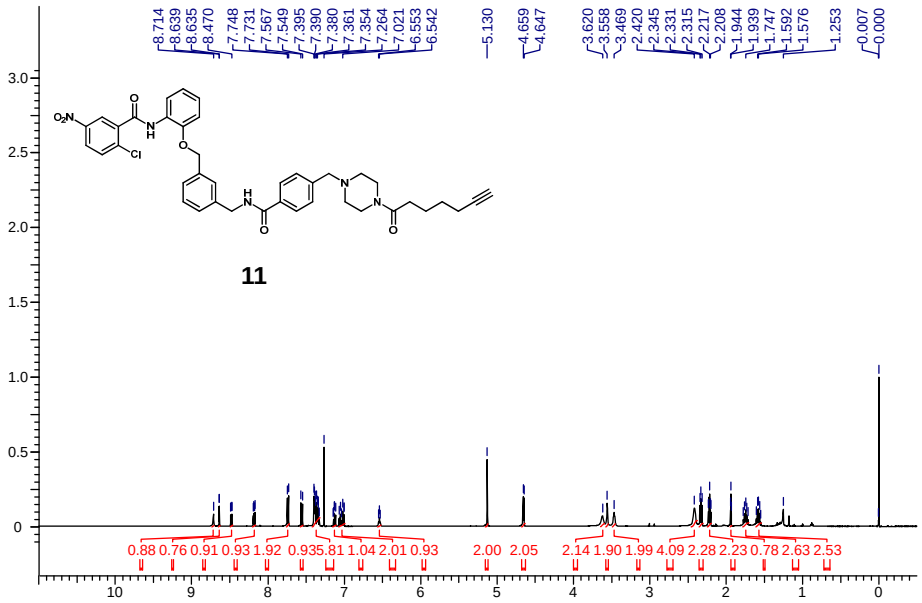
8.714
8.639
8.635
8.470
7.748
7.731
7.567
7.549
7.395
7.390
7.380
7.361
7.354
7.264
7.021
6.553
6.542
5.130
4.659
4.647
3.620
3.558
3.469
2.420
2.345
2.331
2.315
2.217
2.208
1.944
1.939
1.747
1.592
1.576
1.253
0.007
0.000
O2N
Cl
O
N
H
O
N
H
O
N
N
O
11
0.88 0.76 0.91 0.93 1.92 0.93 5.81 1.04 2.01 0.93 2.00 2.05 2.14 1.90 1.99 4.09 2.28 2.23 0.78 2.63 2.53

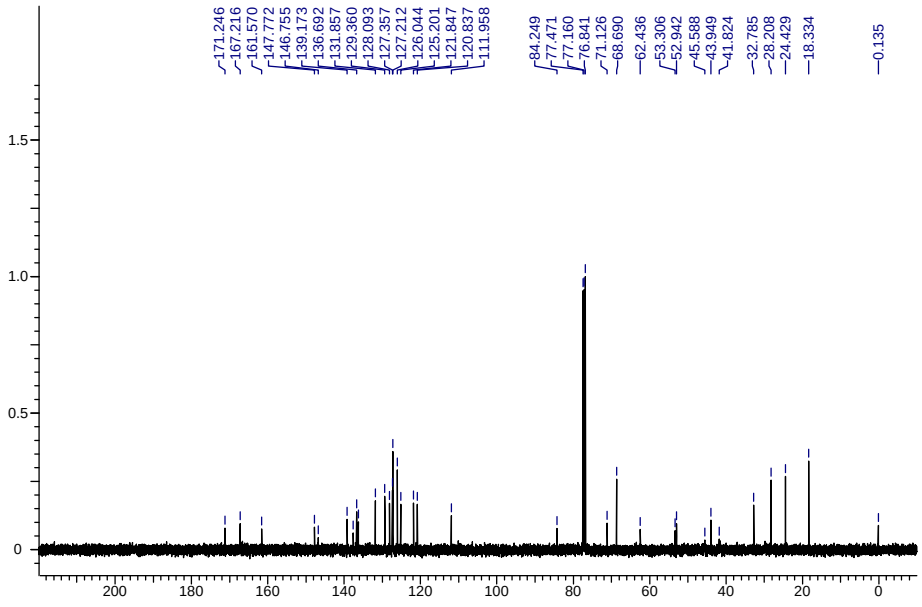
171.246
167.216
161.570
147.772
146.755
139.173
136.692
131.857
129.360
128.093
127.357
127.212
126.044
125.201
121.847
120.837
111.958
84.249
77.471
77.160
76.841
71.126
68.690
62.436
53.306
52.942
45.588
43.949
41.824
32.785
28.208
24.429
18.334
0.135